2014

Object-Based Coastal Morphological Change Analysis Based on LiDAR and Hurricane Events

Bedoor Adel Mohammad
Louisiana State University and Agricultural and Mechanical College, bmoham1@lsu.edu

OBJECT-BASED COASTAL MORPHOLOGICAL CHANGE ANALYSIS BASED ON LIDAR AND HURRICANE EVENTS

A Dissertation

Submitted to the Graduate Faculty of the
Louisiana State University and
Agricultural Mechanical College
in partial fulfillment of the
requirements for the degree of
Doctor of Philosophy

in

The Department of Geography and Anthropology

by
Bedoor Adel Mohammad
B.A., Kuwait University, 2005
M.A., California State University, Northridge, 2009
May 2015

“Not all treasure‘s silver and gold, mate.”

Jack Sparrow, Pirates Of The Caribbean: The Curse Of The Black Pearl.

I couldn't have done it without you!

Acknowledgments

As I approach the end of my doctoral program, I am conscious of those without whom I would not have completed my studies. Therefore, I would like to take this opportunity to express my gratitude.

This dissertation would never have been accomplished without our God Almighty, the Creator and the Guardian, to whom I am thankful and grateful for His blessings and His power to guide me on the right path.

I would like to express my deepest appreciation to all my committee members for their continuous encouragement and guidance. A sincere gratitude goes to my advisor and committee chair, Dr. Lei Wang, for directing me through the analysis process and guiding me in completing my dissertation writing. Special thanks go to Dr. Patrick Hesp, who was not only one of my committee members, but also a mentor, a father figure, and a friend. Also, I would like to thank Dr. Shelley Xuelian Meng for always being sweet and helpful.

I wish to give great thanks to the love of my life, my family, for always supporting me throughout this journey. This dissertation would not have been possible without the love, support, and encouragement I received from my parents to achieve my goals; they are my inspiration in life. I would also like to thank my sisters Sara, Noor, and Atharie, my brother Hamad, my aunt, and my cousin Lulu for constantly standing by my side and believing in me.

I appreciate all the help from my friends in the United States who made it possible for me to overcome my homesickness while I was away from my country, Kuwait, especially Yanqing, who always had my back whenever I needed a friend. I would also like to extend my appreciation to all my friends in Kuwait for their encouragement.

Special thanks to my scholarship sponsors in Kuwait University and the Kuwaiti embassy in the United States; my dreams wouldn‘t have come true without this scholarship.

Table of Contents

List of Tables

List of Figures

List of Abbreviations

ATM	Airborne Topographic Mapper
CART	Classification and Regression Tree
CHARTS	Compact Hydrographic Airborne Rapid Total Survey
CMA	Coastal Morphology Analyst
CSC	Coastal Services Center
DAV	Data Access Viewer
DEM	Digital Elevation Model
DGPS	Differential GPS
DSAS	Digital Shoreline Analysis System
DSM	Digital Surface Model
DSMS	Digital Shoreline Mapping System
DTM	Digital Terrain Model
FEMA	Federal Emergency Management Agency
GCP	Ground Control Points
GIS	Geographic Information Systems
GPS	Global Positioning System
IFSAR	Interferometry Synthetic Aperture Radar
IMU	Inertial Measurement Unit
JALBTCX	Joint Airborne LiDAR Bathymetry Technical Center of Expertise
Laser	Light Amplification by Stimulated Emission of Radiation
LiDAR	Light Detection and Ranging
MLLW	Mean Low Low Water
MLW	Mean Low Water
MSW	Maximum Sustained Wind
NAD	North American Datum
NAVD88	North American Vertical Datum of 1988
NCDC	National Climatic Data Center
NDBC	National Data Buoy Center
NED	National Elevation Dataset

NOAA	National Oceanic and Atmospheric Administration
OGMS	Orthogonal Grid Mapping System
OID	Object ID
OLS	Ordinary Least Square
PRF	Pulse Repetition Frequencies
RMS	Root Mean Square
RMSE	Root Mean Square Error
SSHS	Saffir-Simpson Hurricane Scale
SSHWS	Saffir-Simpson Hurricane Wind Scale
SW	Swath Width
TIN	Triangulated Irregular Network
USGS	U.S. Geological Survey
ZTS	Stereo Zoom Transfer Scope

Abstract

Storms are considered one of the rapid climatic events that have a dramatic impact on coastal morphology, hence they require further investigation and quantifying of coastal changes and responses. Light detection and ranging (LiDAR) is the most advanced technology to be widely used by researchers for coastal geomorphological studies. The purpose of this study is to apply an object-based approach using repeated LiDAR surveys to understand the short-term morphological changes that occurred on Santa Rosa Island, Florida after category 3 hurricanes Ivan (2004) and Dennis (2005), making it the first study to apply this method, as opposed to previous studies' commonly used field-based approaches. The first analysis was conducted using a coastal morphology analysis (CMA) tool. In the second analysis, the extracted mean elevation change values were linked to three factors—mean vegetation, mean slope, and mean elevation—to demonstrate their contribution to the change using ordinary least square (OLS) analysis. The third analysis was carried out using the classification and regression tree (CART) analysis. Of the study area, 18.64% encountered erosional processes and 11.35% with depositional processes during Hurricane Ivan, whereas during Hurricane Dennis, 5.91% faced erosional processes and 8.18% was affected by depositional processes. Both hurricanes resulted in a net sediment loss; 283,167 m3 during Hurricane Ivan and 52,440 m3 during Hurricane Dennis. Generally, objects tended to be irregular, asymmetrical, and shaped with smooth boundaries. Along the coast, most objects tended to have an elongated shape, but inland the shapes were more irregular. The overall OLS model during Hurricane Ivan yielded statistically significant results for the three factors, with a confidence level of 0.00 and an adjusted r-square of 0.40; and during Hurricane Dennis, the mean vegetation and mean

elevation results yielded significant statistical results (p-value 0.00), while slope did not show significance and had an adjusted r-square of 0.47. CART analysis of both hurricanes ranked the mean elevation as the most important factor in predicting the mean elevation change, followed by the mean slope and finally the mean vegetation variable.

Chapter 1 Introduction

1.1 Background

Coastal areas have always been a source of attraction for numerous purposes, including recreational, industrial, agricultural, transportational, or waste disposal purposes (Goudie 2004; Zhou and Xie 2009). The increasing demands of people who want to live close to coastal regions are putting residents at risk of exposure to coastal hazards and making them vulnerable to sea-level changes, and they are disturbing natural habitats and resources on the coasts. On a global scale, by 1998, about two-thirds of the world's population of 4.0 billion resided within 400 km of the coast, around 3.2 billion people lived within 200 km of the coast (Hinrichsen 1999, 2010), and 38% lived 100 km strip from the coast (Stewart 2009).

In the United States, Coastal Shoreline Counties have been defined by the Federal Emergency Management Agency (FEMA) as 452 counties representing a subset of counties that are directly adjacent to open ocean, estuaries, and great lakes. In 2010, 39% of the U.S. population lived in these Coastal Shoreline Counties; in other words, 123.3 million people out of the total of 313 million people in the United States live directly on the shore. Florida alone revealed a historical change in population of 165% in its Coastal Shoreline Counties between 1970 and 2010, and it is predicted to increase by 16% from 2010 to 2020 (NOAA 2013b).

Storms have a dramatic impact on coastal morphology, and they are considered one of the rapid climatic events that can produce profound changes in coastal zones (Schwartz 2005). Every storm has a different degree of impact, depending on the storm's intensity in terms of duration and path, and depending on the inner shelf and coast antecedent geology (Schwartz 2005). Therefore, as every coast is impacted differently, quantifying coastal changes has become a critical matter.

In the past, ground surveys on the beach were challenged by several limitations, such as being costly, time-consuming, and labor-intensive, as well as having limited spatial extent in the study area (White and Wang 2003; Zhou and Xie 2009). Acquiring detailed and dense spatial measurements over large coastal zones can be challenging with the use of traditional survey methods (Stockdon, Doran, and Sallenger 2009). Satellite and airborne imagery is another method used for coastal change analysis. This method may have the advantage of covering the full extent of the area of interest, but it is still considered to be time-consuming in the analytical process (Zhou and Xie 2009) and it lacks altimetry and elevation attributes. Recently, the most advanced technology, called Light Detection and Ranging (LiDAR), has been widely used for coastal geomorphological studies to map coastal erosion and deposition changes, determine shoreline changes, map overwash, and much more.

1.2 Research Objectives, Questions, and Hypothesis

The purpose of this study is to show the morphological changes that occurred after major hurricanes by analyzing the selected coastal region using LiDAR data. The overall objective of this research is to apply an object-based method to understand the short-term morphological changes occurring on coasts as a result of two major hurricanes: Hurricane Ivan in 2004 and Hurricane Dennis in 2005. Specifically, the research aims to address several research questions:

- Is LiDAR data efficient in predicting hurricane-induced coastal morphological changes and volumetric changes in term of erosion and deposition?
- When assessing coastal changes as a result of hurricanes, is the object-based approach (discrete objects method) more detailed than the field-based approach (continuous field method)?
- Does the analysis of pre- and post-hurricane data suggest the coastal morphological changes and volumetric changes in the study area between 2004 and 2005?

- Are there consistent patterns in surface and shape attributes in the erosion and deposition patches occurring after hurricanes?
- Does the morphological change orientation correspond with the major forces of the hurricane (like high winds)?
- Is there a relationship between factors like vegetation cover, slope, and elevation and the geometric change of the object in term of erosion and deposition? Do the factors make the results different? Which of the three factors dominates as the most important factor?
- How can the mapped results be used to manage the restoration projects? Can coastal managers, scientists, and geomorphologists rely on the object-based method in quantifying and examining coastal erosion and accretion?

The proposed hypothesis for this research is that the object-based method yields a better representation of the coastal morphological changes when encountered by major storms. Another proposed hypothesis is that the mean elevation changes in landforms are significantly related to several factors like vegetation distribution, slope, and elevation. In order to test the hypothesis, a quantitative analysis is applied using linear and nonlinear regression analyses.

1.3 Methods

The study investigates the spatio-temporal changes in coastal morphology induced by hurricanes, and its approach is by applying an object-based representation method using repeat LiDAR surveys collected in a selected area in Santa Rosa Island, Florida, between 2004 and 2005. Liu et al. (2010) developed a numerical algorithm that represents an object-based conceptual framework that can be used for coastal morphological change analysis and volumetric changes. The ArcGIS extension module used in this research is called the Coastal Morphology Analyst (CMA) tool. Two sequential dates of the LiDAR data are required in order to detect the changes:

for example, data before a storm and data after a storm. The method concentrates on identifying and delineating discrete objects that represent individual zones or patches of erosion and deposition.

Using the CMA tool, numerous sets of attributes can be derived, such as: 1) planimetric attributes to explain the object's dimensions, position, perimeter, and area of the erosion and deposition object; 2) shape attributes to display the shape characteristics as simple or complex, the orientation, compactness, elongatedness, and ellipticity; 3) surface attributes to explain the surface morphological changes, for example, the elevation, slope, and curvature; 4) volumetric attributes to explain and quantify the sediment change rate of erosion and deposition, for example, the volume change rate and the vertical change rate; and 5) summary statistical attributes to show an overall calculation of all objects, for example, the number of erosion and deposition objects, the average size of erosion and deposition objects, the total erosion and deposition volume, and the net volume change rate (Liu et al. 2010).

1.4 Significance and Contribution of the Study

The major contribution of this research is in being the first to apply an object-based representation for understanding coastal morphological changes created by major hurricanes, as opposed to previous studies that commonly used grid cells field-based approaches. This study will be the first to provide geometric properties and a description about the erosional and depositional patches or areas that develop following a hurricane pass. This goal is pursued by deriving several sets of attributes such as planimetric attributes, shape attributes, surface attributes, volumetric attributes, and summary statistical attributes. For example, for each delineated and identified erosional patch, several attribute values can be extracted like the orientation, width, length, thickness, perimeter, area, compactness, vertical change, volume change rate, elevation, slope, and

much more. This approach represents real-world entities and can be visually easier in the analysis process in mimicking the human perception (Liu et al. 2010) as they tend to identify objects separately rather than giving them a continuous description. For example, geomorphologist tend to identify topographic feature as hills, rivers, roads, dunes etc., rather than giving a general description of the surface.

Another element that differentiates this study from previous research is that it focuses on the physical processes of the change by classifying and applying only LiDAR points that represent bare earth or ground data, and excluding vegetation, building, and noise points within the area.

In addition to the technical advantages of this tool, this study is significant for advancing scientific knowledge in the coastal geomorphology field. Recording topographic information about the coasts and investigating it are necessary to understand sedimentary processes (Brock et al. 2002). This new conceptual framework and analysis will bring new insights to the coastal research community to further understand the sedimentary processes and coastal dynamics of barriers undergoing hurricane driven change.

It is essential to map coastal changes in order to understand coastal dynamics, and therefore provide further recommendations for decision makers. The information and analysis conducted in this study can be of great significance to coastal management and planners, and for coastal analysis after major storms, especially in the process of dune restoration projects. Providing erosional and depositional estimates makes it easier for coastal managers in restoring and nourishing damaged areas, and therefore making this method reliable and time-efficient.

The proposed research contributes to the academic literature by providing quantitatively precise and accurate information about storm effects on coastal morphology within a local scale.

Explicit quantitative and precise, high-level information can be extracted within a large area extent, and therefore a quantitative assessment can be applied rather than a qualitative assessment. The extracted mean elevation change values of each object can be further linked to several factors, including vegetation cover, landform slope, and elevation, to show the contribution of each factor on the change and to run linear and nonlinear regression analysis. For example, a vegetated area can be linked with an eroded object to show if the change was controlled by this factor and if the shape or pattern is interpreted differently. Without having precise geometric properties and attributes, it will be hard to link the results with several factors and to run regression analysis in order to show the significance between them.

Finally, in addition to the efficiency of the method, it is provided freely to the public, which makes it accessible for further testing and analysis.

1.5 Dissertation Organization

The present dissertation consists of seven chapters. The first chapter includes an introduction of the general topic, the research objectives, methods used, and significance of this topic. Chapter 2 covers a review of the literature in order to establish the context of the topic. Chapter 3 discusses the research methodology and consists of the study area description, brief descriptions of the two chosen hurricanes, information about the variables measured in the field, images acquired remotely, and data processing. Chapter 4 presents the coastal morphology analysis results and a discussion of the both hurricanes' spatial distributions in the changes. Chapter 5 presents the linear regression analyses results and discussion using OLS method. Chapter 6 presents the non-linear regression analyses results and discussion using CART method. Chapter 7 is the conclusion of the dissertation.

Chapter 2 Literature Review

2.1 Introduction

This chapter discusses the key literature of this research. It includes an introduction to the background of coastal geomorphology studies. This is followed by an object-based and field-based approach comparison. Next, a LiDAR overview is presented in terms of its definition, the technicalities behind it, and its widespread uses. Finally, hurricanes are discussed in terms of their development, categories, and effects on coastal morphology by linking it to the field of coastal geomorphology.

2.2 Coastal Geomorphology

Coastal regions are considered to be dynamic systems on earth and are prone to continuous changes. These changes are different from one location to another, depending on different factors such as sand supply, climate conditions, tectonic movement, sand size, beach profile, and much more.

Rachel Carson (1955, 1) describes the edge of the sea as:

"…an area of unrest where waves have broken heavily against the land, where the tides have pressed forward over the continents, receded and then returned. For no two successive days is the shore line precisely the same. Not only do the tides advance and retreat in their eternal rhythms, but the level of the sea itself is never at rest. It rises or falls as the glaciers melt or grow, as the floor of the deep ocean basins shifts under its increasing load of sediments, or as the earth's crust along the continental margins warps up or down in adjustment to strain and tension. Today a little more land may belong to the sea, tomorrow a little less. Always the edge of the sea remains an elusive and indefinable boundary."

Carter (1989, 1) defines the coastal zones as the "space in which terrestrial environments influence marine (or lacustrine) environments and vice versa." Changes occur within this zone, and therefore it varies in width over time. Short (1999, 1) defines beaches as "wave-deposited accumulation of sediment lying between modal wave base and the upper swash limit, where the

wave base is the maximum depth at which waves can transport beach material shoreward, and the swash limit, the landward limit of sub-aerial wave action and sediment transport."

Spatially, beaches have two- or three-dimensional characters. The two-dimension type is represented by the cross-shore dimension as shown in Figure 1, and the three-dimension considers the longshore extension in addition to the cross-shore dimension. Beach morphodynamics are affected by three wave processes: wave shoaling, wave breaking, and swash zones. The "nearshore zone" is the submerged seaward limit that extends from the wave base or the inner continental shelf to the breakpoint. The "surf zone" lies between the break point and the swash zone limit where the wave collapses to become a swash. This zone contains dynamic processes and is influenced by the tide range. The "swash zone" extends from where the wave collapses on the shoreline up to the swash limit (Short 1999).

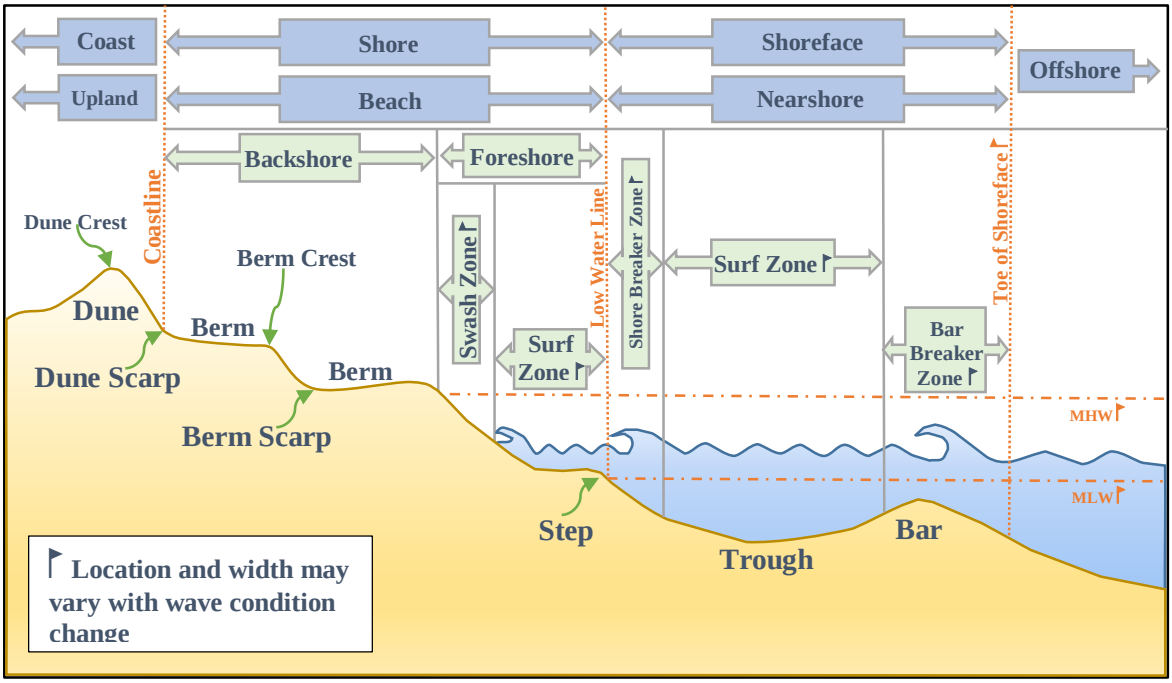

Figure 1 Two-dimensional cross-section beach profile in a wave-dominated beach system. Figure re-drawn from (CHL 2003) (Appendix A).

The time scale of beach morphology oscillation can range from hours up to years and decades (Zhou and Xie 2009). Time scale is recognized differently depending on the purpose of study. For example, a geologist may emphasize events occurring at different geological times (like in the Quaternary period), engineers and coastal managers may focus on single or multiple events (like a storm or a season) to try to estimate changes related to the event, and coastal geomorphologists focus on landforms in several time scales.

Changes in coastal landforms occur within a space and time scale, and they are used in studying coastal morphodynamics. The scale includes four classes of time scales. The smallest is the "instantaneous" time scale, represented by single cycles of physical processes, for example, examining the force of a passage of a wave or tides on the coast. The "event" time scale is represented in processes in recurrent sequences, such as understanding beach responses to seasonal events, storms, floods, or tidal cycles. The "engineering/historical" time scale is represented over several decades and combines several events, such as understanding barrier migrations and evolution over decades. The "geological" time scale is represented in long-term geological times or over a millennia, for instance, the relationship between sand movement and sea level change (Cowell and Thom 1997; Woodroffe 2002).

Coastal geomorphology studies focus on understanding and explaining coastal landform types and the factors and processes that contribute to shaping them (Woodroffe 2002). The interest in studying coastal geomorphology has been long proceeded by scientists. In the 19th century, notable work was done by Charles Lyell, Charles Darwin, and William Morris Davis when they tried to describe coastal landforms. Many efforts in Europe and North America continued throughout the 20th century, and in recent times the work continues but with much more extensive coastal research (Bird 2008).

Several techniques have been developed and applied to map shoreline changes through the late 20th century. Such examples include the "point measurements" developed by Stanford in 1971, which were used to study shoreline erosion (Moore 2000). The Orthogonal Grid Mapping System (OGMS) was introduced by Dolan, Hayden, and Heywood (1978) in an effort to generate a continuous representation of shoreline mapping using aerial photography and an orthogonal grid system. Stereo Zoom Transfer Scope (ZTS) was used to trace shoreline features in order to quantify and recognize shoreline changes. Other techniques included the Metric Mapping developed by Clow and Leatherman in 1984 that used a computer to resolve mathematical models and solutions to apply an analytical treatment of photogrammetry; a combination of ZTS and geographic information systems (GIS) technology used by McBride and others in 1991 to map changes in Louisiana's barrier islands; GIS Strategies, Digital Shoreline Mapping System (DSMS), and Digital Shoreline Analysis System (DSAS); and Softcopy Photogrammetry/GIS Methodology (Moore 2000).

Barriers are defined as "shore-parallel, sub-aerial and sub-aqueous accumulation of detrital sediment (sand/boulders) formed by waves, tides and aeolian processes" (Hesp and Short 1999, 307). The term "barrier island" differentiates from a "barrier" in being detached or separated by a lagoon from the mainland (Woodroffe 2002). Three types of barriers can form, depending on these existing factors: the sea-level movement (being the prime control), the energy of the waves, sediment supply, tidal range, onshore wind energy, and plate tectonics. Consequently, one of three barrier development types can form: regressive (progradational), stable (stationary), or transgressive (retrogradational) (Hesp and Short 1999). Within the United States, barrier island systems are found along the Gulf of Mexico coasts and the Atlantic coasts, containing around 300

islands from Texas to Maine (Beatley, Brower, and Schwab 2002). Barrier islands act as a protection for the mainland against waves, storms, and hurricanes.

2.3 Object-based Approach vs. Field-based Approach

In GIS, there are two concepts used to represent the data: 1) the vector data model, 2) and the raster data model (Chang 2013; Price 2013; Shekhar and Chawla 2003):

1) The vector model, also called discrete or object-based model, shows geographic entities in a single or in a series of *x*-*y* coordinate locations, and spatial features are shown as distinct, and identified object. Spatial information is saved as a point, line, or polygon. For example, a line representing a road or a river, a polygon representing a building or a lake, and a point representing a city. In this case, geospatial data are represented as a geometric object. The object-based data model has the ability to store geometries and attributes within a single system.
2) The raster model, also called the field-based model, shows the spatial data as a series of pixels, cells, or small squares over a region in space that is laid out as rows and columns. Every pixel has a numeric code set to represent the attribute. This approach is used to model a continuous spatial trends, for example, the variation of precipitation, elevation, or temperature. Within the raster model there are two approaches:
    a. Discrete raster: it represents features or objects in a discrete and delineated matter saved in raster format. This represents vector features that have been converted to raster models, and hence are called discrete raster. For example, different colors can be assign to land cover, or roads.
    b. Continuous raster: the method stores information as a map quantity values changing over a surface. The geographic phenomena is shown in a smooth transition from one

cell to its neighboring cell forming a continuous field, for example, in slope surface, elevation surface, or aspect surface rasters.

2.4 LiDAR Overview

LiDAR is a technology that "emits intense, focused beams of light and measures the time it takes for the reflections to be detected by the sensor" (NOAA 2012, 3). The most common acronym for this technology is LiDAR, but it can also be referred to as LADAR, Lidar, or laser altimetry. For the purposes of this research, LiDAR will be used.

There are several approaches used to acquire elevation values about the surface, *in situ* or ground surveys, photogrammetry, Interferometry Synthetic Aperture Radar (IFSAR), and LiDAR technology (Jensen 2009). LiDAR is a reliable and accurate method in providing a representation of landscape elevation, areas with shallow water, and project sites. In remote sensing, there are two systems used to measure energy: passive and active systems. In the passive system, the sensors record natural and external sources of energy, for example, the sun. In the active system, the energy is generated toward the desired object. In this case, LiDAR is considered an active system emitting discrete pulses of laser light toward the target in an attempt to record the reflected light. The recorded points represent three-dimensional coordinates (x, y, and z) of the surface. Airborne platforms and a scanning LiDAR sensor are common techniques used to generate LiDAR data for large areas, while helicopters, ground-based stationary (also water-based), and mobile platforms are used for smaller areas (NOAA 2012).

Two basic methods for the active system are used to measure the three-dimensional surface: time-of-flight or LiDAR measurement, and the Triangulation-based measurements. In time-of-flight measurement, the method works when the light waves travel with a finite and

constant known velocity within a given medium (like air, water, vacuum, etc.) with the aim of measuring the time delay, starting from the time the light is generated to travel from the source toward the target surface and reflect back to the sensor or detector (in other words, the generated light makes a round trip). Laser is an acronym for "light amplification by stimulated emission of radiation," and it produces light that is considered to have high monochromaticity, directionality, brightness, and spatial coherence (Beraldin, Blais, and Lohr 2010). The pulse of light, *t*, travelling time is expressed as follows:

$$t = 2\,\frac{R}{c}$$

Where *R* is the range or distance between the sensor and the object, and *c* is the speed of light ($3 * 10^8$ m s^{-1}) (Jensen 2009). When collecting the three-dimensional data of a surface using a single laser beam, it is essential to have a scanning mechanism to move the laser beam above the desired surface. Several scanning mechanisms are used. The first, the oscillating mirror technique, is widely used in airborne systems, and it works by using a swiveling mirror that directs the pulse of the laser across the swath width to collect points in both directions of the scan in a zigzag pattern. Because the mirror accelerates and decelerates continuously, various distances between laser points are found across the track or scan line. The main advantage is that it can provide an adjustable scan angle, ranging from zero to 75º, and variable scan rate. The second is the rotating polygonal mirror. Here, a rotating polygon mirror is utilized to detect the laser beam. It scans points of data in a parallel, one-directional way with a uniform pattern of equal spaces between the laser points in the scan lines (along and across track), and a range of 30º to 60º scan angles can be provided. The third is the Palmer scanner, which is used mostly in terrestrial laser scanning, but for airborne systems it generates laser pulses in an elliptical pattern on the ground. The fourth is

the glass fibre scanner that uses a scanning mirror, and one laser pulse is fed to several glass fibres (typically 128) that are arranged and glued in a linear array toward the ground with a fixed scan angle of 14º. The advantage of this mechanism is that it is extremely stable (Beraldin, Blais, and Lohr 2010).

Airborne LiDAR data is a widespread technique used for producing a high-quality representation of the continuous surface in three dimensions that is collected from aircraft and helicopters (NOAA 2012). Some of the advantages of this system include having a high measurement density, high accuracy in elevation data, rapid recording for the acquisition of data, the ability to penetrate the canopy and record the floor of forests, and the minimum amount of ground truth that is required. Since LiDAR is an active system, operations for data collection can be done both during the day and at night, giving this system an advantage. Some of the basic components of the airborne laser scanning are as follows: 1) the scanner assembly involves the laser, scanning mechanics, and optics; the basics of the laser system are the same as the previously mentioned measurement (time-of-flight), and it is mounted in the aircraft's fuselage that is set over a hole and sends repeated laser pulses while the aircraft is flying; 2) the Airborne Global Positioning System (GPS) antenna requires signals from satellites, so it is usually mounted on top of the aircraft to get an exposed and undisturbed position; during the flight, the GPS is used to get accurate position information; 3) the inertial measurement unit (IMU) requires a stable platform that can either be fixed directly to the laser scanners or close to it, and it is used to acquire acceleration data and rotation rates (orientation of the platform); IMU provides the survey platform's roll, pitch, and yaw angles, and in order to reconstruct accurate flight paths or trajectory, a combination of GPS and IMU measurements are required, and by merging them, a set of altitude and attitude data are derived; 4) the control and data recording unit can control the entire system

as it stores the gathered data from the previously mentioned devices and therefore becomes responsible for time synchronization; 5) the operator laptop is used during the survey so the operator can observe the performance of the system, set parameters for the mission, and monitor the control and data recording unit; and 6) the flight management system provides the pre-planned flight lines required for the pilot to display before starting the mission. In addition to all the previously mentioned components for airborne laser scanning, a GPS ground station is also required, and it can be used as a reference station for calculating the off-line differential GPS (DGPS). The spatial relationship and time dependencies of the three components, scanner assembly, IMU, and GPS, must be known in order to integrate accurately between them, which contributes to the final elevation data accuracy (Beraldin, Blais, and Lohr 2010).

In coastal applications, there are two airborne LiDAR systems used to obtain topographic data: the subaerial and bathymetric systems (Sallenger et al. 2003). Bathymetric data are obtained in circumstances where the water is clear and shallow in the nearshore zone (NOAA 2012). For land applications, a wavelength between 800 nm and 1,550 nm and a spectral width between 0.1 nm and 0.5 nm are commonly used in airborne laser scanning. It is required to use eye-safe laser beams in order to avoid any damage to human eyes (Beraldin, Blais, and Lohr 2010). The commonly used region of the electromagnetic spectrum is the eye-safe, near-infrared laser light from 1040 nm to 1060 nm for mapping topographic data. Other sensors may also operate the blue-green lasers at 532 nm for bathymetric mappings since they have the ability to penetrate water and reach bottom features and measure sea floor elevations (Jensen 2009). Laser systems that use wavelengths near the visible portion of the spectrum will have high absorption in water bodies, and water surface will therefore be hard to be recorded. Also, at wavelengths close to 1550 nm,

ice and snow tend to have a low reflection, making it poor for snow field surveys (Beraldin, Blais, and Lohr 2010).

Laser beams travel within the cross-track swath width (*sw*) as:

$$sw = 2h \tan \frac{\theta}{2}$$

Where θ is the scan angle, and *h* is the height or altitude of the aircraft above-ground level (Jensen 2009). LiDAR can emit pulses rapidly at about 50,000 to 150,000 pulses per second, and in 2012 it reached 300,000 pulses per second (NOAA 2012), also referred to as the pulse repetition frequencies (PRF) (Jensen 2009). As PRF increases, the ground point density increases. When the PRF is high, the cruising speed is low, the survey height is low, and scan angle is small, all of these contribute to obtaining the highest point density. The return echo number and form can be influenced by the surface type and direction or orientation of the form. Receivers in time-of-flight measurement can obtain several return echoes per pulse, like first, second, third, and last return (Beraldin, Blais, and Lohr 2010). Return numbers are used to determine what feature the reflected pulse came from (NOAA 2012). For example, flat areas or surfaces can provide one return echo, while trees or vegetation can provide several returns because of their sloping surface and complex orientation.

Each survey project of airborne laser scanning can be derived within three different phases: 1) Flight planning: The setup and configuration of the laser scanner has to be initially defined based on the purposes and demands of the project and based on the performance of the scanner parameters. Input information like the height of platform, the speed of platform, and the scan angle are required to produce output parameters like the average point density and swath width. When choosing scan angles for surveys in flat areas, it is better to use larger scan angles, while for urban

or densely vegetated areas, it is better to choose smaller angles. Some software is used to get the required parallel flight lines and overlaps, normally a 20% overlap, in order to cover the project area. 2) Survey flight: based on the parameter chosen in the previous step, the survey flight can start to collect the data depending on the demands of the project, for example, in choosing a certain season for collecting vegetated areas and choosing specific weather condition. 3) Data processing: This phase consists of deriving DGPS data by correcting the airborne GPS measurements when comparing them with data from the ground GPS station and by merging and integrating IMU measurements with the obtained DGPS data. Other corrections include data calibration and atmospheric correction. After LiDAR point cloud data are corrected and classified, the data will be ready for interpolation processes into Digital Elevation Models (DEM), whether it is a Digital Surface Model (DSM) that covers all surface objects like vegetation, buildings, and ground surface, or a Digital Terrain Model (DTM) that produces only the bare-earth or ground terrain surface (Beraldin, Blais, and Lohr 2010).

Airborne LiDAR data's level of accuracy can be different from one vendor to another, depending on the flight parameters and instrument use, and usually LiDAR data are tested after collection and processing and then documented in the metadata section (NOAA 2012). Several factors can affect the accuracy of LiDAR data, for example, errors can occur from errors in the calibration of the GPS, IMU, and scanner assembly; flight path errors; surface complexity; laser beam reflection on moveable objects rather than the ground; and errors during coordinate transformation (Beraldin, Blais, and Lohr 2010). Accuracy assessment techniques are applied to measure and compare ground control points (GCP) with the collected airborne LiDAR data. A known point in the field will be compared with a surface of LiDAR points in the three nearest points using the triangulated irregular network (TIN) method. Since it is unlikely to be able to

collect a point using airborne LiDAR that exactly matches the ground point, a surface of LiDAR points is used instead in the comparison process. To avoid getting biased test results, the surface is preferred to be in open areas that are not sloped or irregular. Data accuracy is measured using a statistical measure of variability in elevation called the root mean square error (RMSE) with a typical measure ranging between five and 30 centimeters (NOAA 2012). For topographic surveys, LiDAR has a high vertical accuracy (Stockdon, Doran, and Sallenger 2009) when compared with older methods like the National Elevation Dataset (NED) that produces elevation datasets for U.S. Geological Survey (USGS) using photogrammetric techniques with a vertical RMSE of 2.4 m (NOAA 2012). Sallenger et al. (2003) evaluated the accuracy of the Airborne Topographic Mapper (ATM) survey data by comparing them with extensive ground measurements, and they estimated the vertical accuracy of ATM to be ≈ 15 centimeters root mean square (RMS). This makes using LiDAR essential in studying dune fields since the topography and elevation of dune fields tend to be highly variable in nature (Stockdon, Doran, and Sallenger 2009).

A study done by Sallenger et al. in 1999 aimed to investigate the impact of two extreme storms on the coastal topography of Assateague Island, Maryland and Virginia, during 1998 using ATM by comparing pre- and post-storm profiles. The results show a vertical erosion change of about two meters (Sallenger et al. 2003). This indicates that the two meter value is much greater than the common vertical accuracy measurement ranging between five and 30 centimeters (NOAA 2012), and that morphological change values are not close to measurement accuracy. When studying the impact of storms on coastal morphology changes over a regional scale, the interest in vertical accuracy will not be on a sub-centimeter level (Sallenger et al. 2003).

It is also essential to reflect upon the horizontal resolution of the data point spacing as it can affect the vertical accuracy. The common measured horizontal resolution using airborne

LiDAR is between 1.0 m and 2.0 m or better. Using the oversampling technique in recording multiple overlaps in the flight passes, the data can increase the total collected points, and therefore provide higher horizontal resolution. In addition to its high vertical and horizontal accuracy, the temporal resolution also plays a great role in the accuracy of the data analysis process since in using airborne LiDAR data collection, it can be easier than with photogrammetric techniques to renew the data collection in a short time and therefore can be a good source of accurate elevation measurement for coastal studies (NOAA 2012).

Many coastal change surveys and studies have proven the efficiency of this technology (Shrestha et al. 2005). Numerous applications have been applied using LiDAR data including quantifying coastal changes impacted by storms (Zhang et al. 2005; Sallenger et al. 2006; Robertson, Zhang, and Whitman 2007; Stockdon, Doran, and Sallenger 2009; Claudino-Sales, Wang, and Horwitz 2010), for mapping and determining modern shoreline positions (Stockdon et al. 2002; Robertson et al. 2004), or for long-term rates of shoreline movement or change (Morton, Miller, and Moore 2004; Morton and Miller 2005; Hapke et al. 2006). The field-based or cell-by-cell differencing approach is usually used in association with the LiDAR survey when analyzing morphological and volumetric coastal changes, and the results are presented as a continuous field over the spatial extent (Gutierrez et al. 2001; White and Wang 2003; Shrestha et al. 2005; Gares, Wang, and White 2006).

2.5 Hurricanes and Coastal Geomorphology

Hurricanes are one of the most destructive natural disasters that can produce morphological changes along coastal zones. Hurricanes are a type of tropical cyclone that forms in the western hemisphere's tropical oceans, mostly between the latitudes of 5º and 20º. The warm temperature of the ocean's surface of 27ºC (80ºF) or greater, and the warm moist air are important factors that

help enhance and sustain the hurricane's formation. In other regions around the world, tropical storms are also called typhoons, if formed in the western Pacific, or cyclones, if formed in the Indian Ocean.

Tropical cyclones develop through different levels until reaching the hurricane stage, as indicated from the weakest to the strongest respectively: 1) Tropical Disturbance, 2) Tropical Depression, 3) Tropical Storm, and 4) Hurricane. As an international agreement, if the wind reaches 74 miles (119 km) per hour or more, and it has a rotary circulation over tropical waters, it is called a hurricane. Hurricanes are formed within a low-pressure system ranging from 980 to 920 mb at the center (Lutgens and Tarbuck 2007).

The Saffir-Simpson Hurricane Scale (SSHS), developed by Herbert Saffir and Robert Simpson in the early 1970s (Channel 2012; NOAA 2010), categorizes the intensity level of hurricanes into five categories as a result of studying previous storms (NOAA 2013d; Lutgens and Tarbuck 2007). Recently, NOAA's National Weather Service updated the scale to a new scale called Saffir-Simpson Hurricane Wind Scale (SSHWS) that excludes the storm surge range and reflects minor modifications on the wind speed boundaries between category 3/4 and category 4/5 (NOAA 2010, 2013d).

By using this scale, meteorologists can predict the level of storm severity on homes, people, and vegetation. When the tropical storm becomes a hurricane, the National Weather service assigns a scale depending on its strength by using the SSHWS. Table 1 gives different SSHWS hurricane categories and the level of damage related to it. Damages encountered by hurricanes can be found in three ways (Lutgens and Tarbuck 2007):

Table 1 The Saffir-Simpson Hurricane Wind Scale (SSHWS), modified (NOAA 2013d; Lutgens and Tarbuck 2007).

Category	Sustained Wind* (mile/hour)	Sustained Wind* (knot)	Sustained Wind* (kilometer/hour)	Central Pressure (millibars)	Description
One	74–95	64–82	119–153	greater than 980	Minimal damage: Very dangerous winds will produce some damage
Two	96–110	83–95	154–177	965–979	Moderate damage: Extremely dangerous winds will cause extensive damage
Three	111–129	96–112	178–208	945–964	Extensive damage: Devastating damage will occur
Four	130–156	113–136	209–251	920–944	Extreme damage: Catastrophic damage will occur
Five	157 or more	137 or more	252 or more	less than 920	Catastrophic damage: Catastrophic damage will occur

* Sustained wind is “wind speed determined by averaging observed values over a two-minute period” (NWS 2009).

a) Storm surge: With extreme weather events, a temporal increase in the seawater level occurs above the normal astronomical high tide level and results in devastating damage on the coast (Thomas, Goudie, and Dunkerley 2000; Lutgens and Tarbuck 2007). The strong onshore winds during storms help pile up the water in the ocean, pushing it toward the coasts to cause a storm surge. Several factors play a role in the amplitude of a storm surge on coasts: the orientation of the coastline with the path of the storm; the storm's strength, speed, and extent; and the bathymetry of the coast (NOAA 2013c). Coasts facing the Gulf of Mexico are subjected to strong storm surges because of their shallow continental shelf and gentle slope. In the Northern Hemisphere, hurricanes circulate counterclockwise, and therefore the right side of the eye has the strongest storm surge where winds blow toward the shore (Lutgens and Tarbuck 2007).
b) Wind damage: Onshore winds can be a strong force that cause damage on the coast during hurricanes. The morphological coast can be dramatically changed and eroded, and buildings are susceptible to damage from debris. Hurricane-forced wind velocities can reach outstanding speeds, such as in the case of category 3, 4, and 5 shown in Table 1. Damage produced by winds can extend to about 200 kilometers inland from the coast. Tornados can also form during hurricanes and can enhance the destructive level (Lutgens and Tarbuck 2007).
c) Flooding: Severe and heavy rain associated with hurricanes are another way of triggering a threat to coastal zones and to humans. This torrential rain can cause flash floods and mudflows as the hurricane track moves inland. Despite the fact that a hurricane usually weakens as it moves inland, it can still cause extensive flooding, and the effects can reach far inland from the coast (Lutgens and Tarbuck 2007).

Morton (2002) listed principal factors that control and influence storm impacts on coastal barrier islands and beaches in the western Atlantic and Gulf of Mexico, including the

characteristics of an individual storm, coastal location relative to the path of the storm, storm successiveness on the same region, storm coincidence with local astronomical tides cycle, backshore flooding duration, wind stress on coastal water bodies, beach and barrier island topography, the texture of coastal sediment, coastal vegetation types and coverage, and the artificial structure type and density.

The range of vertical morphological change in landform for pre- and post-hurricane studies can be catastrophic and rapid in coastal zones. Depending on the strength and intensity of the storm, coastal topography can change overnight as a result of strong winds, high storm surge, and rainfall. The range of morphological change depends on the storm's magnitude and intensity, such as storm surge, wave energy, and wave run-up (Sallenger 2000); the storm path; the topography and morphology of the beach system, such as low-level dunes being susceptible to destruction and sections of the barrier being vulnerable to submersion in low-lying barrier islands; and other factors like vegetation cover and distribution and human constructions.

Barrier islands' vulnerability to hurricanes depends on the storm-induced mean water level elevation, which is expressed as the sum of storm surge, wave run-up, and the astronomical tides, when compared to the elevation of sand dunes' located most seaward. Dunes are likely to submerge if the mean water level exceeds the sand dune crest, and therefore those conditions cause significant changes on the coast (Stockdon, Doran, and Sallenger 2009).

Many studies have been done in the field of coastal geomorphology and aided further understanding of morphology changes impacted by storms and hurricanes. Studies by Shepard and LaFond (1940) and Shepard (1950) contributed to the coastal geomorphology field and brought new insight about the beach profile responding to the varying wave energies (low- and high-wave energy). Records were obtained by surveying beach profiles along the Scripps Institution pier at

La Jolla, California, over a period of two years. Their observations indicated that beach systems can be changed depending on the season. During calm weather with low, flat waves (swell waves), the sediment tends to be pushed onshore, building a berm and a somewhat steeper beach profile. On the other hand, during stormy weather, taller and steeper waves tend to erode the berm and beach and transport sediment offshore, building sand bars or submarine bars in the surf zone.

Hayes (1967) contributed significantly with his study on two hurricanes—Carla in 1961 and Cindy in 1963—that made landfall in Texas, showing the coastal morphological response to those hurricanes. His study brought new understanding about sediment movement and redistribution during hurricanes between the three zones: the inner shelf, the nearshore, and the subaerial. He indicated that the inner neritic zone played two important roles in being the supplier and the receiver of deposits during the hurricane.

Dolan and Godfrey (1973) examined the impacts of Hurricane Ginger on coastal morphology on two barrier islands in North Carolina, and they indicate that the response is different in every location. In the north, the dunes stabilized by human suffered from extreme erosion and recession, and the sediment was mostly transported offshore and alongshore during the hurricane. In the south, the area comprises natural dunes, and deposition was the main process noticed.

Some other studies focused on the Gulf of Mexico area with the attempt to examine the impact of hurricanes on coastal morphology (e.g., Morgan et al., 1958; Wright et al., 1970; Kahn and Roberts 1982; Stone and Salmon 1988; Stone 1998; and Stone and Wang 1999). They indicated that high wave energy and high water levels occurring during hurricanes can result in substantial erosions in the beach systems (Keen and Stone 2000).

Sallenger (2000) categorized and defined four levels of storm-impact regimes on barrier islands. The impact depends on four elevation parameters: R_{High} and R_{Low}, representing landward margin of the swash from a fixed vertical datum, where R_{High} is the highest elevation and R_{Low} is the lowest elevation, and D_{High} and D_{Low}, representing the elevation of the barrier islands' first line of defense measured relative to a fixed datum, where D_{High} is the highest crest of elevation, and D_{Low} is the lowest elevation. The scale is presented from the weakest to the strongest, respectively: impact level 1 is the "swash" regime, where R_{High} and R_{Low} is lower than D_{Low} or the dune base; impact level 2 is the "collision" regime, where R_{High} reaches and collides with the dune base, causing net erosion; impact level 3 is the "overwash" regime, where R_{High} is higher than D_{High} and R_{Low} is lower than D_{High}; and impact level 4 is the "inundation" regime, when all landward water swash parameters exceed D_{High}, causing submergence of the barrier island.

Numerous researchers have attempted to investigate coastal morphological changes induced by Hurricane Ivan (Wang et al. 2006; Sallenger et al. 2006; Houser, Hapke, and Hamilton 2008; Claudino-Sales, Wang, and Horwitz 2010) and Hurricane Dennis (Claudino-Sales, Wang, and Horwitz 2008) while some focused on using LiDAR data to quantify coastal changes impacted by storms (Sallenger et al. 2006; Houser, Hapke, and Hamilton 2008; Claudino-Sales, Wang, and Horwitz 2010).

Wang et al. (2006) examined the northwest coasts of Florida by surveying an eastward extent of areas from Fort Walton Beach to St. George. They applied several cross–barrier island profiles and beach-dune profiles with an attempt to understand the short-term storm impact and recovery induced by Hurricane Ivan. The author indicated four impacted level regimes along the shore: inundation and overwash in regimes resided within 100 km east of the hurricane center, collision regime occurred within 100–150 km, and swash regimes were noticed up to 300 km.

Despite the efforts in this research to show post-hurricane recovery over a large area, only a few profiles were recorded (3 cross-barrier-island profiles and 7 beach-dune profiles). This results in gaps between every profile and causes others to be missing comprehensive topographic data, and therefore an accurate estimation of the change over a large area within the barrier island cannot be provided.

Sallenger et al. (2006) studied four different hurricanes that made landfall on Florida's coast during 2004 with an attempt to understand the different characteristics of change on every coast using photography and airborne LiDAR surveys of pre- and post-hurricanes. The authors indicated that each hurricane produced a unique response. The averaged longshore shoreline change varied roughly from +1 m up to 20 m, while the average longshore volume change ranged between -11 $m^3 m^{-1}$ and -66 $m^3 m^{-1}$. They indicated that the intensity of hurricanes is not the only indication of intense shoreline changes. For example, although Hurricane Charley made landfall as category 4, making it the highest category out of the other three hurricanes during the 2004 season, it showed the lowest mean shoreline change.

Claudino-Sales, Wang, and Horwitz (2008) applied a combination of methods, including rectified aerial photos of before and after Hurricane Ivan and Dennis, ground observation, and pre- and post-storm dune beach profile surveys with an attempt to qualitatively examine the factors that affected the regional scale dune fields' destruction and survival that took place along Santa Rosa Island, Florida. They discussed an interaction of several factors that play a role in dune survival, such as hurricanes' characteristics and the barrier islands' morphological parameters. They emphasized the role of vegetation density in survival and continuity of the dune fields. This research lacks vertical topographical data across the barrier island. By using the dune-beach profile for the ground or field investigation, only limited linear portions are investigated in the large spatial

extent. The research also encountered loss in some pre-storm beach-dune profiles as some benchmarks were destroyed after storms. The authors only examined the qualitative factors controlling the change, and not the quantitative measurement. Only visual evaluations of dune destruction/survival were constructed, which enhances the chance of human error in distinguishing different features (like berm, dune, water, and more).

Houser, Hapke, and Hamilton (2008) studied dune morphology variation alongshore Santa Rosa Island, Florida, in relationship to Hurricane Ivan and the historical and storm-related change rates of shoreline using LiDAR data, bathymetry data, historical shoreline change rates data, and statistical analysis. The authors discussed how the variation is driven by the inner-shelf transverse ridges, and the cuspate headland in the backbarrier or the barrier island width. In this research, the results of morphological change are not exclusively concentrated on single storm effects as they include historical storm-related rates of shoreline erosion in the analysis. This brings a limitation in this research in not emphasizing the role of Hurricane Ivan on the change.

Another study by Claudino-Sales, Wang, and Horwitz (2010) expanded on their previous study on Santa Rosa Island by quantifying the changes in the regional-scale dune system elevation characteristic and calculating volume changes pre- and post-Hurricane Ivan using cross-island airborne LiDAR profile surveys and ground surveys. The authors indicated 70% destruction in incipient and hummocky dunes along the study area, and more sand was eroded from the barrier island than deposited with profile volume losses of 100–200 m^3/m. This research only applies a continuous representation of change by using several lines of cross-sectional profiles along the barrier island. This approach is limited as it lacks thorough and homogeneous quantitative topographic information on change over the regional scale and only provides a linear change across the barrier island. In addition, the research uses “first return” LiDAR data, and therefore the

evaluation could include errors due to mistaking ground features with vegetation features or with noise.

In the literature described previously, the studies concentrated on different aspects and used different methodologies to understand hurricane impacts on coastal regions; however, many gaps were indicated. This research will cover the missing gap by extracting erosional and depositional objects and provide volumetric changes. Also, when studying coastal morphological changes induced by hurricanes, attributes like shape and pattern were not previously examined, and this requires further detailed analysis.

Chapter 3 Research Methodology

3.1 Introduction

This chapter discusses the methodology used in this research. In the first section, the extent of the chosen location is described, and characteristics of the landform are discussed. Section two includes detailed meteorological characteristics of both Hurricane Ivan and Hurricane Dennis in addition to their impacts. Section three describes the dataset downloaded and utilized in this research, in addition to detailed pre-processing steps to prepare the data. The following section explains the CMA processes used to generate the final identified object map, in addition to the set of attributes calculated. The Zonal Statistics as Table tool was discussed to explain how several factors' values were generated. Next, the ordinary least square is discussed. Finally, the classification and regression tree (CART) method is explained.

3.2 Study Area

For this research, a portion is chosen from Santa Rosa Island, Florida, located in Escambia County, as shown in Figure 2. To facilitate the analysis process, the study area was divided into three sections as (I-1, I-2, and I-3) for Hurricane Ivan and (D-1, D-2, and D3) for Hurricane Dennis. The area-bounding coordinates extend approximately from latitude N30.344º to N30.356º, and from longitude W87.019º to W87.068º, stretching alongshore from east to west to approximately 4.8 km long, and extending inland to approximately 0.6 km wide from south to north. The mean center of the selected study area is surrounded by Pensacola Beach from the west and Navarre Beach from the east, and it is located fairly close to both hurricanes' landfalls: approximately 92 km east from the center of Hurricane Ivan as it made landfall in Gulf Shores, Alabama; and 8 km

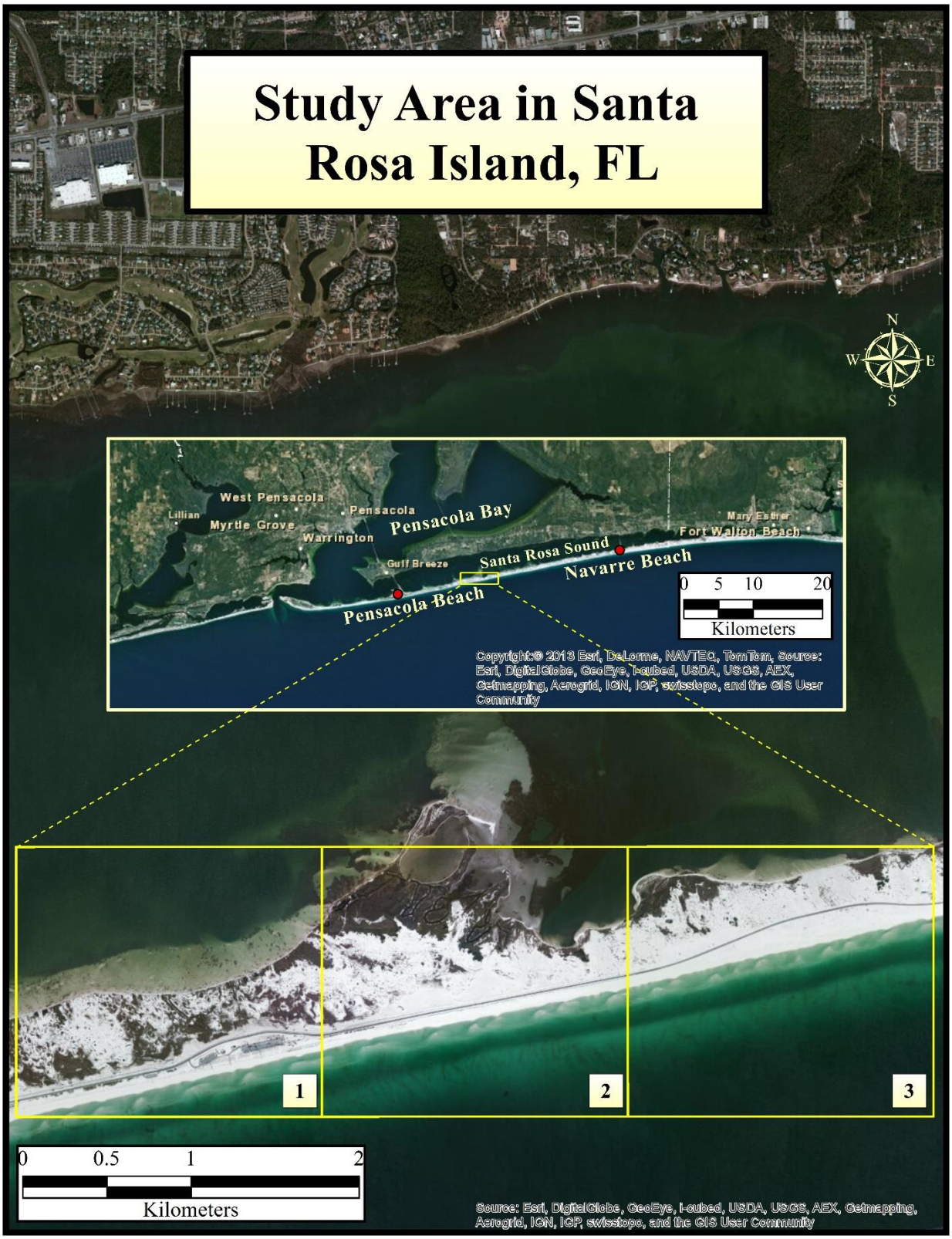

Figure 2 Study area in Santa Rosa Island, Florida. Basemap from (ESRI 2013b).

east from the center of Hurricane Dennis as it made landfall in Santa Rosa Island, Florida, as shown in Figure 3.

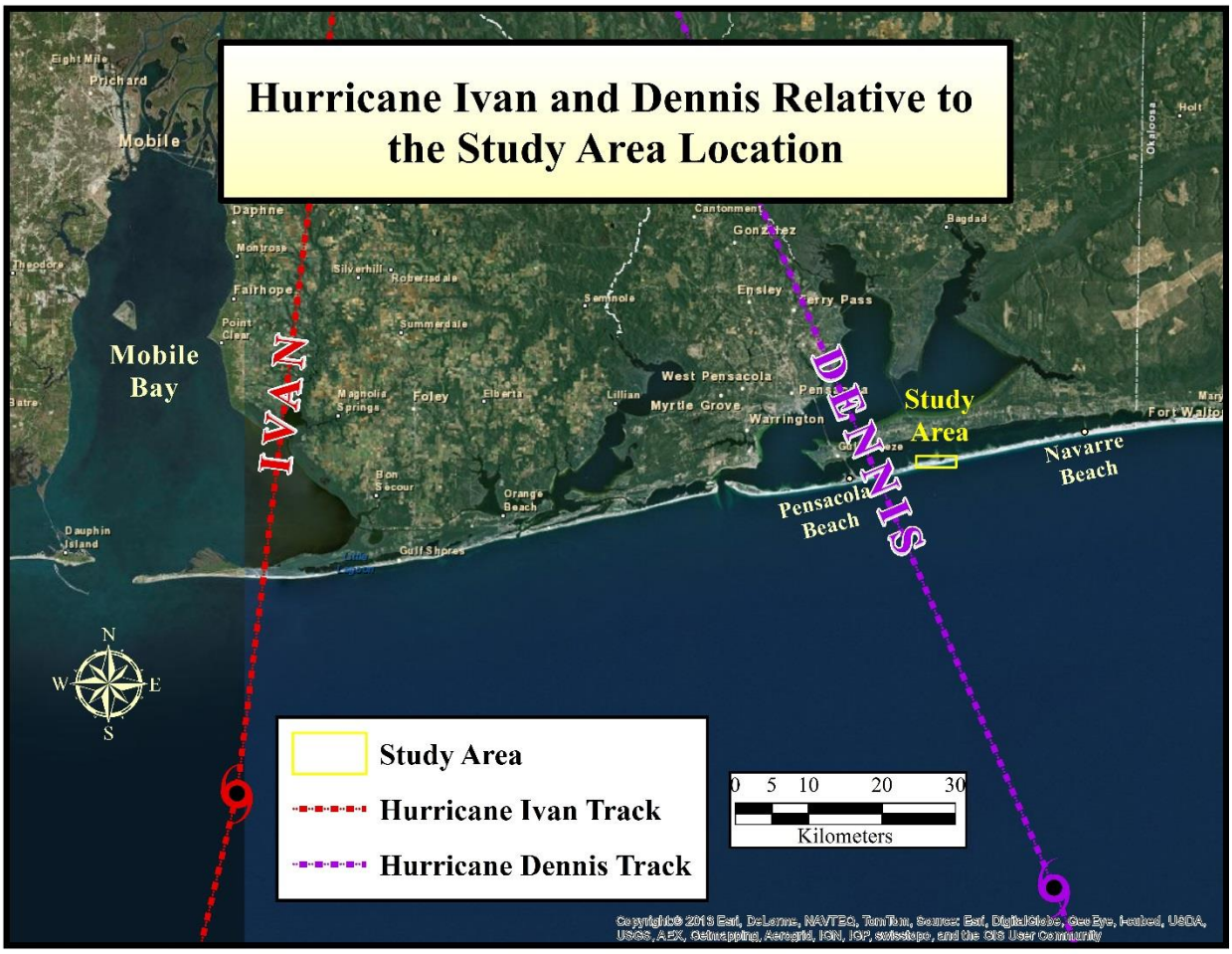

Figure 3 Hurricane Ivan and Hurricane Dennis track distance from study area. Basemap from (ESRI 2013b).

The selection process of the study area is based on several factors, including the quality of LiDAR data in having a small average point spacing between points and avoiding datasets that included missing points or survey errors during the flight, resulting in line gaps. The selected site consisted of mostly sand and vegetation and is relatively undeveloped with minimal infrastructure when compared to other regions in this barrier island. It only included one building, a few wooden crossover trails, parking, and roads, making it ideal for understanding the physical processes of morphological change.

Santa Rosa Island is a barrier island located in the western Florida Panhandle, elongating from east to west, and extends through three different counties: Escambia County, Santa Rosa County, and Okaloosa County. This barrier island is narrow, with an average of 500 m wide, and extending 85 km from Pensacola Bay in the west to Choctawhatchee Bay in the east. It has a low-lying profile with relatively low incipient and established foredunes, ranging from 2.5 to 10.0 m above mean low water (MLW). The barrier island originated in the late Holocene period to build on top of a Pleistocene core (Claudino-Sales, Wang, and Horwitz 2010). The coastline depositional landforms are mainly produced by waves, currents, and aeolian processes. The elongated barrier island faces the Gulf of Mexico from the south, Pensacola Bay on the northwest, and Choctawhatchee Bay on the northeast, and it is separated from the mainland by Santa Rosa Sound in the north. The area is primarily wave dominated and microtidal (Kish and Donoghue 2013) with a tide average range of 0.43 m, and the prevailing winds are southwesterly with moderate speeds. The sediment is composed of 99% quartz and 1% heavy materials like illmenite and rutile (Stone et al. 2004). The back of the island consists of maritime forest patches along the Santa Rosa Sound.

Stone and Stapor (1996) created a model showing sediment transport rates in the Santa Rosa Island Region. The longshore transport of sediment is toward the west. Nearly 57,000 m^3 yr^{-1} of the sediment is eroded from the west side of Land's End Canal and then transported to Destin East Pass. Out of this amount, about 44,000 m^3 yr^{-1} is transported south into the shelf. Around 50,000 m^3 yr^{-1} of sediment is being transported from the east of Santa Rosa Island toward Navarre Beach, and 47,000 m^3 yr^{-1} of that total gets transported south offshore into the shelf. In the region between Pensacola Beach and Pensacola Pass, about 58,000 m^3 yr^{-1} of the net litteroral transport moves to the west, and 34,000 m^3 yr^{-1} out of that total gets transported to the south into the offshore inner shelf. An approximate rate of 26,000 m^3 yr^{-1} is deposited westward in Pensacola Pass.

3.3 Hurricanes Ivan and Dennis

The 2004 and 2005 hurricane season was an active season that affected many coastal areas in Florida that face the Gulf of Mexico (Claudino-Sales, Wang, and Horwitz 2008). The study areas chosen in this research have historically been in a range of several tropical cyclones' paths. Figure 4 shows a historical record between 1851 and 2010 of tropical cyclones in northwest Florida.

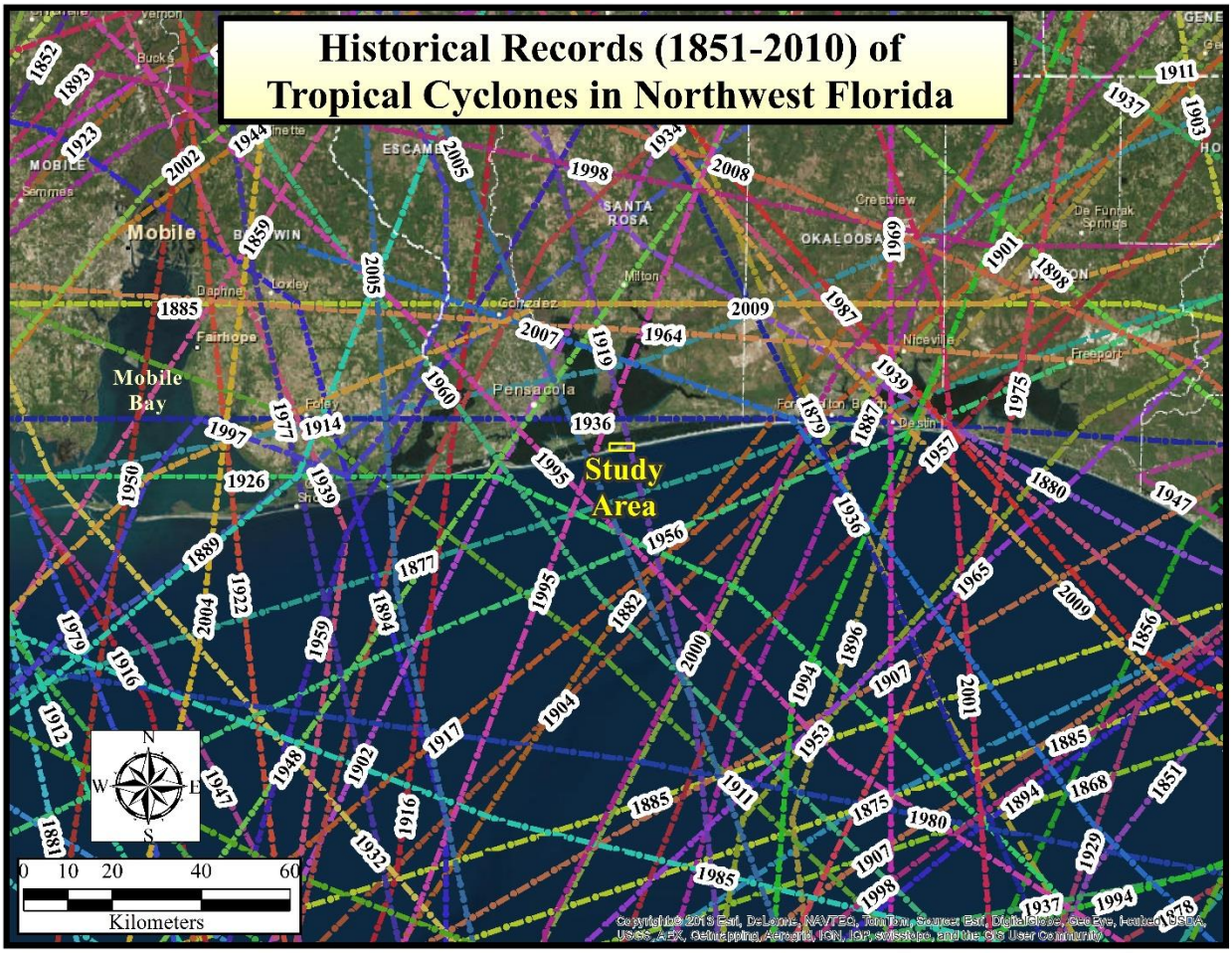

Figure 4 Historical records between 1851–2010 of tropical cyclones in northwest Florida. Basemap from (ESRI 2013b).

3.3.1 Meteorological Characteristics and Impacts of Hurricane Ivan

Hurricane Ivan was one of the most destructive hurricanes on the coasts of Florida (FDEP 2004). The initial development of Ivan started from a large tropical wave on August 31, 2004 on the west coast of Africa. Ivan was a Cape Verde–type hurricane because it started to develop into a tropical storm on the east side of the Atlantic Ocean near the Cape Verde Islands (less than approximately 1,000 km), and because it reached a hurricane category before entering the Caribbean Sea (NOAA 2006; Stewart 2006).

On September 2 at about 1800 UTC, it continued to develop into a tropical depression and became Tropical Storm Ivan on September 3 at 0600 UTC; it continued to move westward over the Atlantic Ocean. On September 5 at 0600 UTC, it reached hurricane status (Stewart 2006). On its path in the Caribbean Sea, Hurricane Ivan intensified three times to reach category 5 before entering the Gulf of Mexico (FDEP 2004). Ivan made landfall on September 16 at about 0650 UTC as a category 3 west of Gulf Shores, Alabama (Stewart 2006) and east of Mobile using the SSHS (FDEP 2004), and it extended 170 km from the hurricane center (Claudino-Sales, Wang, and Horwitz 2010). Figure 5 displays the track of Hurricane Ivan by showing the maximum sustained wind (MSW) gust (10-min) in knots along the path.

The hurricane came to the shore with extensive wind speeds, waves, and surge, and therefore resulted in severe damage (Claudino-Sales, Wang, and Horwitz 2008). The most impacted coastal areas from Hurricane Ivan were the ones extending to the east of the storm's landfall, where severe beach erosion and structural damage occurred. Counties located to the east of the hurricane's landfall in Santa Rosa Island, Florida (like Escambia, Santa Rosa, and Okaloosa) suffered severe erosional damage while Gulf County suffered less damage because when moving further away from the hurricane landfall, the strength diminishes (FDEP 2004).

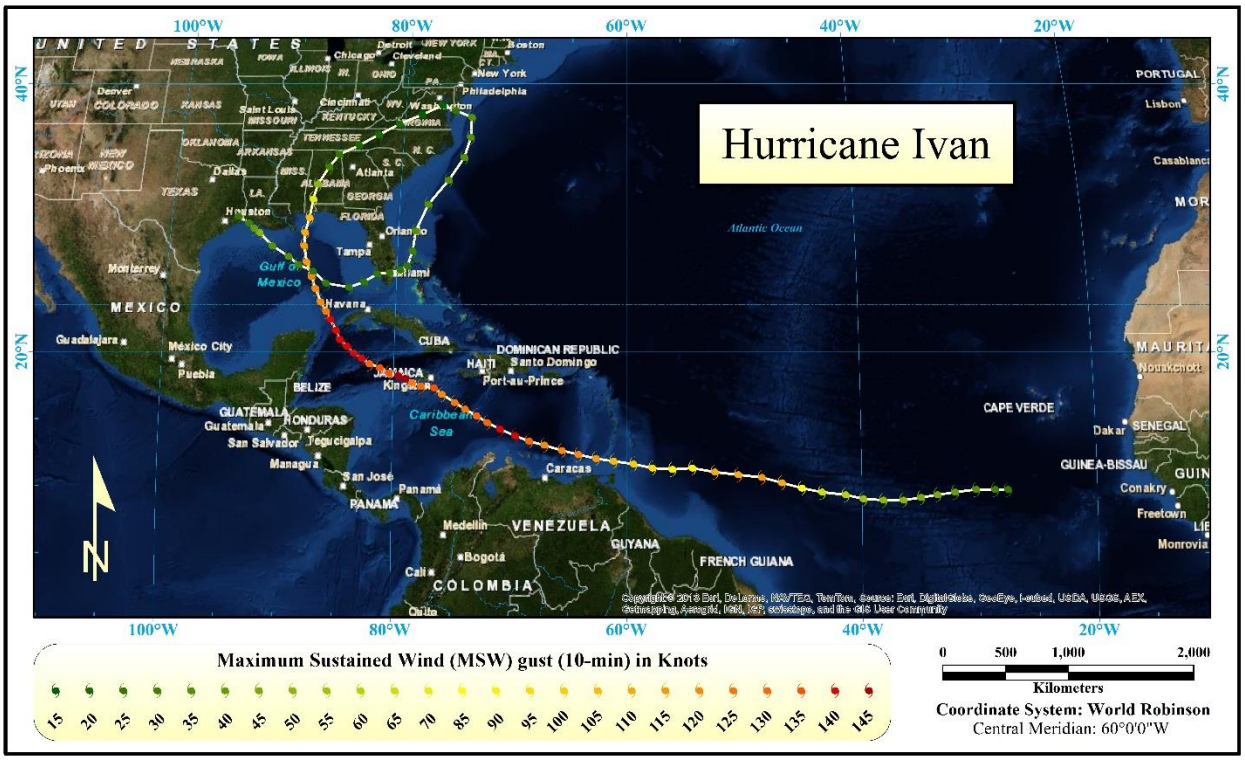

Figure 5 Hurricane Ivan path, showing the MSW gust (10-min) in knots. Basemap from (ESRI 2013b).

As the hurricane crossed the barrier island in Alabama and headed northeast inland, it weakened into a tropical storm and gradually into a tropical depression on September 17 at 0000 UTC. Although the hurricane weakened, it still produced tornados and extraordinary rain that caused damage to the southeastern United States and caused flash floods. A total of 117 tornados developed over three days in different states. Table 2 shows the count of tornados formed in several southeastern states. Storm surge occurred on coastal regions reaching 10–15 feet (3–4.5 m) above mean sea level from Destin, Florida to Mobile Bay, Alabama, and 6–9 feet (1.8–2.7 m) from Destin, Florida to St. Marks, Florida (Stewart 2006). Pensacola tide gage measured a 2.06 m high surge above mean low low water (MLLW) (Wang et al. 2006). Buoy 42040 from National Data Buoy Center (NDBC) located offshore near the path of Hurricane Ivan recorded extremely high waves reaching 16 m just offshore before landfall (Claudino-Sales, Wang, and Horwitz 2010).

Table 2 Total count of tornados formed in several U.S. states during Hurricane Ivan in 2004 (Stewart 2006).

States	Tornado Count
Virginia	37
Georgia	25
Florida	18
Pennsylvania	9
Alabama	8
South Carolina	7
Maryland	6
North Carolina	4
West Virginia	3

3.3.2 Meteorological Characteristics and Impacts of Hurricane Dennis

Hurricane Dennis is one of the most damaging hurricanes to have occurred on the coast of Florida's Panhandle (FDEP 2005). Dennis initially developed from a tropical wave on June 29, 2005 from the west coast of Africa. The system became a tropical depression on July 4 at 1800 UTC over the south of Windward Islands and moved westward. On July 5, the system developed into a tropical storm with a general movement toward the west and northwest. On July 7, it developed into a hurricane level and intensified in strength quickly to reach category 4. Hurricane Dennis made landfall on July 8 near Punta del Ingles, Cuba, and then continued its path toward the north-northwest as it emerged into the Gulf of Mexico on July 9 at 0900 UTC. Dennis made landfall as a category 3 using the SSHS on July 10 at about 1930 UTC on Santa Rosa Island, Florida, approximately two miles (3.2 km) east of Pensacola Beach with a wind speed of 115–120 mile/hr. (185–193 km/hr.) (Beven 2005; FDEP 2005). Figure 6 displays the track of Hurricane Dennis by showing the MSW gust (10-min) in knots along the path.

As in the case of Hurricane Ivan, the most impacted coastal areas from Hurricane Dennis were the ones extending to the east of the storm's landfall. A combination of factors played a role

Figure 6 Hurricane Dennis path, showing the MSW gust (10-min) in knots. Basemap from (ESRI 2013b).

on the impact, such as the strong winds, the storm surge, and the breaking waves. Coastal areas extending from Navarre Beach to Wakulla County were severely impacted (FDEP 2005).

Pensacola beach in Escambia County, Florida experienced a wind speed ranging from 95–115 mile/hr. (153–185 km/hr.) occurring from the northwest, and a storm tide of 8–10 feet (2.4–3 m). Navarre Beach in Santa Rosa County, Florida, was about 7.5 miles (12 km) east of the center of the Hurricane Dennis track. This area experienced a maximum 121 mile/hr. (195 km/hr.) wind velocity occurring from the south and southeast, and a storm tide of 10–12 feet (3–3.6 m). This led to flooding, overwash, and major beach and dune erosion. St. Joseph Peninsula State Park in Gulf County, Florida, experienced some major beach and dune erosion, storm surge flooding, and overwash (FDEP 2005). The highest recorded waves reached 10 m (Claudino-Sales, Wang, and

Horwitz 2008). Pensacola tide gage measured a 1.5 m high surge above MLLW (Claudino-Sales, Wang, and Horwitz 2008).

As the hurricane crossed the western Florida Panhandle and Alabama moving north-northwesterly, it weakened into a tropical storm and gradually became a tropical depression on July 11 as it reached Mississippi. Ten recorded tornados were produced from Hurricane Dennis: nine recorded in Florida and one in Georgia (Beven 2005).

3.4 Datasets and Data Pre-Processing

Several software packages and tools were used in pre-processing and analyzing the data, including ESRI ArcGIS software version 10.1 and 10.2.2, the CMA tool, LAStools, Google Earth Pro, IBM SPSS, and WRPLOT View.

The LiDAR datasets used in this research were downloaded using Data Access Viewer (DAV) published by the National Oceanic and Atmospheric Administration's (NOAA) Coastal Services Center (CSC) (NOAA 2013a). The datasets were collected by the Joint Airborne LiDAR Bathymetry Technical Center of Expertise (JALBTCX) using the Compact Hydrographic Airborne Rapid Total Survey (CHARTS) system, and it contained topographic and hydrographic data. The purpose for their data collection was to depict the elevations above and below water along the immediate coastal zone. The downloaded datasets covering the study areas were in a LAS format file containing numerous LiDAR point cloud data. LiDAR datasets were projected to the North American Datum (NAD) 1983 Universal Transverse Mercator (UTM) zone 16N, and to North American Vertical Datum of 1988 (NAVD88), and included the following:

1) Pre-Hurricane Ivan datasets: two datasets were downloaded, which were collected beginning on April 1, 2004, and ending on May 30, 2004. Vertical accuracy is believed to be within the order of 15 cm RMSE. The downloaded datasets were unclassified to several

class codes. They included a total point cloud data of 3,758,897 points, and the elevation z value ranged from -1.74 m to 19.5 m.

2) Post-Hurricane Ivan datasets: one dataset was downloaded, which was collected beginning on November 1, 2004, and ending on December 31, 2004. Vertical accuracy is believed to be within the order of 15 cm RMSE. The downloaded dataset was unclassified to several class codes. It included a total point cloud data of 2,730,783 points, and the elevation z value ranged from -2.11 m to 18.75 m.
3) Post-Hurricane Dennis datasets: two datasets were downloaded, which were collected beginning on July 13, 2005, and ending on July 25, 2005. LiDAR data were tested against ground truth data using post processed KGPS methods and showed a vertical accuracy of better than +/- 20 cm and horizontal accuracy of better than +/- 75 cm. The downloaded datasets were unclassified to several class codes. They included a total point cloud data of 8,160,839 points, and the elevation z value ranged from -2.24 m to 16.02 m.

Within every timeframe of a hurricane event, LiDAR datasets were merged into one dataset and clipped within the extent of the study area polygon. Each LiDAR dataset's cloud points were classified for the purpose of extracting ground or bare-earth points. (1) Pre-Hurricane Ivan datasets: A total of 3,518,919 points were classified as ground with elevation ranging from -1.74 m to 10.29 m. (2) Post-Hurricane Ivan datasets: A total of 2,642,664 points were classified as ground with elevation ranging from -2.11 m to 10.11 m. (3) Post-Hurricane Dennis datasets: A total of 7,756,567 points were classified as ground with elevation ranging from -0.31 m to 10.06 m.

After all LiDAR datasets were classified, raster interpolation processes were applied to convert LAS files to raster DTM grid files. An Ordinary Kriging method was utilized to interpolate

the cloud points into raster DTM using a cell size of 2 m as shown in Figure 7. The total area size covered 2,264,790.84 m^2 for pre–Hurricane Ivan, and covered 2,248,176.77 m^2 for pre–Hurricane Dennis. Several surface rasters were generated using the pre-hurricane DTM raster in both hurricane events. Two slope surface rasters were generated to show each cell surface gradient or rate of maximum change in z value measured in degree values as shown in Figure 8 with slope ranging between 0 and 43 degrees prior to Hurricane Ivan, and 0 to 45 degrees prior to Hurricane Dennis.

Other datasets used in this research included aerial and satellite imageries. All imageries were projected to NAD83/ UTM zone 16N. The high-resolution orthorectified imagery included aerial photographs acquired on March 1, 2004, and these were downloaded in a GeoTIFF format from USGS EarthExplorer (USGS 2014), consisting of eight imageries. An orthoimage was corrected to a uniform scale and rectified to obtain a geometric quality of the map. Imageries consisted of three bands combined to create natural color (RGB) imagery, and with a high spatial resolution of 0.61 m. All images were mosaicked into one image raster to represent pre–Hurricane Ivan image.

Several high-resolution satellite images were downloaded from Google Earth Pro acquired on February 27, 2005, with a spatial resolution of 0.36 m. A total of eighteen images were saved with attached control points representing (x , y) points or longitude/latitude coordinate points, and later imported into ArcMap to be georeferenced, rectified, and mosaicked into one image raster to represent a pre–Hurricane Dennis image.

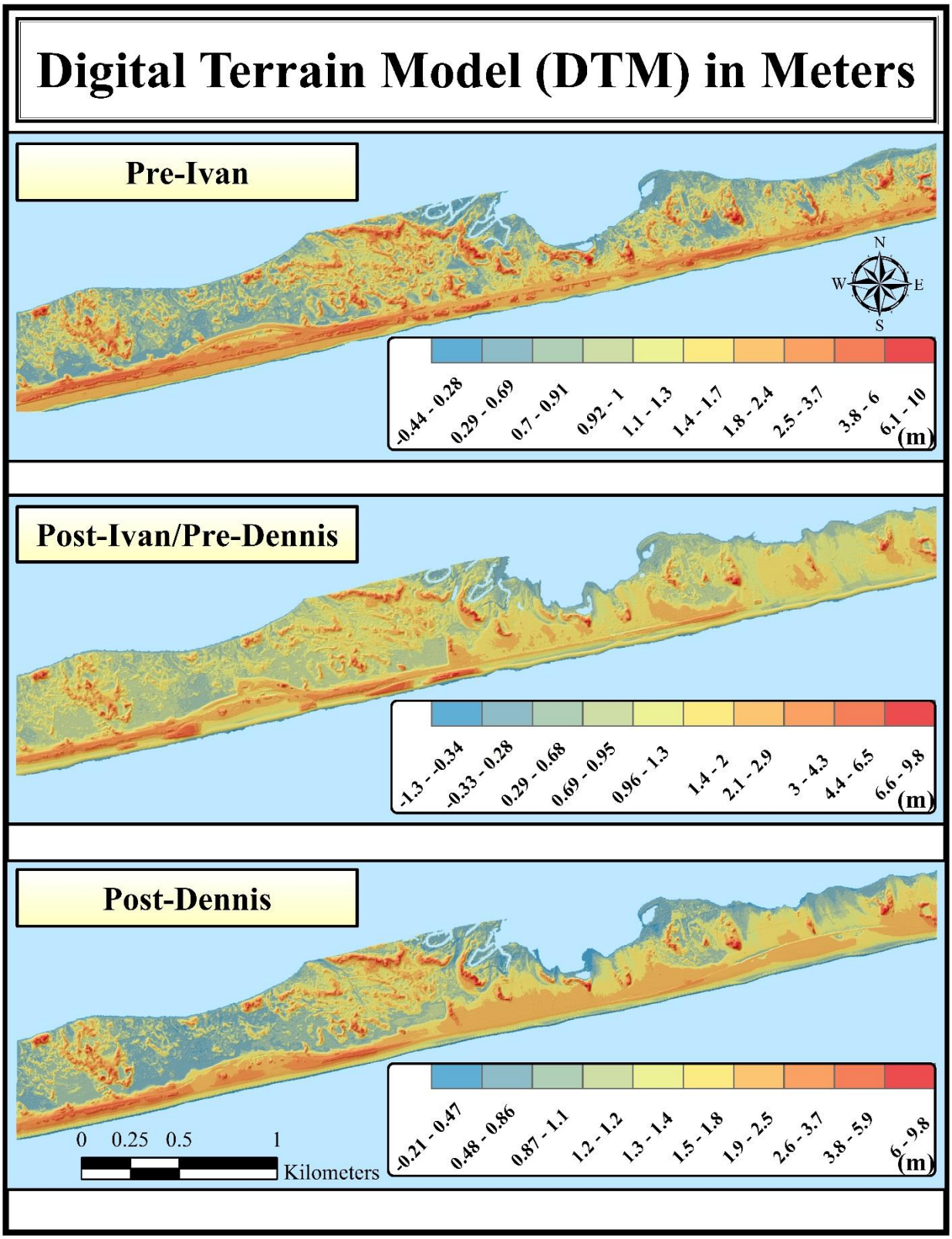

Figure 7 The three generated digital terrain models (DTM), measured in meters, for pre-Hurricane Ivan, post-Hurricane Ivan/Pre-Hurricane Dennis, and Post-Hurricane Dennis.

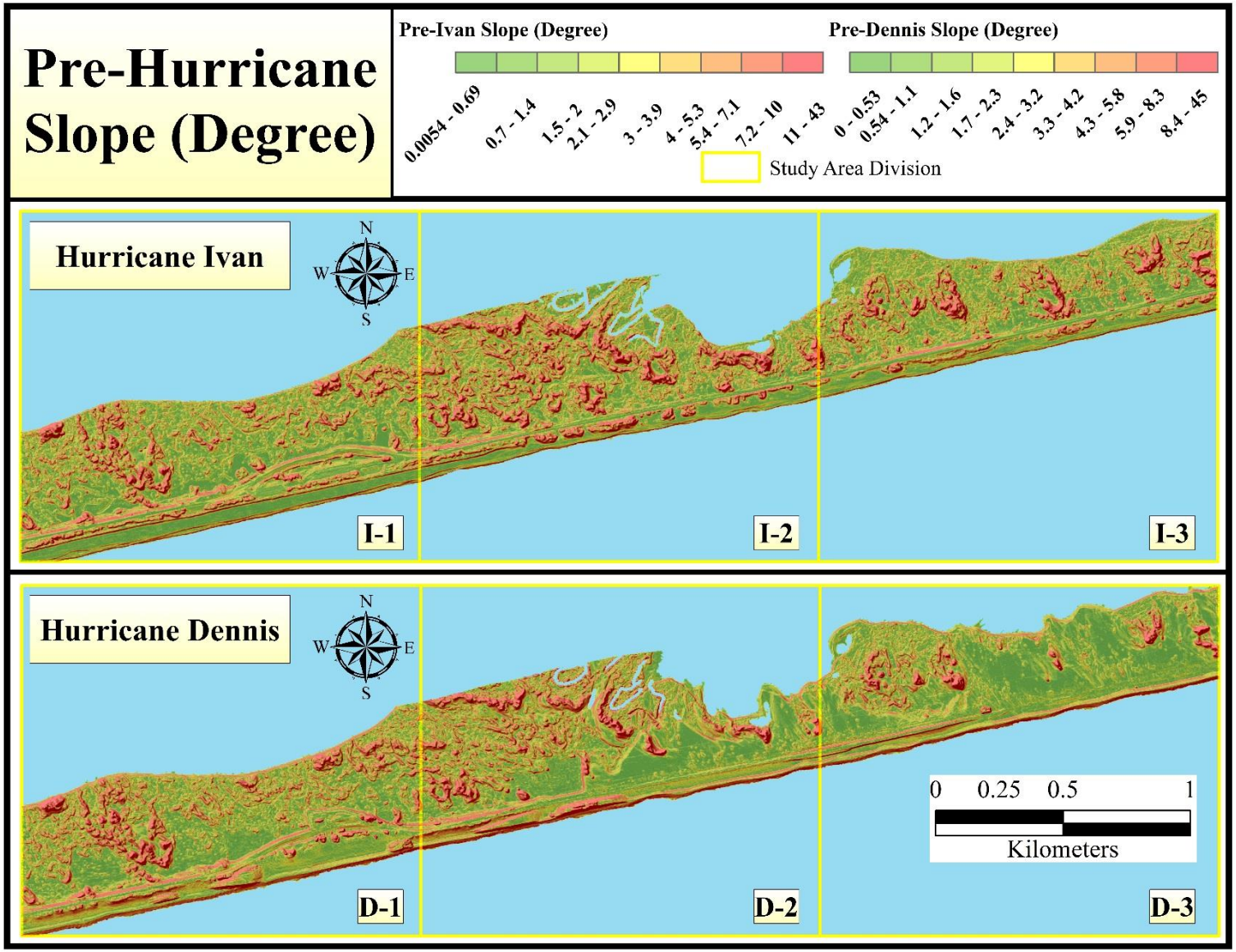

Figure 8 Pre-hurricane slope rasters were generated using DTM grid files, measured in degrees.

Aerial and satellite imageries acquired before each hurricane were used to generate vegetation coverage rasters and to digitize local roads into polygon shapefiles as shown in Figure 9. Using the ISO Cluster Unsupervised Classification tool from ArcGIS, an initial output classified raster was generated and later reclassified into (0, 1) classes, where 0 represents cells that are not vegetated, and 1 represents cells with vegetation. Two reclassified rasters were generated: one for vegetation cover prior to Hurricane Ivan, and another for vegetation cover prior to Hurricane Dennis.

Hourly observations of US local climatological data recorded from the Pensacola Regional Airport station were downloaded from the National Climatic Data Center (NCDC) (NOAA 2014a) to produce wind rose models. Several wind rose models were generated in different timeframes during Hurricane Ivan in Figure 10 and Hurricane Dennis in Figure 11. For each hurricane, the model represents wind speed in meters per second (m/s) and frequency during the day of hurricane landfall. The wind rose model displays the frequency distribution of occurrences of winds in each of the defined direction sectors and wind speed classes for the specified date, year, and time period. Each sector indicates that the frequencies shown are related to winds blowing from an angle, such as a 90-degree indicate wind blowing from the east.

Finally, historical records of tropical cyclone track were downloaded from NCDC (NOAA 2014b) in a shapefile format to display the track of both studied hurricanes as seen in Figure 5 and Figure 6, in addition to a larger extent view of historical tropical cyclone tracks passing within the northwest of Florida as seen in Figure 4.

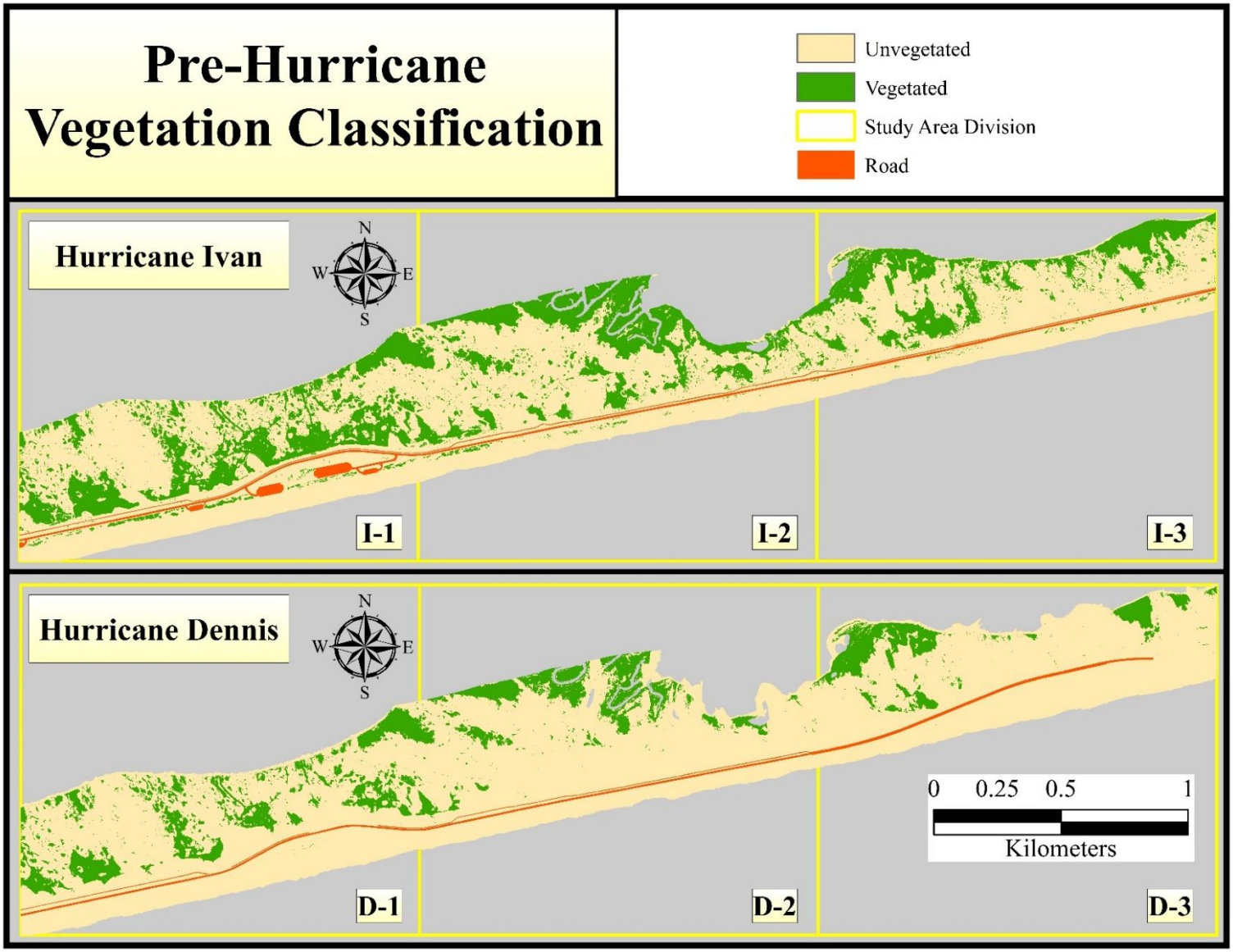

Figure 9 Pre-hurricane vegetation rasters were generated using ISO Cluster Unsupervised Classification tool, and cells were reclassified into two classes: (0) representing non-vegetated cells, and (1) representing completely vegetated cells.

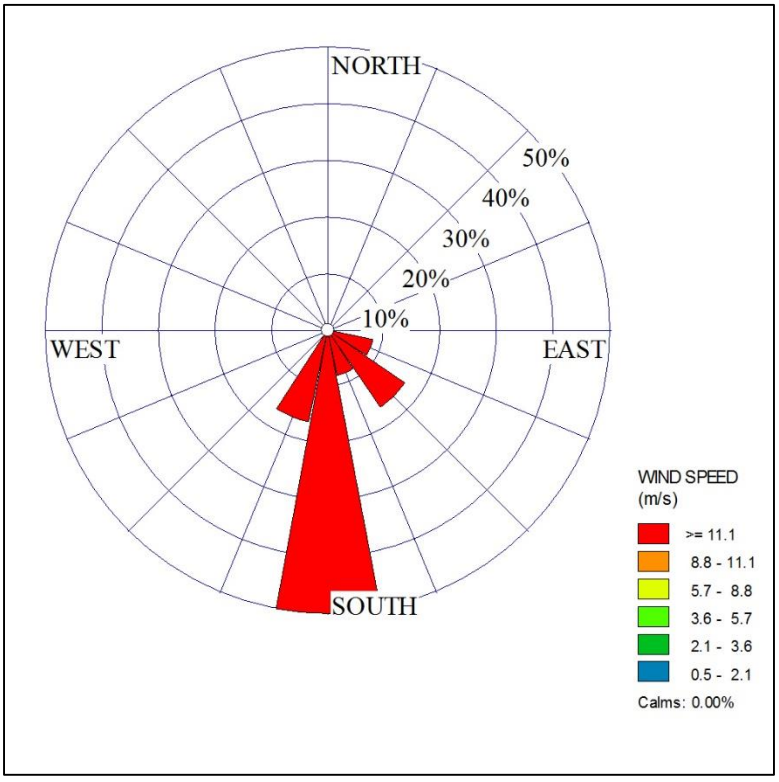

Figure 10 Hurricane Ivan wind rose in m/s during landfall starting on September 16, 2004, at 01:00 am, and ending on September 16, 2004 at 05:00 am.

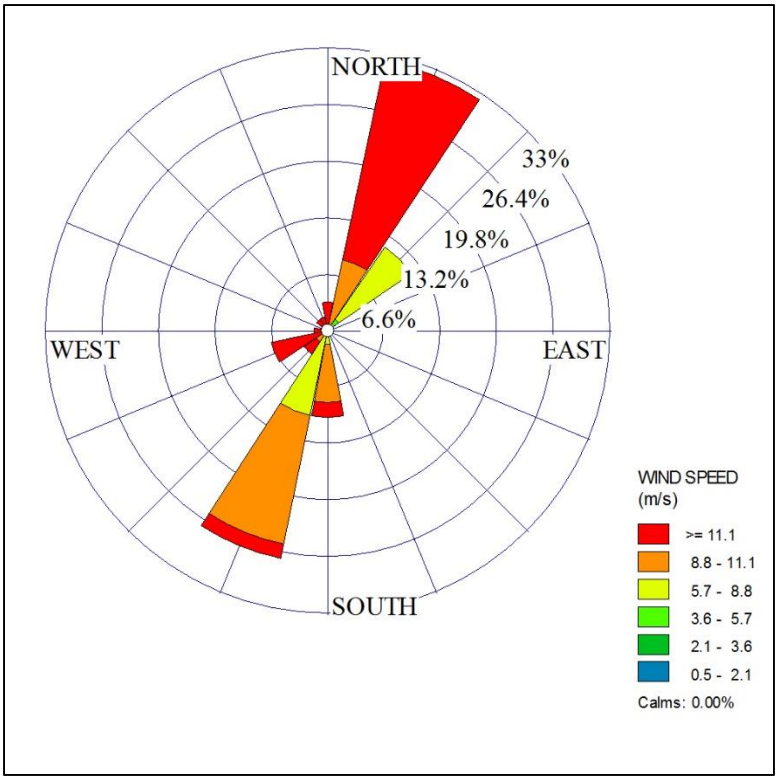

Figure 11 Hurricane Dennis wind rose in m/s during landfall starting on July 10, 2005, at 00:00 am, and ending on July 10, 2005 at 11:00 pm.

3.5 CMA Processes

In order to use the CMA tool, two sequential elevation DTMs were used within the same boundary extent, with the same map projection and datum, and the same spatial resolution for before an event and after an event. The processes applied here were done first for the Hurricane Ivan event and then for Hurricane Dennis.

A change map was initially generated from the two sequential DTM rasters using the Generate Change Map tool by subtracting the pre-hurricane raster from the post-hurricane raster as shown in the equation (Liu et al. 2010):

$$\Delta z_{ij} = z_{ij}^{post\ hurricane} - z_{ij}^{pre\ hurricane}$$

Where $z_{ij}^{post\ hurricane}$ and $z_{ij}^{pre\ hurricane}$ represent elevation values for cells (*i, j*), respectively, at the post-hurricane event, and the pre-hurricane event, and Δz_{ij} represents the elevation difference for the cells (*i, j*). As a result, a field-based elevation difference grid is generated as shown in Figure 12, and a change map is generated as shown in Figure 13.

Object filtering operations were performed by applying the Remove Small Objects tool to remove objects with number of grid cells less than 18 for the Hurricane Ivan change map, and 15 for Hurricane Dennis in order to avoid noisy objects. Fill operation was performed to connect and close small holes within the objects. The result map is shown in Figure 14.

Based on the generated filtered change map, objects were identified using the Identify Object tool, and a table was generated in which each object was delineated and recognized with a unique Object ID (OID) number, and a change status was set to categorize each object as either being an erosional or depositional object. A conversion tool was applied to convert the raster datasets into polygon shapefiles. Fields labeled “no change” were deleted from the map.

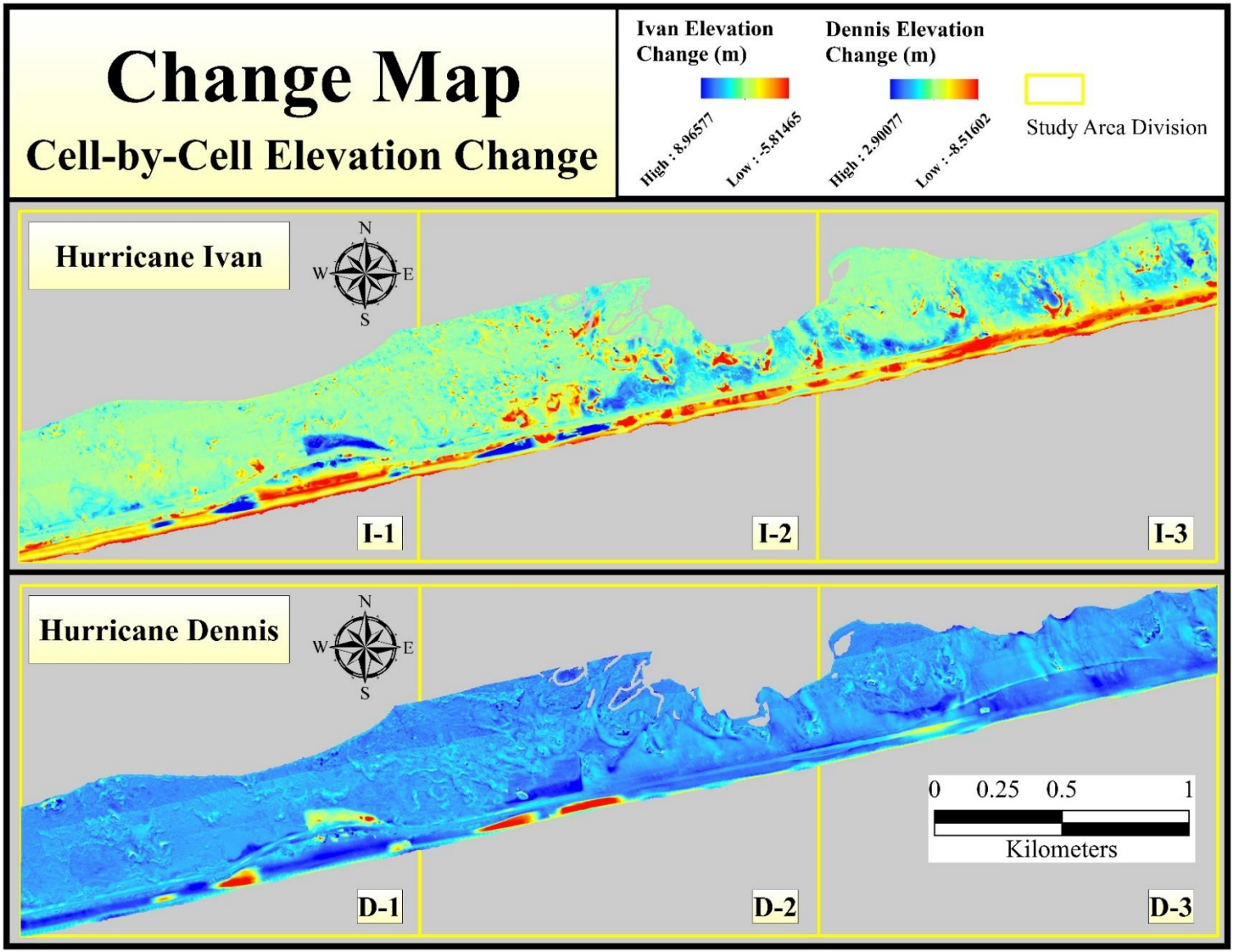

Figure 12 During the CMA process, a change map representing the field-based elevation difference grid was generated by subtracting the pre-hurricane raster from the post-hurricane raster, measured in meters.

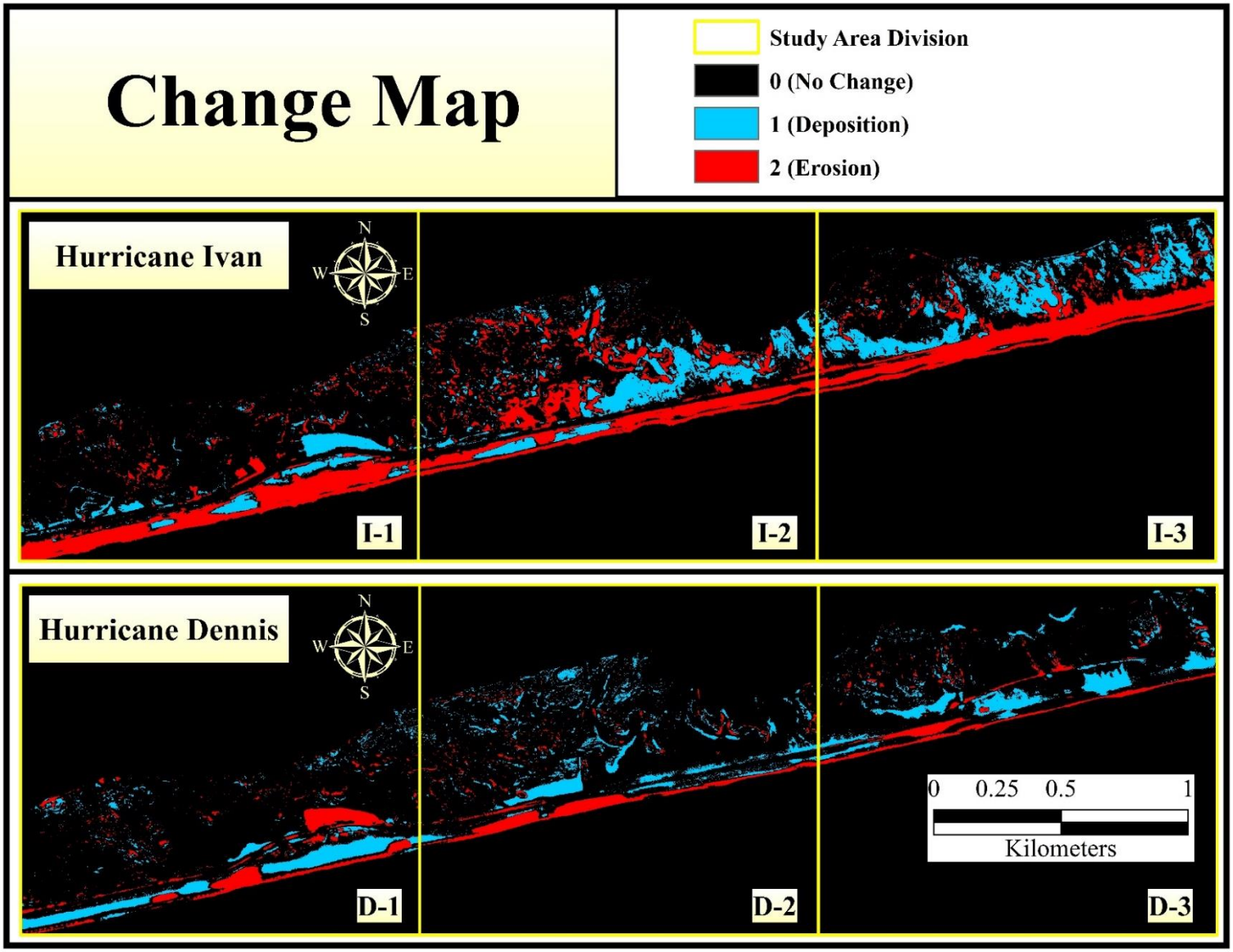

Figure 13 During the CMA process, a change map of all delineated objects was generated representing the object's status of erosional objects, depositional objects, or no change.

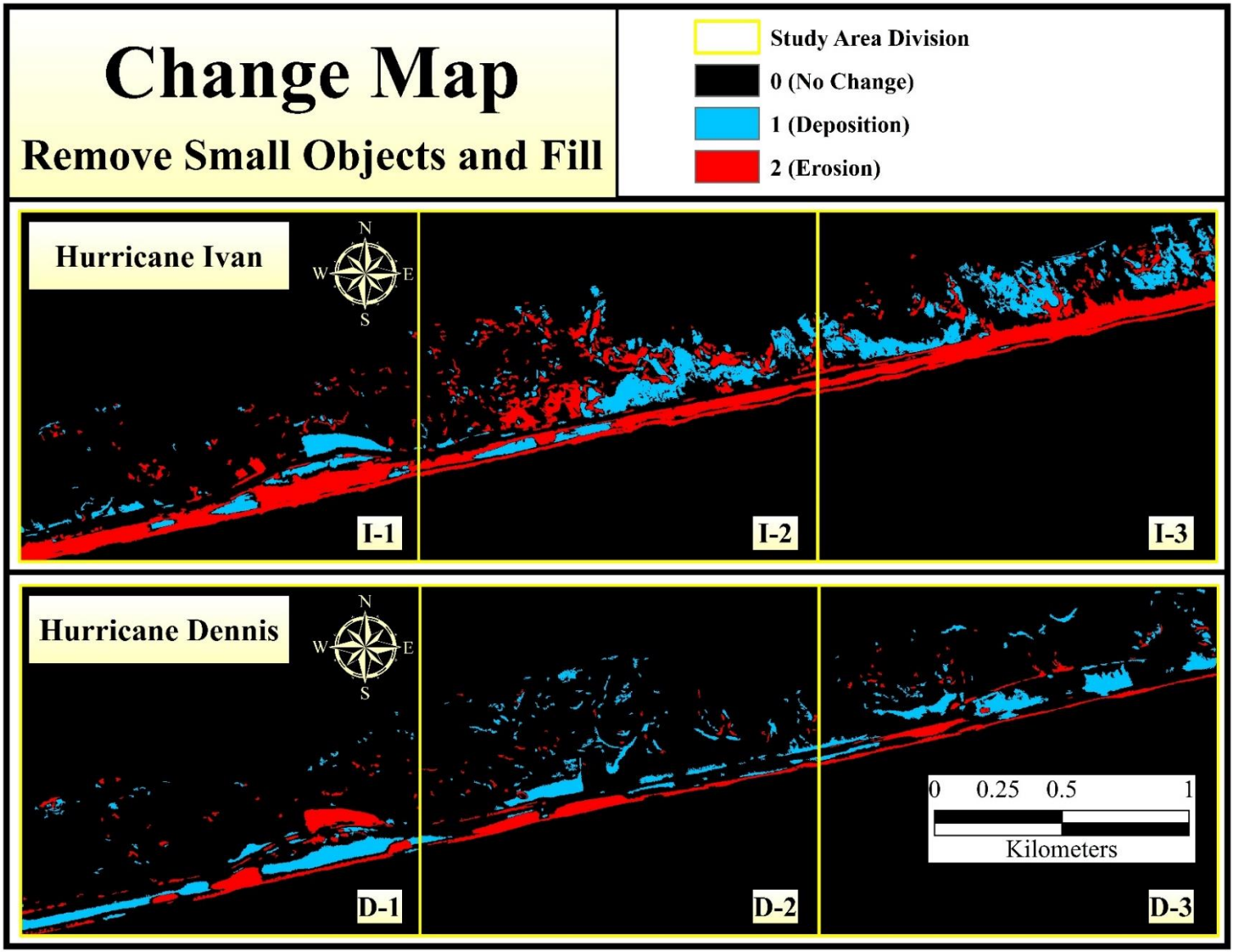

Figure 14 During the CMA process, object filtering was performed on the change map in order to remove small and noisy objects, and a fill operation was performed to connect and close small holes within the objects.

Sharp angles and edges of the objects were smoothed to enhance the cartographic quality. The output object map is shown in Figure 15. Another object map was generated by applying a quadrat segmentation to split the objects into smaller sizes as shown in Figure 16 in order to avoid outlier values during the linear regression analysis.

As a result, a set of attributes were computed within the segmented objects like planimetric, shape, volumetric, and surface attributes. In the process of generating planimetric and shape attributes, two bounding polygons are fitted to all objects: the minimum bounding rectangle polygon as shown in Figure 17, defined as the rectangle bound lines of the major and minor principle axis along the objects' centroid, comprising all object cells within it; and the best-fit ellipse polygons as shown in Figure 18, expressed using the objects' low-order central moments on all the cells within the object (Liu et al. 2010).

The planimetric attributes describe the objects' dimension and position and include the objects' centroid point coordinates (x_c, y_c), the perimeter, the area, and the minimum bounding rectangle length and width. The shape attributes explain the characteristics of the erosional and depositional objects, and in this research, the focus is on the following: compactness index *(CI)*, elongatedness *(ELG)*, asymmetry *(ASM)*, orientation *(∅)*, fractal dimension *(D)*, rectangularity *(REC)*, ellipticity *(ELP)*, and triangularity *(TRI)*. The compactness index *(CI)* explains the deviation of an object from a typical shape—which in this case is how far it deviates from a circular shape—but it does not explain the geometric form of an object (Wentz 2000). The object is described in circularity measure, where a circle is the most compact the shape can be assigned, with a value of 1.0. This means the greater the value of compactness index, the more compact and circular the shape is, whereas smaller values are less compact. Elongatedness *(ELG)* is explained by the length and width ratio within the minimum bounding rectangle of an object. The smallest

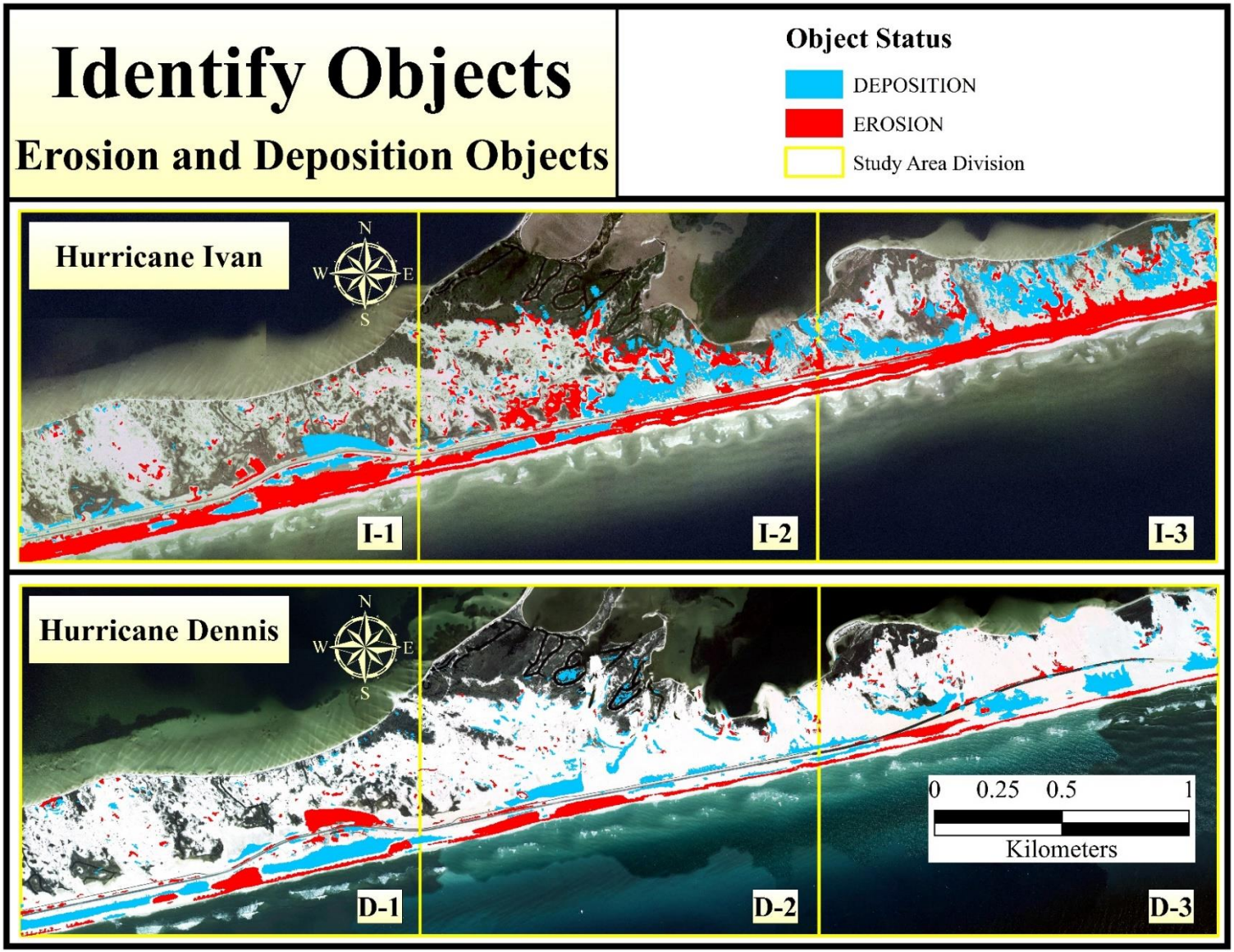

Figure 15 During the CMA process, objects were identified and delineated to be categorized as erosional and depositional objects, and each object was recognized with a unique OID.

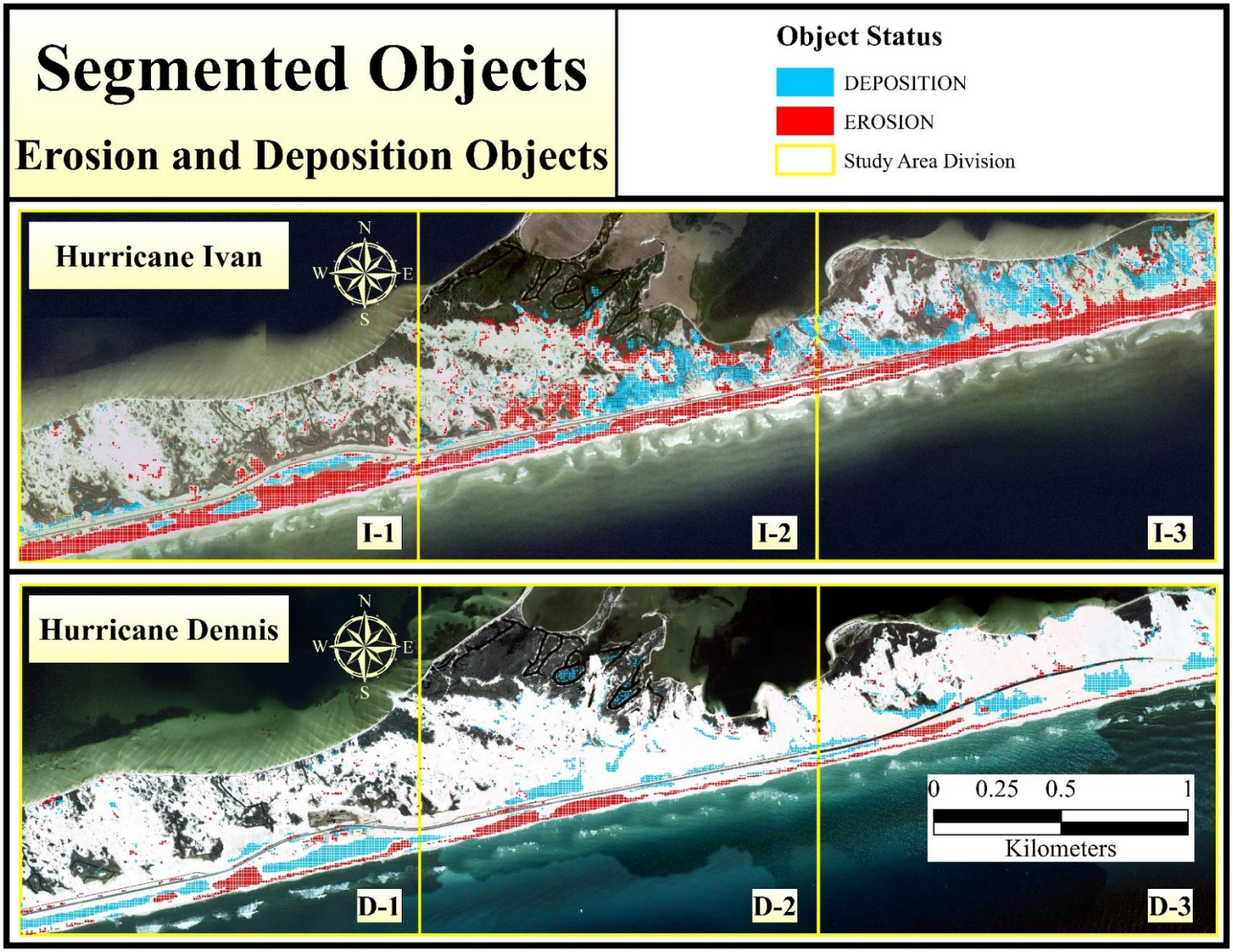

Figure 16 During the CMA process, an objects identification map was generated using the quadrat segmentation method in order to split objects into smaller sizes, and avoid outlier values during the regression analysis. Each object was recognized with a unique OID.

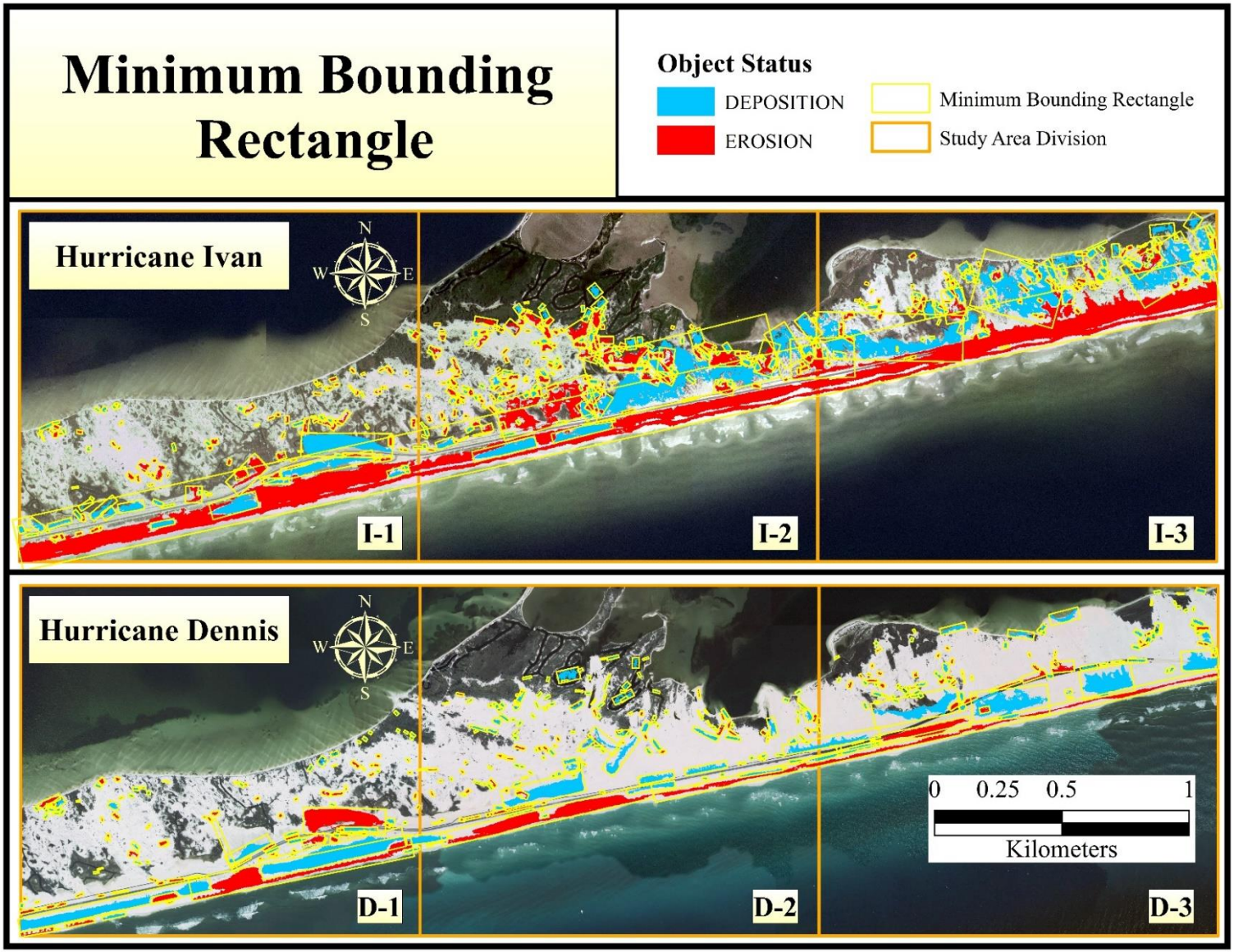

Figure 17 During the CMA process, a minimum bounding rectangle shapefile was generated representing the rectangle bound lines of the major and minor principle axis along the objects' centroid, and comprising all object cells within it.

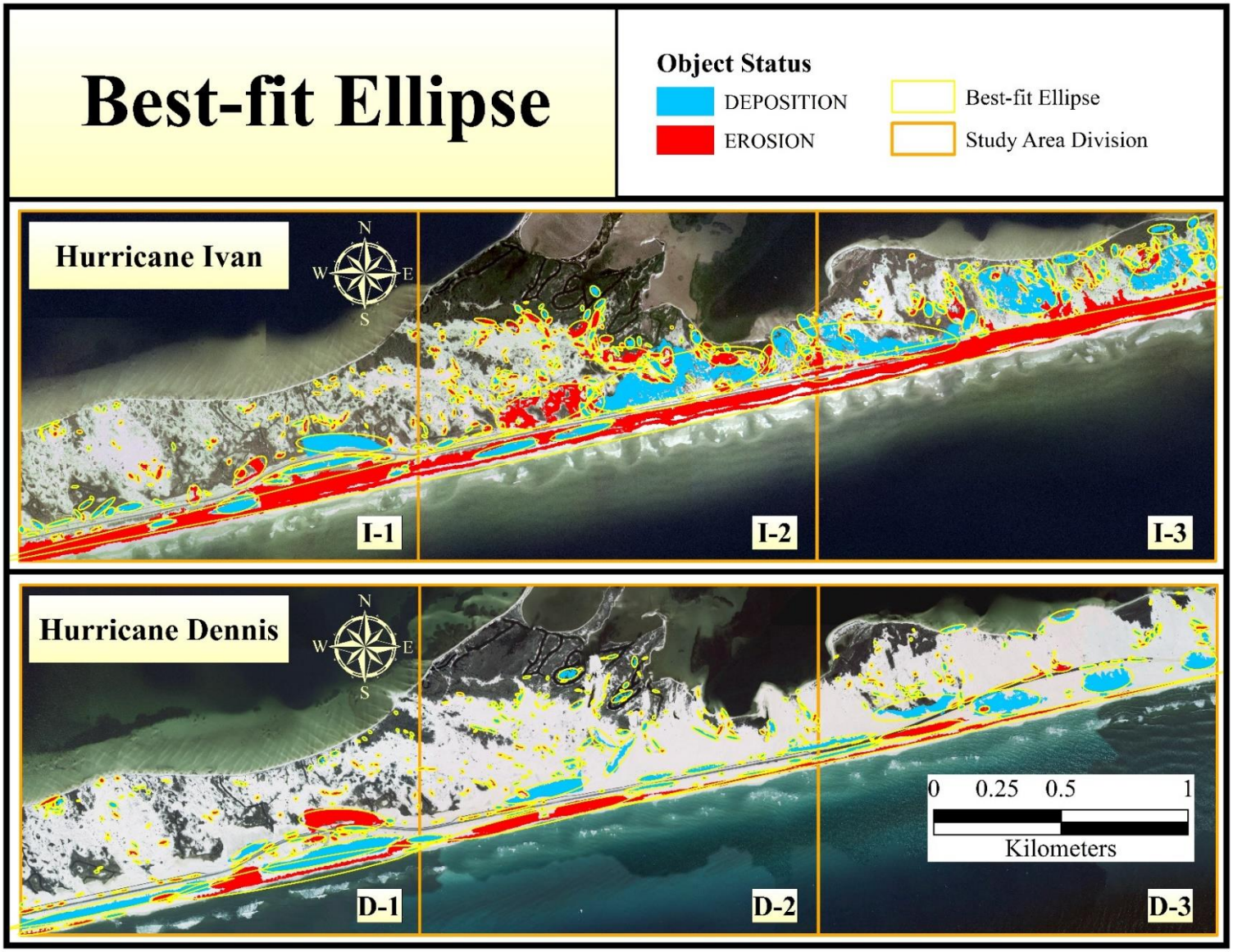

Figure 18 During the CMA process, a best-fit ellipse shapefile was generated using the objects' low-order central moments on all the cells within the object.

calculated value describes an object close to a circle or square shape with equal length and width, and as values get larger, the shape becomes more elongated. Asymmetry *(ASM)* can be expressed in terms of the object's major and minor axis ratio on the best-fit ellipse. Lengthier objects are described as having an asymmetrical shape. The value of 0 is the lowest asymmetry value and is found in circle and square shapes. Orientation *(Ø)* is the ellipse angle from the horizontal x-axis and the semi-major axis measured counterclockwise and ranging between 0º and 180º, shown in Figure 19.

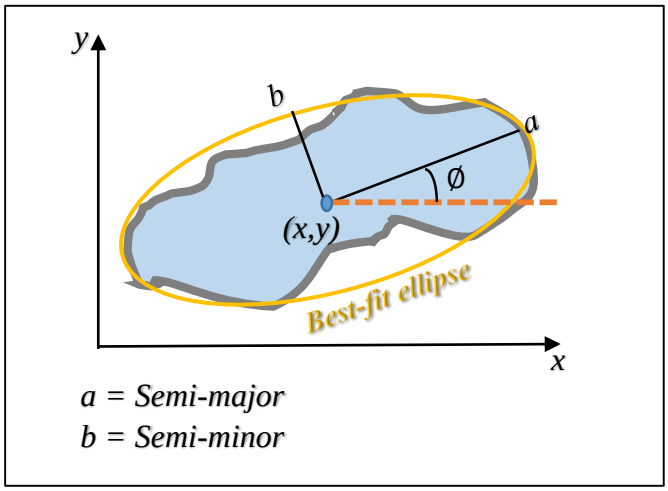

Figure 19 Orientation (Ø) parameters of *semi-major* (*a*), and *semi-minor* (*b*) within the best-fit ellipse. Redrawn from (Liu et al. 2010).

For better representation, the counterclockwise ranges were (1) flipped to a clockwise range of 0º to 180º and (2) converted to compass point and degrees in order to show object orientation direction as shown in Figure 20. For example, a value of 10º in the counterclockwise range would be flipped to a clockwise range to become 170º, and it would also be converted to a compass range to become 80º. Fractal dimension *(D)* explains the shape boundaries of an object in terms of its complexity or smoothness. Larger fractal dimensions indicate a more complex object boundary, while smaller values indicate smoother boundaries of the object. The ellipticity *(ELP)* is described in terms of a resemblance and likeness of an object to an ellipse shape whereas larger

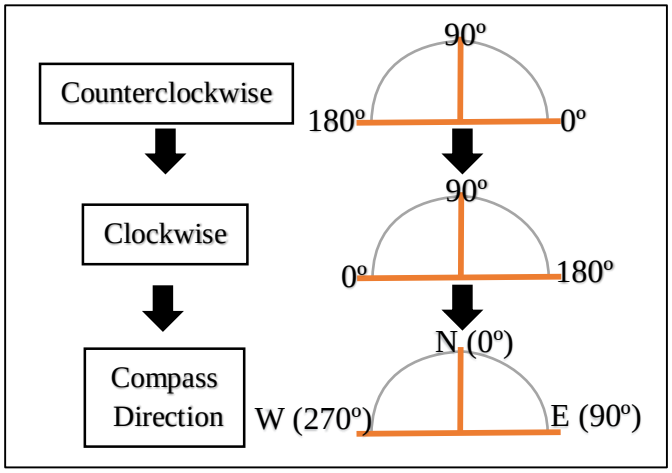

Figure 20 The counterclockwise range was converted to (1) clockwise ranging from 0º to 180º and (2) compass directions ranging from 270º to 90º.

values indicate greater similarity to the shape, and they range between 0 and 1.0. Refer to Appendix B for shape attribute equation definitions. The surface attribute explains three-dimensional morphological changes in the surface, and in this research the focus was on the mean elevation change measured in meters, the mean curvature change, and the mean slope change measured in percent rise. The mean change values are calculated by extracting the mean values of all cells within the object zones in both the pre-hurricane and the post-hurricane raster and then subtracting the pre-hurricane values from the post hurricane values. The volumetric attribute used in this research include the mean volume change measured in cubic meters and explains the sediment magnitude change (Liu et al. 2010).

3.6 Zonal Statistics as Table

The Zonal Statistics as Table tool was used to calculate statistical values of a raster within the zones of another raster and to return the results as a table. The segmented objects' maps were used as an input rater to provide a boundary zone in each erosional or depositional patch. For the input value rasters, different sets of rasters were performed. (1) Mean vegetation values: the results were in a range of values between 0.0 and 1.0 to show the mean percentage of vegetation cover

within each zone. For example, a value of 0.6 means that 60% vegetation cover resides within one zone. (2) Mean slope values: the results calculate the average of slope degree values within each zone. (3) Mean elevation values: the result calculates the average of elevation values in meters within each zone.

3.7 Ordinary Least Square

Researchers have a common interest in finding the relationship between one variable and several other variables. It is more accurate to measure and identify patterns statistically rather than just looking at the pattern on a map. The term "regression analysis" is a statistical method commonly used to investigate such relationships by discovering the relationship between the dependent variable—or response variable—denoted by *y*, and the independent variable—or explanatory variable or predictor variable—denoted by *x*. Linear regression is a statistical technique and requires that the model is linear in regression parameters (Yan and Su 2009).

Multiple linear regression analysis was applied to understand the relationship between the coastal morphological elevation changes impacted by a hurricane and the factors that may have contributed to the changes, including: vegetation, slope, and elevation. A commonly used form of linear regression is the "least squares fitting." Linear least squares fitting is a mathematical technique used to find the best-fitting straight line that goes through a set of points (Weisstein 2013). Accordingly, the ordinary least square (OLS) regression tool provided in ESRI ArcGIS performs a global linear regression and is used to generate predictions about the relationship, and to produce output feature class and tables with coefficient information and diagnostics (ESRI 2013a). This tool is convenient to provide an initial foundation by providing a global model of the spatial regression analyses. The formula is expressed as followed:

$$Elevatoion\ Change\ (y) = \beta_0 + \beta_1\ Vegetation + \beta_2\ Slope + \beta_3\ Elevation + \varepsilon$$

where y is the dependent variable, $(\beta_0, \beta_1, \beta_2, \beta_3)$ are regression coefficients, $(Vegetation, Slope, Elevation)$ are independent variables in the model, and ε is the random error.

3.8 Classification and Regression Tree

The classification and regression tree (CART) is a data analysis tool that applies a recursive partitioning process to the data in which it splits the data stage-wise into smaller and smaller sections, and the output framework is shown in an inverted tree diagram (Berk 2008). This method is used in order to determine the independent variables most important to the predictions of the dependent variable (Everitt 2002). The decision tree has several sections starting from the root node, in which displays the overall sample observation; a subset of nodes; and finally the terminal nodes or leaf nodes, which are characterized as homogenous nodes in terms of the dependent variable. The tree framework is structured with a set of sequential questions about the feature, starting from the root node, which are answered in several nodes until reaching the final terminal node where a prediction is made. In this research, this technique was conducted through the IBM SPSS software using a growing method called "CRT", which also stands for classification and regression tree.

Chapter 4 Coastal Morphology Analysis

4.1 Introduction

The object-based, hurricane-induced morphological change analysis was applied to both hurricanes. The first section discusses planimetric and volumetric results found following each hurricane. Next, the surface attributes are presented. Subsequently, the shape attribute results following each hurricane are presented. Next, a wind flow and object orientation relationship is discussed. Consequently, the spatial distributions of morphological changes are discussed. Finally, the discussion and conclusions are presented.

4.2 Post-Hurricane Planimetric and Volumetric Attributes

Following Hurricane Ivan, a set of erosional and depositional patches were detected within the study area, comprising a total of 481 objects, from which 274 objects were erosional and 207 were depositional, as shown in Figure 21 section (A). After Hurricane Dennis, a set of erosional and depositional patches were identified within the study area, comprising a total of 428 objects, from which 169 object were erosional and 259 were depositional, as shown in Figure 21 section (B). This indicates a vast change from Hurricane Ivan recorded objects as the total count of objects declined from 481 to 428 objects, a decrease of 11%. Erosional patches decreased greatly in total count from 247 following Hurricane Ivan to 169 following Hurricane Dennis, a decrease of about 32%, while depositional patches increased by around 25% from Hurricane Ivan to Hurricane Dennis. Moreover, post-Hurricane Ivan the total erosional patches exceeded the total depositional patches, while during Hurricane Dennis a reverse count was noticed where the depositional patches were greater in total than the erosional patches.

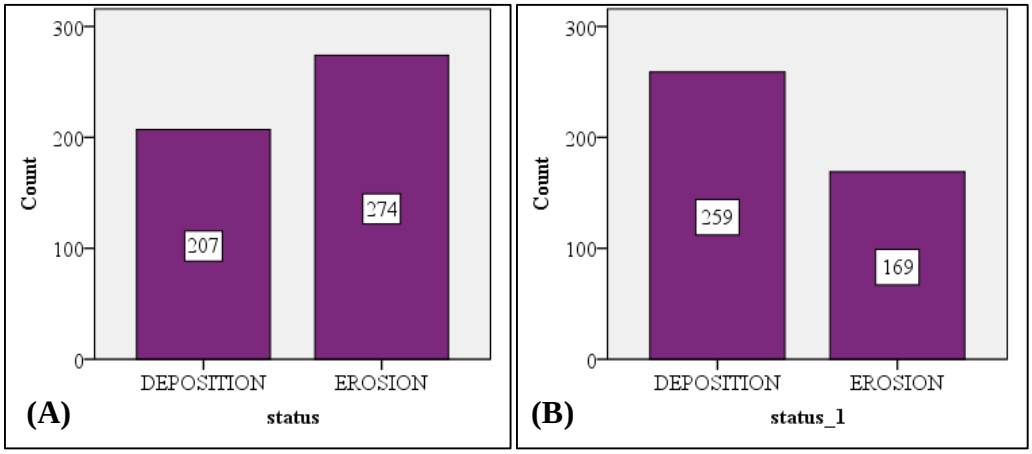

Figure 21 Erosional and depositional objects: (A) Post-Ivan and (B) Post-Dennis.

Table 3 shows the descriptive statistics of objects in both hurricanes. The total area size of the objects after Hurricane Ivan reached 679,116 m^2, ranging from an enormous object with an area of 295,708 m^2 to the smallest object with an area of 72 m^2, resulting in a mean value of 1,411.9 m^2. The results were positively skewed where the majority of objects were distributed within the range of smaller area sizes, as shown in Figure 22 section (A), and 151 objects peaked between 100 to 199 m^2. The total erosional area sizes reached 422,120 m^2, while the total depositional area sizes reached 256,996 m^2. Mean length was 27.9 m, ranging from 5.7 m to 2,992.9 m, while the mean width was 9 m, ranging from 1.9 m to 99.3 m. Following Hurricane Dennis, the objects' total area size reached 316,664 m^2, decreasing by 53% in size from Hurricane Ivan, ranging from a maximum value of 26,880 m^2 to a minimum value of 60 m^2, and having a mean value of 739.9 m^2. Most objects fell within a range of smaller area-sized objects, as shown in Figure 22 section (B), where 156 objects peaked between 0 and 99 m^2. The total erosional area sizes reached 132,868 m^2, while the total depositional area sizes reached 183,796 m^2. The objects' mean length was 26 m and ranged from 5.1 m to 1,292.8 m, while the mean width was 6.6 m and ranged from 2.5 m to 48.6 m.

Following Hurricane Ivan the total erosional volume change reached -508,938.2 m^3, ranging from the minimum value of -380,124 m^3 to the maximum value of -39.4 m^3, and the total

deposition volume change reached 225,771.4 m^3, ranging from the minimum value of 35.3 m^3 to the maximum value of 37,031.4 m^3, as shown in Table 3 and Figure 23 sections (A) and (B). The total sediment volume change reached about -283,166.7 m^3. After Hurricane Dennis, the total erosional volume change reached -170,927.2 m^3, a decrease in volume loss by around 66% from Hurricane Ivan, ranging from the minimum value of -59,931.7 m^3 to the maximum value of -28.5 m^3, and the total deposition volume change reached 118,477.7 m^3, a decrease in total volume deposit by around 48% from Hurricane Ivan, ranging from the minimum values of 26.8 m^3 to the maximum value of 18,822.2 m^3, as shown in Table 3 and Figure 23 sections (C) and (D). The total sediment volume change reached about -52,449.5 m^3.

Table 3 A Descriptive table representing planimetric attributes of area in (m^2), length in (m), and width in (m), and volumetric attribute of volume change in (m^3).

		Area (m^2)	Length (m)	Width (m)	Volume Change (m^3)
Post-Hurricane Ivan					
N	Valid	481	481	481	481
	Missing	0	0	0	0
Mean		1,411.9	27.9	9	-588.7
Median		184	13.7	6.1	-52.8
Std. Deviation		13,853.3	139	10	17,619.6
Variance		191,912,968.8	19,312.4	100.9	310,450,017.1
Skewness		20.2	20.4	5.2	-20.9
Std. Error of Skewness		0.1	0.1	0.1	0.1
Range		295,636	2,987.2	97.4	417,155.4
Minimum		72	5.7	1.9	-380,124.0
Maximum		295,708	2,992.9	99.3	37,031.4
Sum		679,116	13,435.3	4,336.9	-283,166.7
Post-Hurricane Dennis					
N	Valid	428	428	428	428
	Missing	0	0	0	0
Mean		739.9	26	6.6	-122.5
Median		124	11.6	5.3	36.5
Std. Deviation		3,015.6	77.3	5.6	3,962.7
Variance		9,094,111.3	5,973.8	31.8	15,702,769.4
Skewness		6.6	11.9	4.6	-9.8
Std. Error of Skewness		0.1	0.1	0.1	0.1
Range		26,820	1,287.6	46.1	78,753.9
Minimum		60	5.1	2.5	-59,931.7
Maximum		26,880	1,292.8	48.6	18,822.2
Sum		316,664	11,147.2	2,842.6	-52,449.5

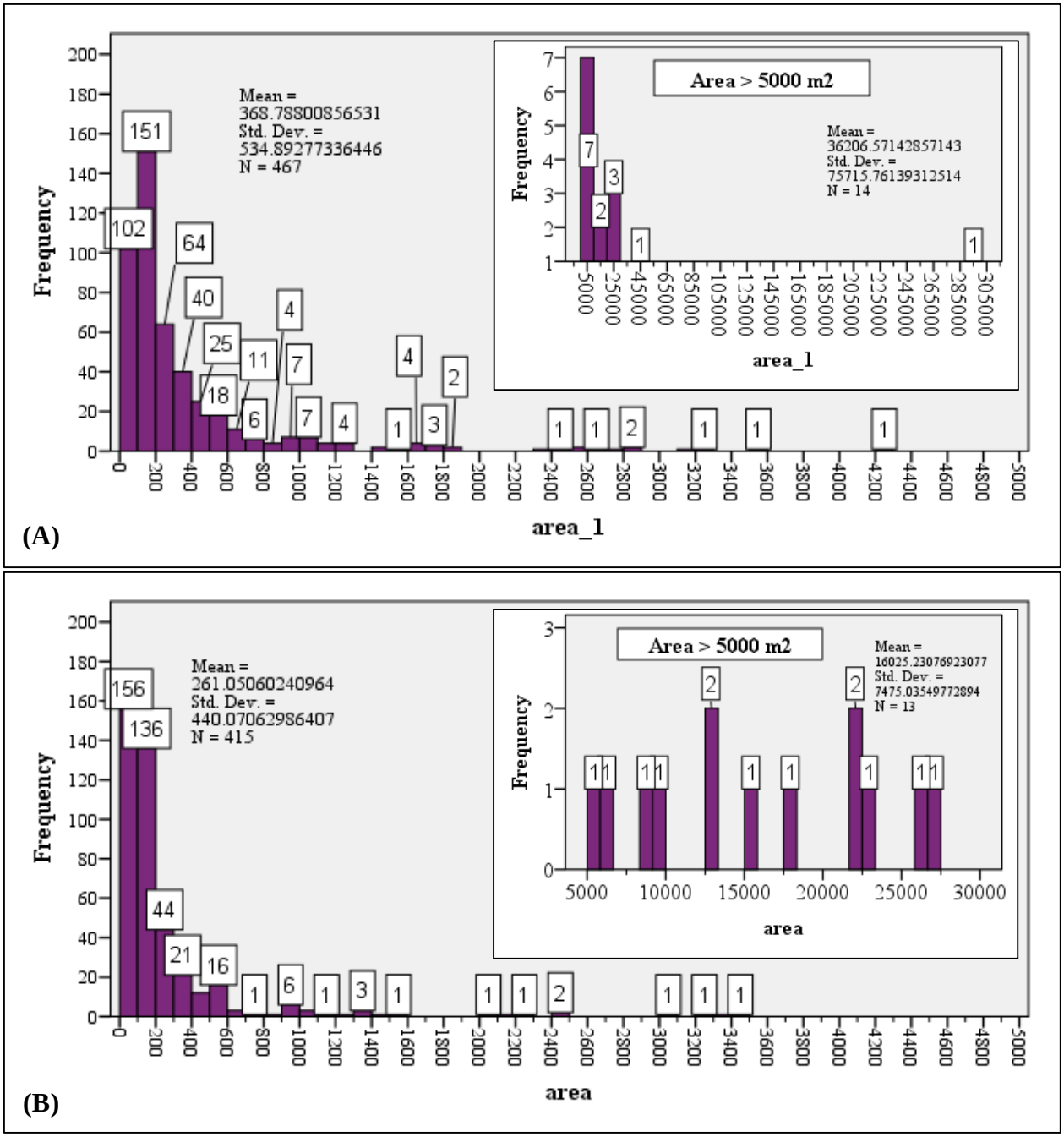

Figure 22 Objects' area size in (m^2): (A) Post-Hurricane Ivan and (B) Post-Hurricane Dennis. Smaller inner histogram represents area values > 5000 m^2.

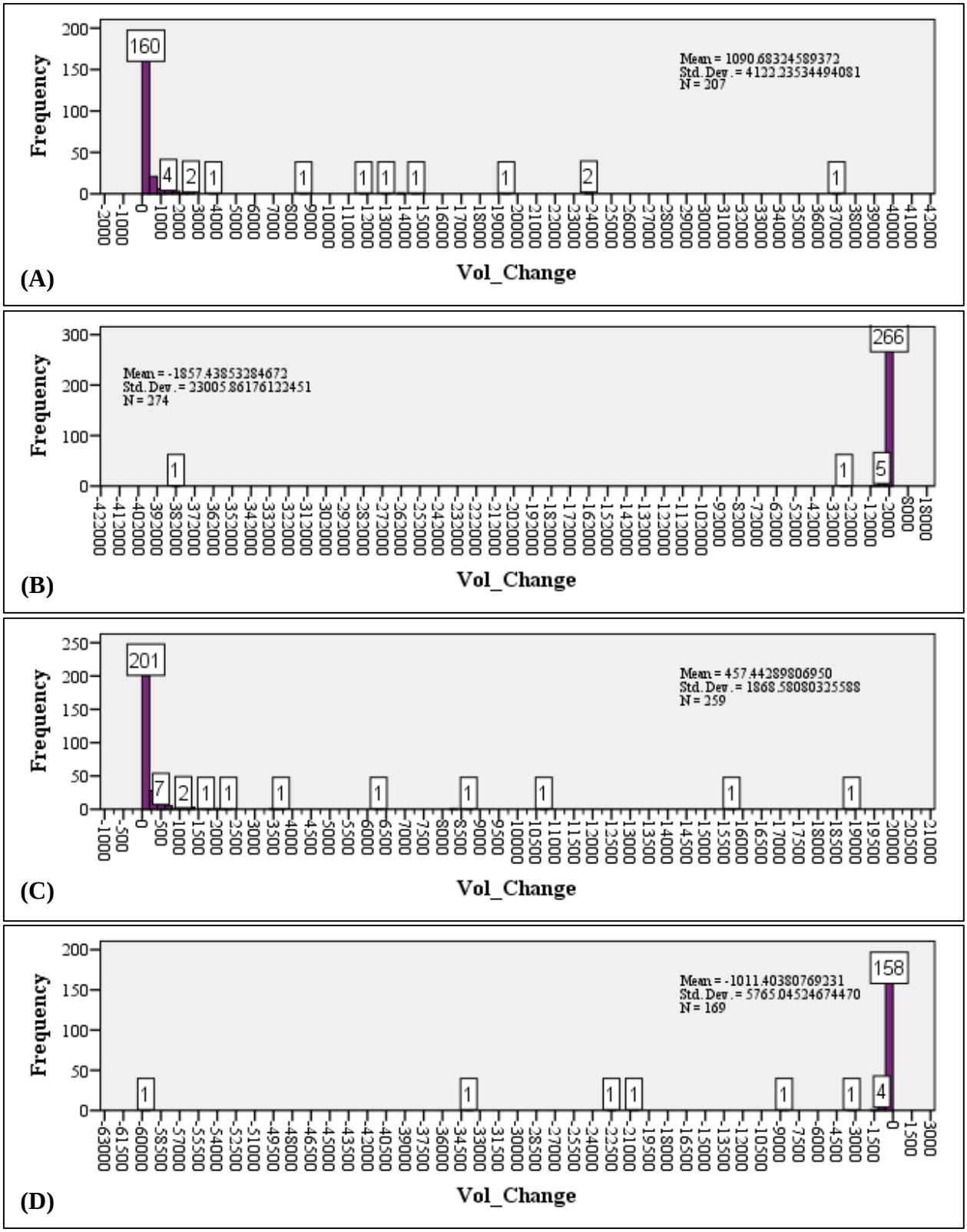

Figure 23 Post-Hurricane Ivan volume change in (m^3): (A) Deposition and (B) Erosion; and Post-Hurricane Dennis volume change in (m^3): (C) Deposition and (D) Erosion.

4.3 Post-Hurricane Surface Attributes

Table 4 shows the descriptive statistics of the objects' surface attributes after each hurricane. Post-Hurricane Ivan, the mean elevation change in each object ranged from the minimum values of -1.8 m to the maximum values of 2 m, with a mean of -0.2 m, as shown in Figure 24 section (A). The majority of erosional mean elevation changes peaked between -0.7 m and -0.6 m with a total of 74 objects, while 73 depositional objects were between 0.5 m and 0.6 m. Following Hurricane Dennis, the mean elevation change ranged from -2.3 m to 1.5 m, with a mean of 0.1 m, as shown in Figure 24 section (B). The peak of erosional mean elevation change ranged between -0.6 m and -0.5 m and consisted of 55 objects, while the depositional mean elevation change peaked between 0.4 m to 0.5 m and consisted of a total of 98 objects. When comparing the two events, it seems that following Hurricane Ivan more erosional objects suffered from an incline in the mean elevation change, especially between -0.9 m and -0.6 m, while there was a greater increase in the mean elevation change noticed in depositional objects following Hurricane Dennis, ex. 0.4 m and 0.6 m.

The mean curvature change is a surface attribute term used to explain the surface curvature in morphological changes as a result of coastal processes, and it is explained in term of convexity or concavity in the surface. Objects with negative difference values indicate having a more concave surface, while positive differences indicate a more convex surface. Following Hurricane Ivan, the mean curvature change had a mean of -2.5 and ranged from the minimum value of -27.2 to the maximum value of 10.9, as shown in Table 4. 56.6% of objects were characterized as having a concave surface, as shown in Figure 25 section (A), from which 98.2% objects were erosional and the remaining 1.8% were depositional. The other 43.5% of objects had a convex surface, from which 3.4% were erosional objects and 96.7% were depositional objects. Following Hurricane

Dennis, the mean curvature change had a mean of 0.3 and ranged from the minimum value of -27.6 to the maximum value of 22.1, as shown in Table 4. The mean curvature change in 39.5% of objects became more concave, as shown in Figure 25 section (B), from which all were erosional objects. The other 60.5% of objects became more convex, from which all were depositional objects. Between these two hurricanes, a repetitive pattern in morphodynamic changes can be determined following major storms, where most erosional patches tend to have concave patterns in their surface, whereas depositional patches tend to have convex patterns.

Table 4 A Descriptive table representing surface attributes of mean elevation change in (m), mean curvature change, and mean slope change in (% rise).

		Mean Elevation Change (m)	Mean Curvature Change	Mean Slope Change (% Rise)
Post-Hurricane Ivan				
N	Valid	481	481	481
	Missing	0	0	0
Mean		-0.2	-2.5	-2.8
Median		-0.6	-2.7	-2.1
Std. Deviation		0.7	6.7	3.6
Variance		0.6	45.2	13.3
Skewness		0.3	-0.4	-0.7
Std. Error of Skewness		0.1	0.1	0.1
Range		3.8	38.1	29.0
Minimum		-1.8	-27.2	-18.1
Maximum		2.0	10.9	11.0
Sum		-86.1	-1,180.4	-1,326.1
Post-Hurricane Dennis				
N	Valid	428	428	428
	Missing	0	0	0
Mean		0.1	0.3	-0.4
Median		0.5	2.6	-0.4
Std. Deviation		0.6	8.7	2.4
Variance		0.4	76.1	5.6
Skewness		-0.5	-0.5	0.3
Std. Error of Skewness		0.1	0.1	0.1
Range		3.8	49.8	26.5
Minimum		-2.3	-27.6	-14.0
Maximum		1.5	22.1	12.5
Sum		39.9	133.5	-151.9

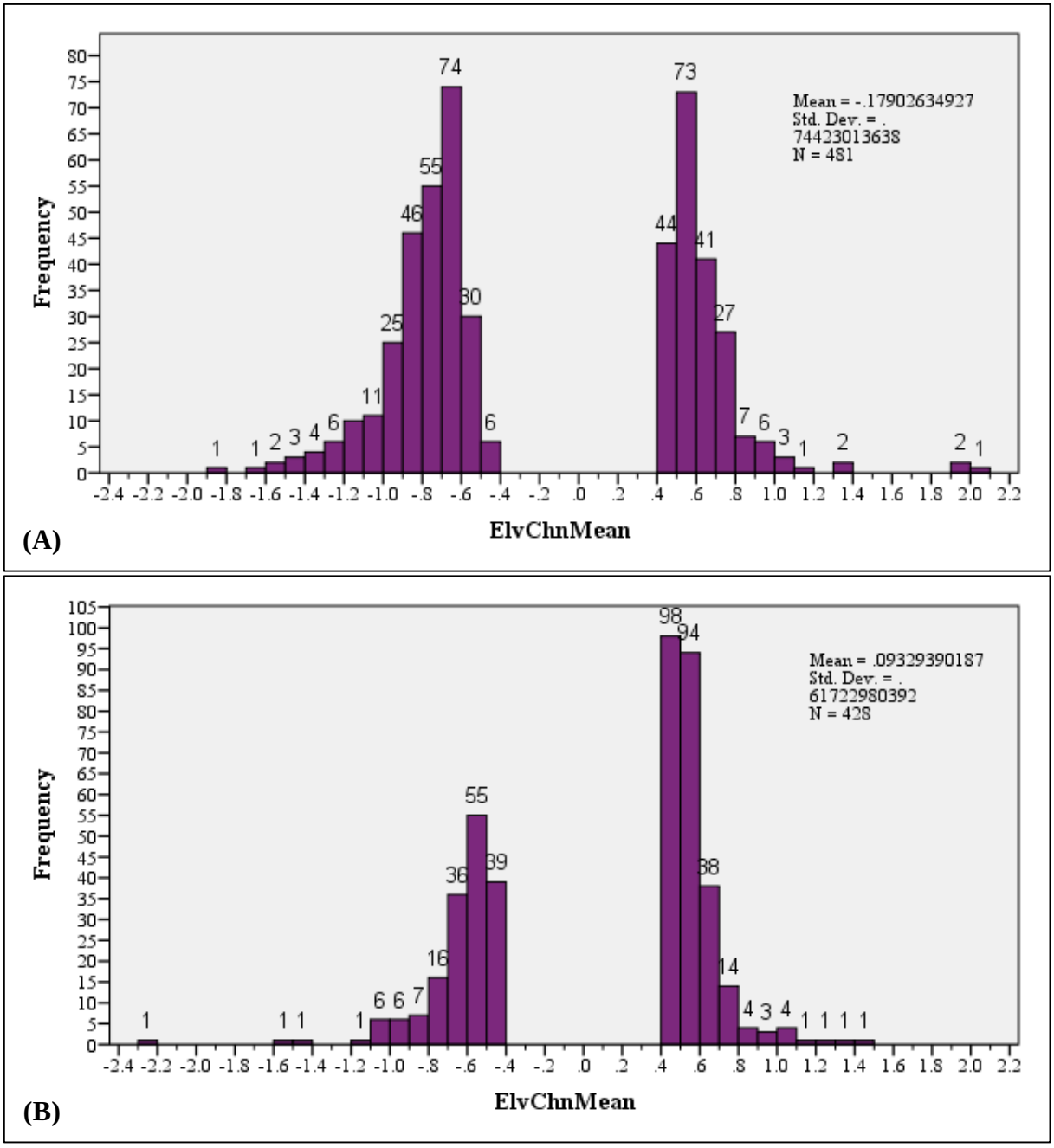

Figure 24 The mean elevation change in (m): (A) Post-Hurricane Ivan and (B) Post-Hurricane Dennis. All interval within the negative values represent erosional objects, and all intervals within positive values represent depositional objects.

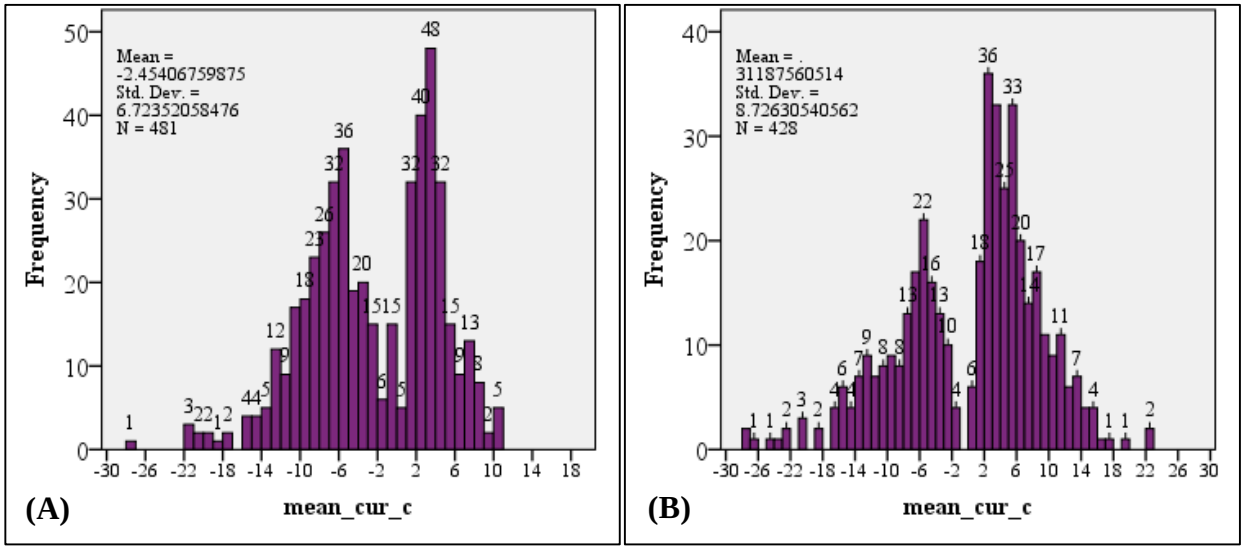

Figure 25 The mean curvature change: (A) Post-Hurricane Ivan and (B) Post-Hurricane Dennis Objects with negative difference values indicate more concave surface, while positive differences indicate a more convex surface.

The mean slope change measures the change in surface gradient in percent rise. Objects with a negative difference value indicate a flatter or less steep surface, while a positive difference represents a steeper surface. Following Hurricane Ivan, 83.4% of the objects turned into flatter surfaces with less steep gradients, as shown in Figure 26 section (A), from which 62.1% of objects were erosional and 37.9% were depositional. The other 16.6% of objects grew steeper, where 31.3% of objects were erosional and 68.8% were depositional. The mean value was -2.8% and ranged between -18.1% and 11%, as shown in Table 4. After Hurricane Dennis, 67.8% of objects became flatter surfaces, as shown in Figure 26 section (B), from which 35.5% were erosional objects and the remaining 64.5% were depositional objects. The other 32.2% objects became steeper surfaces, from which 47.8% were erosional objects and 52.2% were depositional objects. The mean value was -0.4% and ranged between -14% and 12.5%, as shown in Table 4. In both hurricanes, a similar pattern in changes is noticed, where the majority of landforms tended to flatten following a major storm.

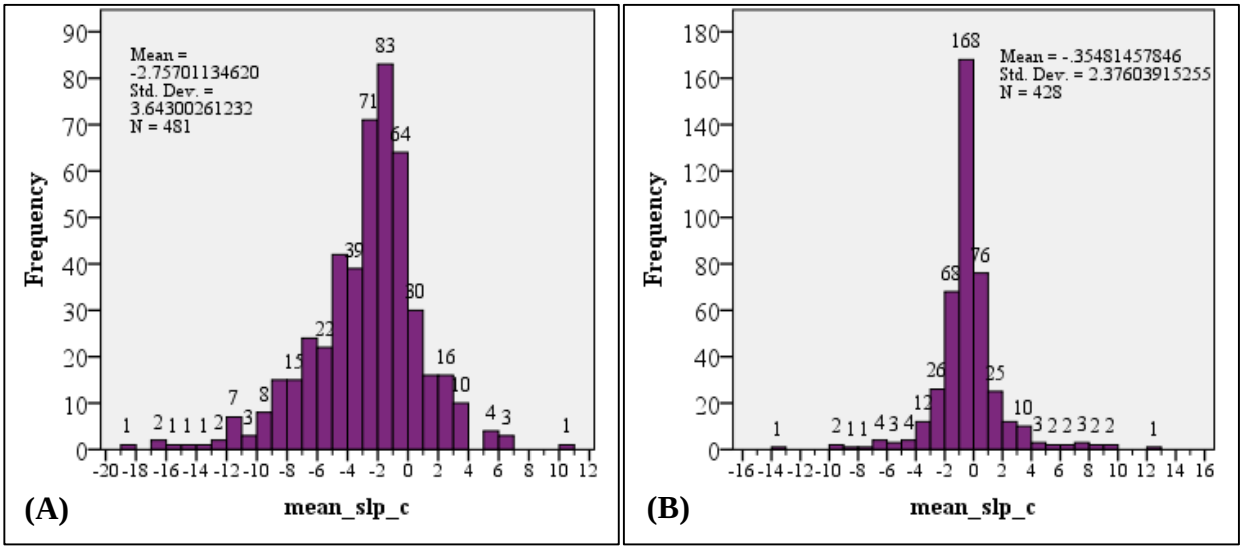

Figure 26 The mean slope change in (% rise): (A) Post-Hurricane Ivan and (B) Post- Hurricane Dennis. Negative differences show flatter surfaces, while the positive show steeper surfaces.

4.4 Post-Hurricane Shape Attributes

Since there are different possibilities to describe geomorphological objects' shape after a storm occurs, a set of numerous shape types were explored in order to provide a complete descriptive analysis. Table 5 show the descriptive statistics of all shape attributes studied in this research.

For the compactness index (*CI*) attribute, the distribution was slightly positively skewed, as shown in Figure 27 section (A), following Hurricane Ivan. The values ranged between 0.01 and 0.66, with a mean of 0.27. The majority of objects were distributed in smaller value intervals, with a peak between 0.25 and 0.29, and most objects clustered between 0.10 and 0.39. These values represent smaller compactness index values, indicating that objects do not have a compactness characteristic and that the majority tend to have irregular shapes. Following Hurricane Dennis, the pattern was consistent with the previous hurricane in having positively skewed distribution in the graph; the majority of values distributed in smaller intervals between 0.1 and 0.34, and the peak was from 0.20 and 0.24, as shown in Figure 27 section (B). The values ranged between 0.01 and 0.63, with a mean of 0.26.

Table 5 Descriptive table of shape attributes.

Post-Hurricane Ivan									
	N	Range	Min.	Max.	Mean	Std. Deviation	Variance	Skewness	
	Statistic	Statistic	Statistic	Statistic	Statistic	Statistic	Statistic	Statistic	Std. Error
CI	481	0.66	0.01	0.66	0.27	0.13	0.02	0.42	0.11
ELG	481	52.00	1.03	53.03	2.62	2.79	7.80	12.90	0.11
ASM	481	0.95	0.03	0.98	0.51	0.20	0.04	-0.19	0.11
D	481	0.40	1.00	1.40	1.05	0.08	0.01	1.80	0.11
ELP	481	0.89	0.08	0.98	0.53	0.18	0.03	0.01	0.11
∅	481	179.67	0.00	179.67	89.07	57.34	3,287.47	0.18	0.11
Valid N (listwise)	481								
Post-Hurricane Dennis									
	N	Range	Min.	Max.	Mean	Std. Deviation	Variance	Skewness	
	Statistic	Statistic	Statistic	Statistic	Statistic	Statistic	Statistic	Statistic	Std. Error
CI	428	0.62	0.01	0.63	0.26	0.12	0.01	0.53	0.12
ELG	428	109.87	1.02	110.90	3.27	5.74	32.90	15.80	0.12
ASM	428	0.97	0.02	0.99	0.56	0.20	0.04	-0.22	0.12
D	428	0.32	1.00	1.32	1.04	0.07	0.01	1.73	0.12
ELP	428	0.93	0.05	0.98	0.51	0.18	0.03	0.07	0.12
∅	428	179.62	0.00	179.62	94.56	64.34	4,140.07	-0.07	0.12
Valid N (listwise)	428								

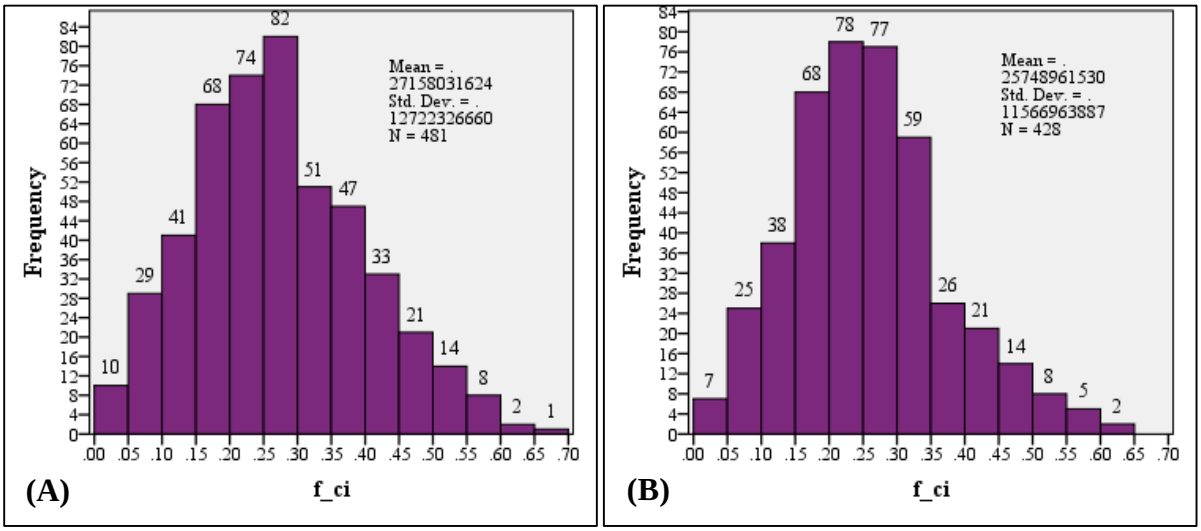

Figure 27 Compactness index (*CI*): (A) Post-Hurricane Ivan and (B) Post-Hurricane Dennis. Greater values mean more compact and circular object, and smaller values show less compact.

In the case of the elongatedness (*ELG*) attribute, the graph was highly positively skewed following Hurricane Ivan, as shown in Figure 28 section (A). The majority of objects were distributed in smaller elongatedness values between 0 and 3.99; there was a peak between 0 and 1.99, explaining that objects have a smaller elongatedness type of a shape, with an exception in one outlier object with a large value of 53, making a large gap in the graph. The values ranged between 1.03 and 53.03 and had a mean of 2.62. A similar pattern was noticed following Hurricane Dennis, where most objects distributed in smaller values, with a peak between 0 and 4.99; one exception was an object with a large value of 111, as shown in Figure 28 section (B) and in Table 5. The mean value was 3.27 and ranged between 1.02 and 110.90. The difference between the two hurricanes is that the range value became larger—52 post-Hurricane Ivan and 109 post-Hurricane Dennis—because the outlier object after the second hurricane had a larger elongatedness value of about 111.

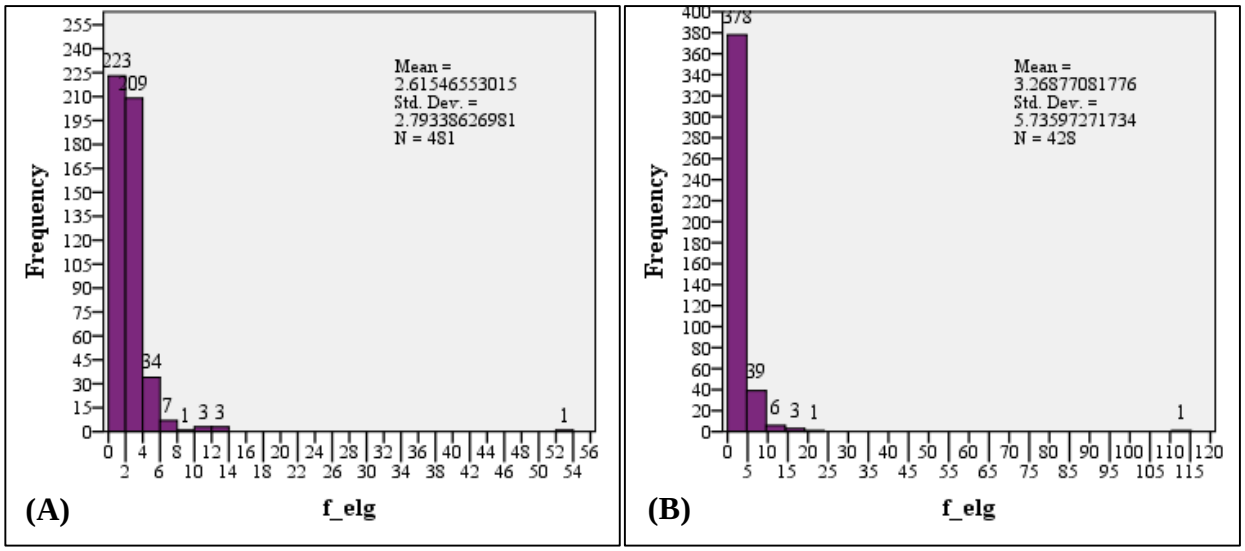

Figure 28 Elongatedness (*ELG*): (A) Post-Hurricane Ivan and (B) Post-Hurricane Dennis. Greater values show more elongated shape, and smaller values show more circle or square shape.

For the asymmetric (*ASM*) attribute, the majority of objects had a normal distribution post-Hurricane Ivan, as shown in Figure 29 section (A), and had a peak between 0.55 and 0.59. The values ranged between a minimum of 0.03 and a maximum of 0.98 and had a mean of 0.51. In

Figure 29 section (B), Post-Hurricane Dennis also showed a reasonably normal distribution in the graph and had a peak between 0.6 and 0.64. The values ranged from the minimum of 0.02 to a maximum of 0.99 and had a mean of 0.56. This shows that most objects in both hurricanes had an asymmetrical type of shape. Storm surge height and the maximum wave heights can trim and erode objects to a more asymmetric shape along the coast.

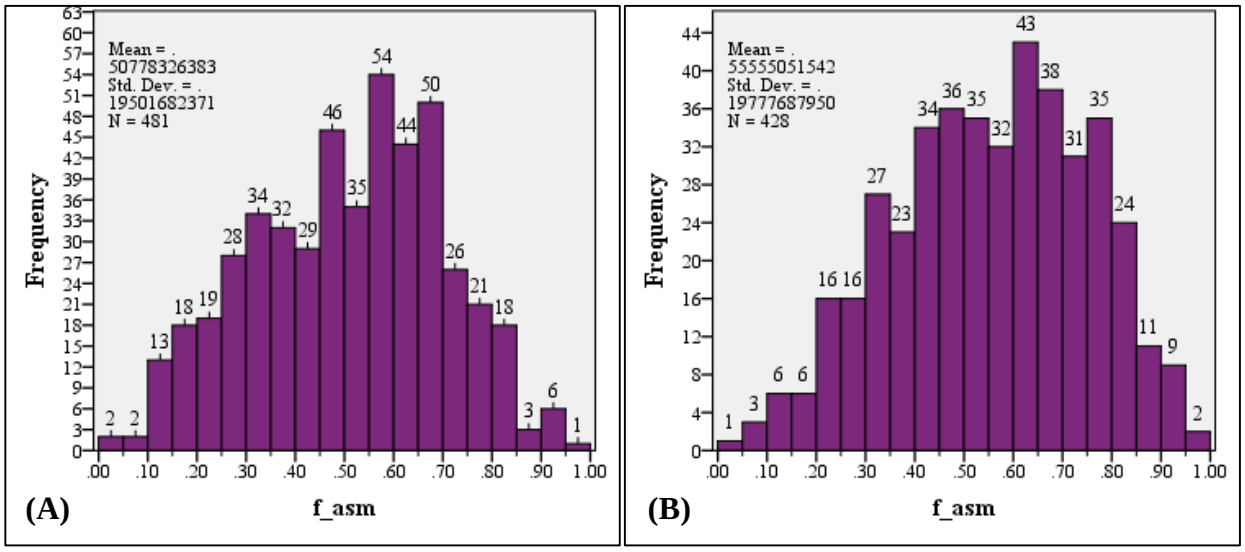

Figure 29 Asymmetric (*ASM*): (A) Post-Hurricane Ivan and (B) Post-Hurricane Dennis. Greater values show more asymmetrical shape, and smaller values show more symmetrical shapes of circle or square.

In the case of the fractal dimension (*D*) attribute, the values ranged between 1 and 1.4 and had a mean of 1.05 after Hurricane Ivan, as shown in Table 5. Figure 30 section (A) shows a positively skewed spread where the majority of objects were distributed within smaller values and peaked between 1 and 1.02. After Hurricane Dennis, the same pattern was seen with a positively skewed distribution where most objects had smaller values, peaking between 1 and 1.02, as shown in Figure 30 section (B). The values ranged between 1 and 1.32 and had a mean of 1.04. In both hurricanes a consistent pattern was noticed where the majority of objects had a smooth boundary shape.

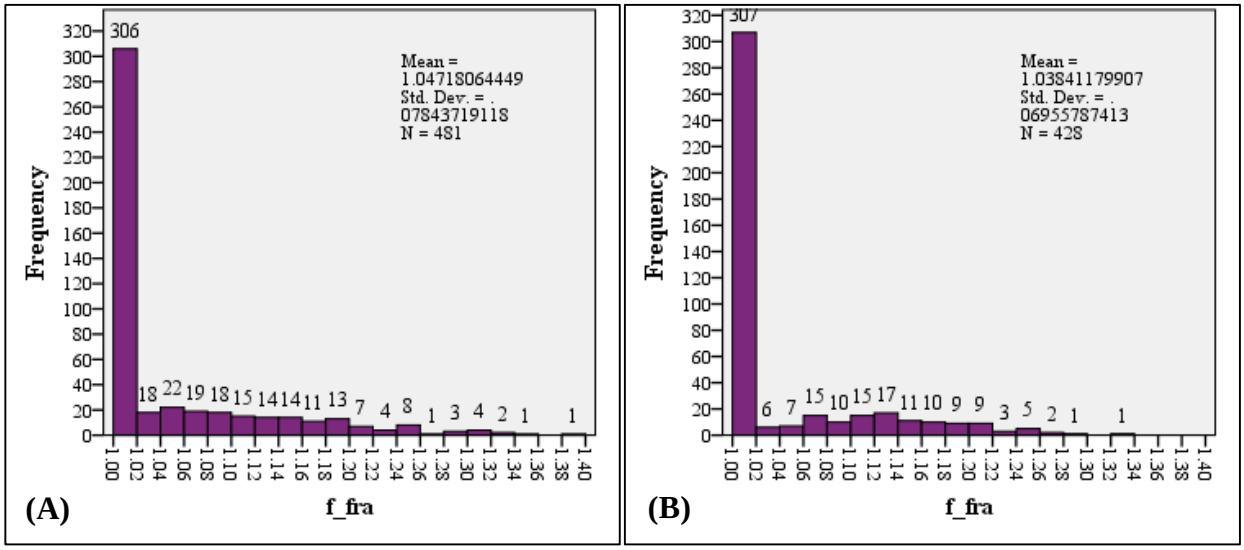

Figure 30 Fractal dimension (*D*): (A) Post-Hurricane Ivan and (B) Post-Hurricane Dennis. Greater values show more complex boundaries, and smaller values show smoother boundaries.

For the ellipticity (*ELP*) attribute, the attributes ranged from 0.08 to 0.98 and had a mean of 0.53 following Hurricane Ivan, as shown in Table 5. The graph had a normal distribution, as shown in Figure 31 section (A). Post-Hurricane Dennis the values ranged from 0.05 to 0.98, with a mean of 0.51. Objects had a normal distribution, as shown in Figure 31 section (A). Objects tended to have greater similarity in shape, though not completely.

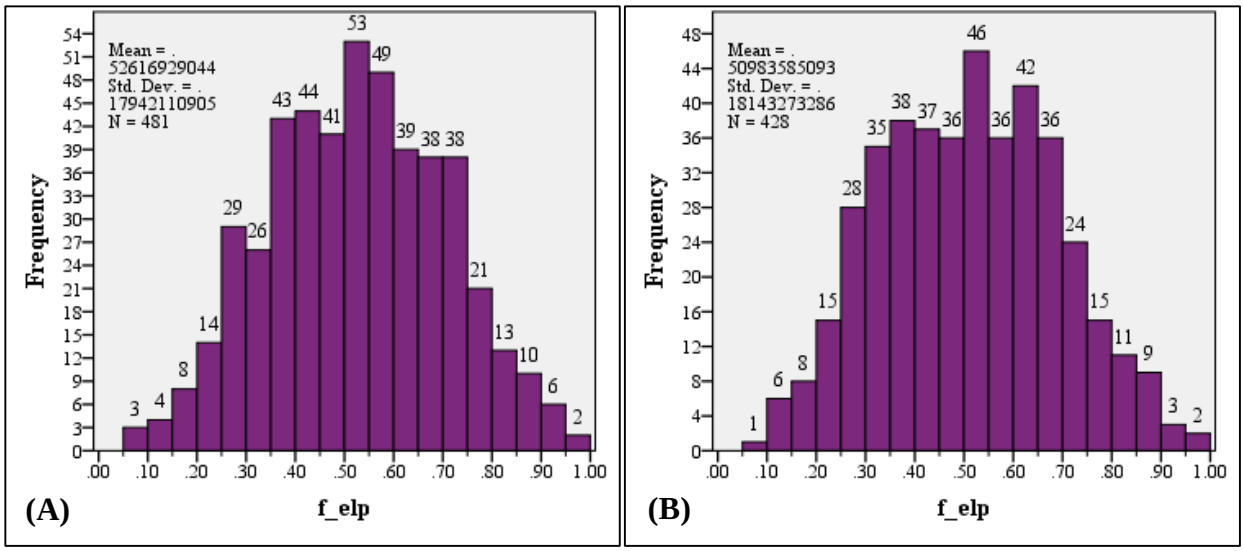

Figure 31 Ellipticity (*ELP*): (A) Post-Hurricane Ivan and (B) Post-Hurricane Dennis. Greater values show more similarity to the ellipse shape, and smaller values show less similarity.

4.5 Post-Hurricane Object Orientation and Wind Flow Relationship

In the case of the clockwise object orientation *(Ø)* attributes, the object' angle of degree ranged from 0º to 179.7º—with a mean of 89.1º—following Hurricane Ivan, as shown in Table 5. A peak of orientation directions ranged between 170º and 180º, as shown in Figure 32 section (A). After Hurricane Dennis the objects' orientation focused more at greater degrees and peaked between 160º and 169º. The values ranged between 0º and 179.6º and had a mean of 94.6º, as shown in Figure 32 section (B).

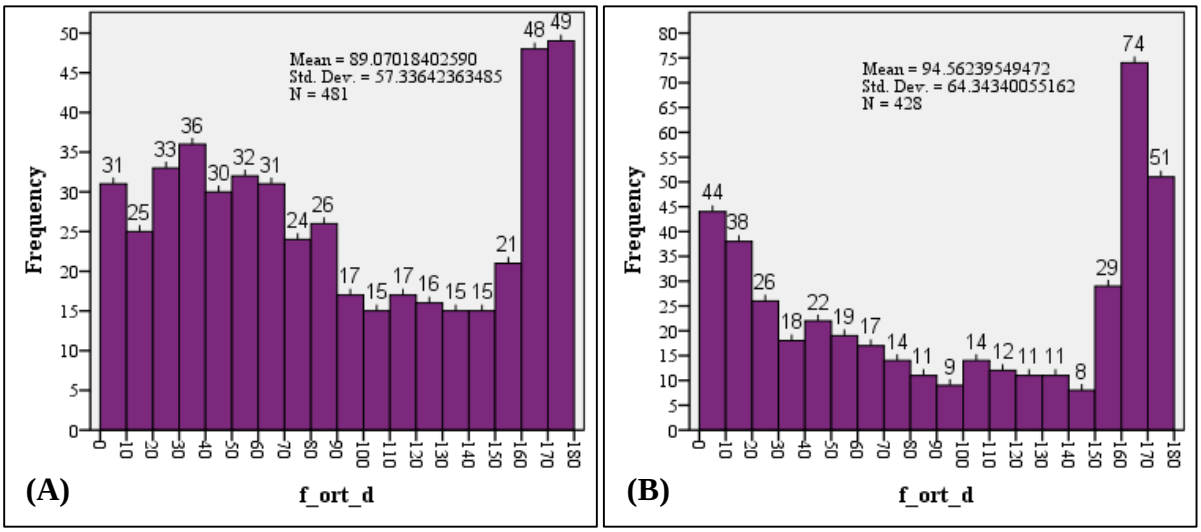

Figure 32 Clockwise object orientation (Ø): (A) Post-Hurricane Ivan and (B) Post-Hurricane Dennis.

An object orientation rose model was generated following each hurricane, representing both erosional orientation and depositional orientation, and subsequently overlaid with the wind rose model from Figure 10 and Figure 11 in order to give a better representation of objects' orientation direction from true north, and to find wind flow contribution in the objects' orientation, as shown in Figure 33 and Figure 34. Each sector of the object orientation rose displays the frequency percentage of occurrence within each compass point, where larger sectors indicate greater occurrence within a compass point. The directions were classified into nine classes, as shown in Table 6 displaying the compass point, degree range, and object frequency percentage

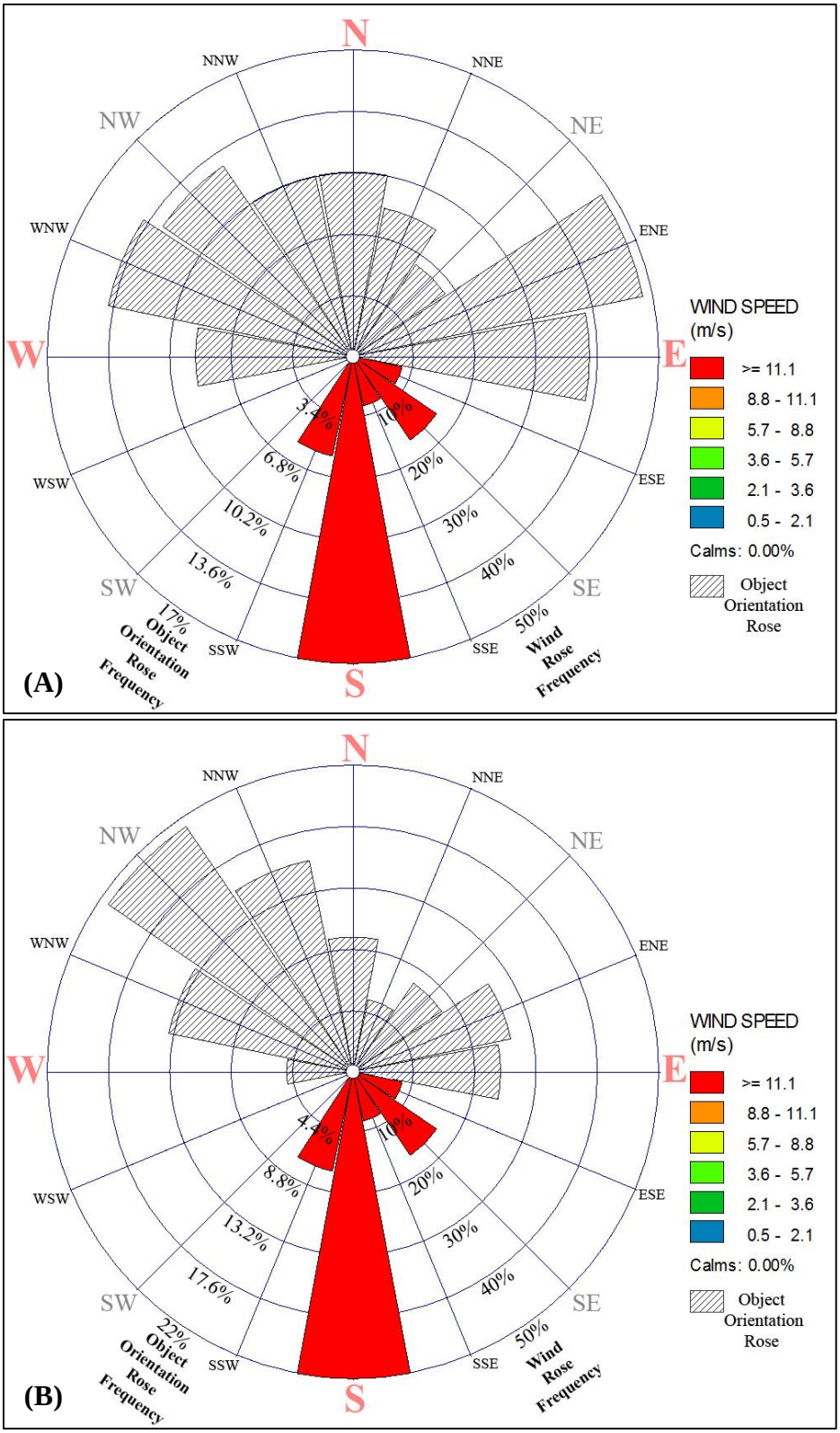

Figure 33 A model of overlaying wind rose during Hurricane Ivan landfall starting on September 16, 2004, at 01:00 am, and ending on September 16, 2004 at 05:00 am, and object orientation rose post-Hurricane Ivan displayed as A) erosional objects and B) depositional objects.

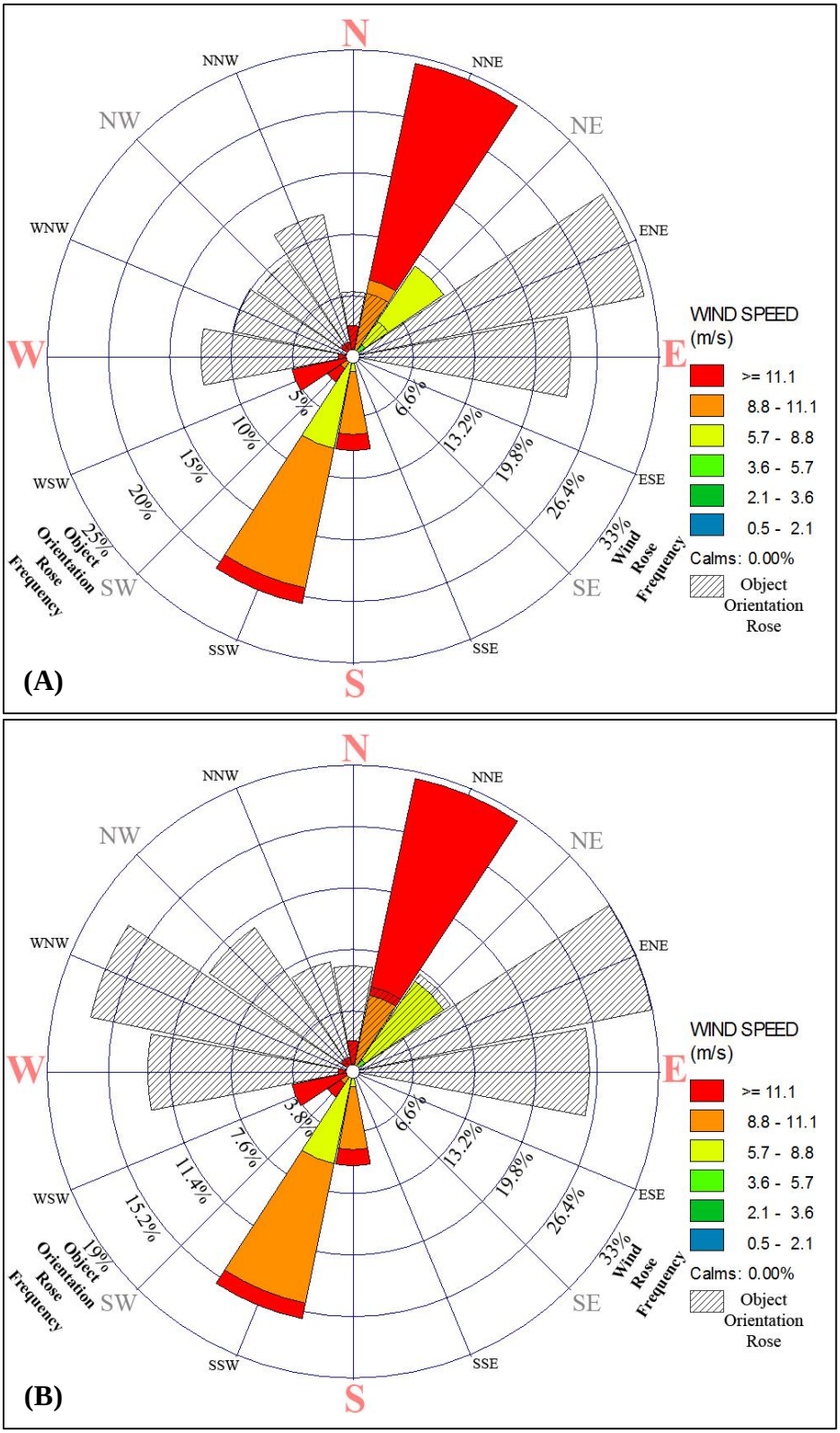

Figure 34 A model of overlaying wind rose during Hurricane Dennis landfall starting on July 10, 2005, at 00:00 am, and ending on July 10, 2005 at 11:00 pm, and object orientation rose post-Hurricane Dennis displayed as A) erosional objects and B) depositional objects.

Table 6 A list of the compass point, degree range, object frequency percentage following Hurricane Ivan and Hurricane Dennis in both erosional and depositional objects are displayed.

Compass Point	Direction (Degree)	Ivan Erosion (%)	Ivan Deposition (%)	Dennis Erosion (%)	Dennis Deposition (%)
W	258.75 - 281.25	8.8	4.8	12.4	12.7
WNW	281.25 - 303.75	13.9	13.5	10.1	16.6
NW	303.75 - 326.25	12.8	21.3	9.5	10.8
NNW	326.25 - 348.75	10.2	15.5	11.8	7.0
N	348.75 - 11.25	10.2	9.7	5.3	6.6
NNE	11.25 - 33.75	8.4	5.3	5.3	5.4
NE	33.75 - 56.25	6.2	7.7	3.6	7.3
ENE	56.25 - 78.75	16.4	11.6	24.3	18.9
E	78.75 - 101.25	13.1	10.6	17.8	14.7

following Hurricane Ivan and Hurricane Dennis in both erosional and depositional objects.

From the wind rose created for Hurricane Ivan during landfall, as shown in Figure 33 in sections (A) and (B), the model revealed that the prevailing wind direction was from the south, with 50% frequency, from which all wind speeds were recorded as >= 11.1 m/s. The two other most frequent wind directions were blowing from the southeast and the south-southwest, both with around 17% frequency, and with wind speeds >= 11.1 m/s. In the erosional object orientation rose model in section (A), objects oriented all over the range from east to west. The east-northeast sector had the dominant orientation occurrence with about 16.4% frequency. This sector can be mostly attributed to erosional processes occurring along the coast from wave run-up and high storm surge forces. In general, when comparing the erosional object orientation rose with the wind rose, wave run-ups were noticed to be more important to the model than wind as waves showed a great role in spreading objects and orienting them along the coast. This means that wind forces did not play the only role in the orientation of objects. In the depositional object orientation rose model in section (B), the northwest sector was the dominant direction of orientation with about 21.3% frequency, followed by north-northwest with about 15.5% frequency, and the west-northwest with

around 13.5%. Those sectors fell within the range of dominant wind directions, indicating that wind can be related to the depositional object orientation.

From the wind rose created for Hurricane Dennis during landfall, as shown in Figure 34 in sections (A) and (B), the model revealed the prevailing wind direction was from the north-northeast direction with about 32% frequency. This sector was dominated by 73.7% wind speeds of >= 11.1 m/s, and the remaining 26.3% was for wind speeds between 8.8–11.1 m/s. Another frequent wind direction was from the south-southwest, with about a 27% frequency. This sector was dominated by 56.3% of wind speeds between 8.8–11.1 m/s; the remaining comprised of 37.5% wind speeds between 5.7–8.8 m/s and 6.3% of wind speeds >= 11.1 m/s. In the erosional object orientation rose, the most dominant orientation was toward the east-northeast with 24.3% frequency, followed by the east direction with around 17.8% frequency. As mentioned previously, those objects' orientation can be accounted for by the strong forces along the coast that shaped them. The remaining object orientation rose sectors likewise did not show explicit relationship with the wind flow in orienting the objects. However, wave run-ups were noticed to be more important to the model as it showed a great role in spreading objects and orienting them along the coast. In the depositional object orientation rose, the dominant orientation was also found to be in east-northeast direction with about 19% frequency. Another major orientation was toward the west-northwest with 17% frequency. Within this sector, objects tended to orient nearly perpendicular to the dominent wind directions. This may be a reason that the wind flow came from both opposite directions, the noth-northeast and south-southwest, and hence aided in elongating the depositional objects.

4.6 Hurricane Ivan Spatial Distribution

Prior to Hurricane Ivan, the crest elevation of foredunes located along the coast seaward from the road ranged between approximately 3 m and 6 m, and foredunes were mostly discontinuous. The inland area was composed of several discrete, high-elevated dunes ranging in crest elevation from approximately 3 m to 10 m. The remaining area was mostly flat with numerous dispersed low-hummocky dunes and nebkha (discrete vegetated dune mounds) along the study area. The cross-shore width of the barrier island extending from the shoreline to the back of the barrier island ranged from the minimum of approximately 270 m to the maximum of about 950 m. Approximately 36% of the study area was composed of vegetation cover.

After Hurricane Ivan the spatial variation in object distribution was noticeable. The identified object's status distribution maps are shown in Figure 35, Figure 36, and Figure 37; the mean elevation change maps are shown in Figure 38, Figure 39, and Figure 40; and the mean slope change maps are shown in Figure 41, Figure 42, and Figure 43.

The berm and foredunes suffered severe erosional changes, comprising a longshore patch represented in OID 72, with an area size of 295,708 m^2 stretching all along the coast, orienting with an azimuth angle of 167.6º from true north (in other words, directed toward the ENE compass point). This object's mean elevation change value declined from 2.6 m prior to the hurricane to 1.5 m after the hurricane, with a difference of -1.1 m in mean elevation change. This object had a mean slope change value of -0.32º, decreasing in gradient from 4.06º to 3.7º. In section I-3 this object expanded further landward than in adjacent areas, and hence, resulted in burial of the road in the east section.

Surfaces with higher elevations were vulnerable to erosional processes, where 216 objects—or 78.8% of the erosional objects—had a mean elevation value ranging from >= 2 m up

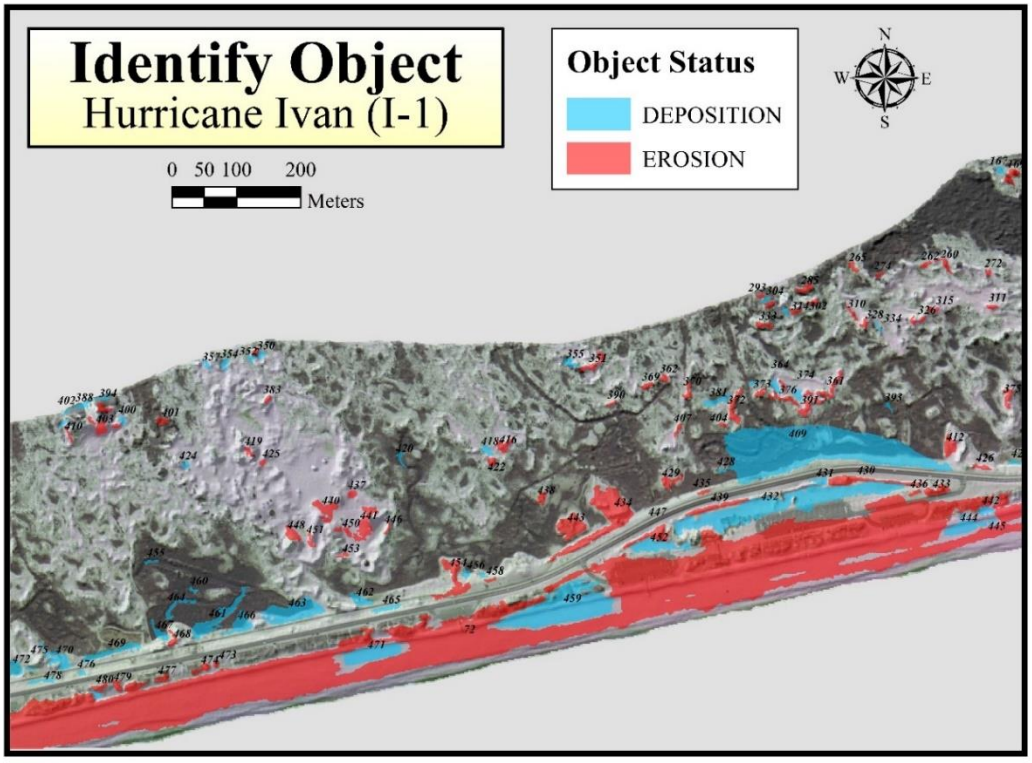

Figure 35 Spatial distribution of the identified objects post-Hurricane Ivan within (I-1). Background image acquired on March 1, 2004.

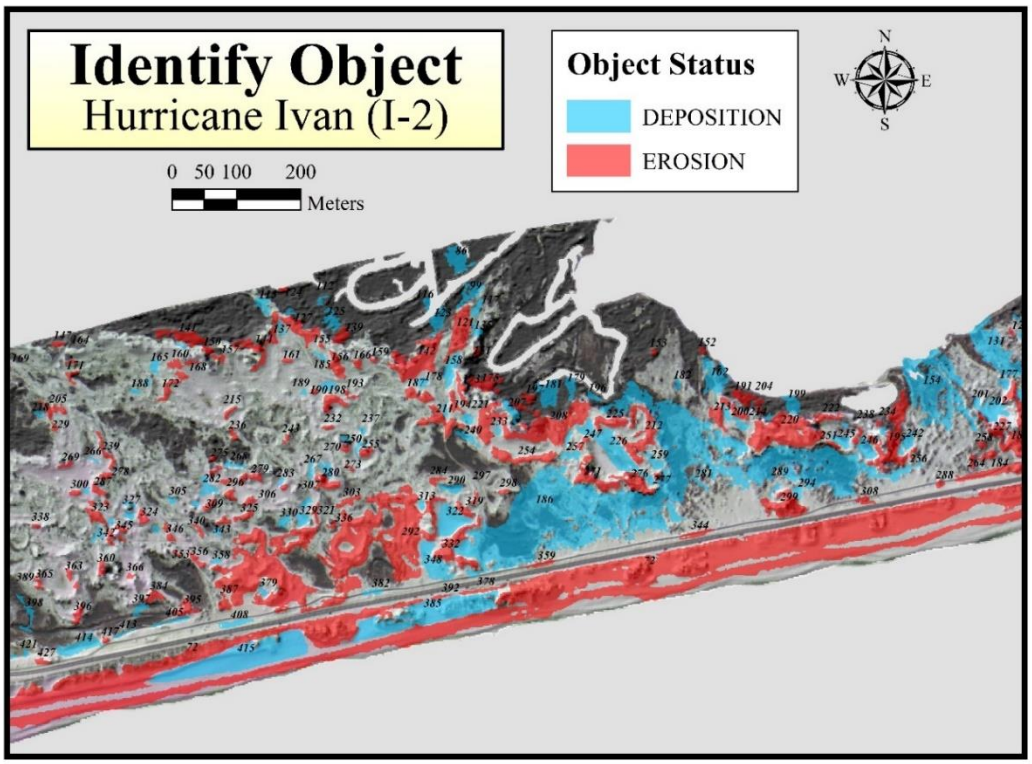

Figure 36 Spatial distribution of the identified objects post-Hurricane Ivan within (I-2). Background image acquired on March 1, 2004.

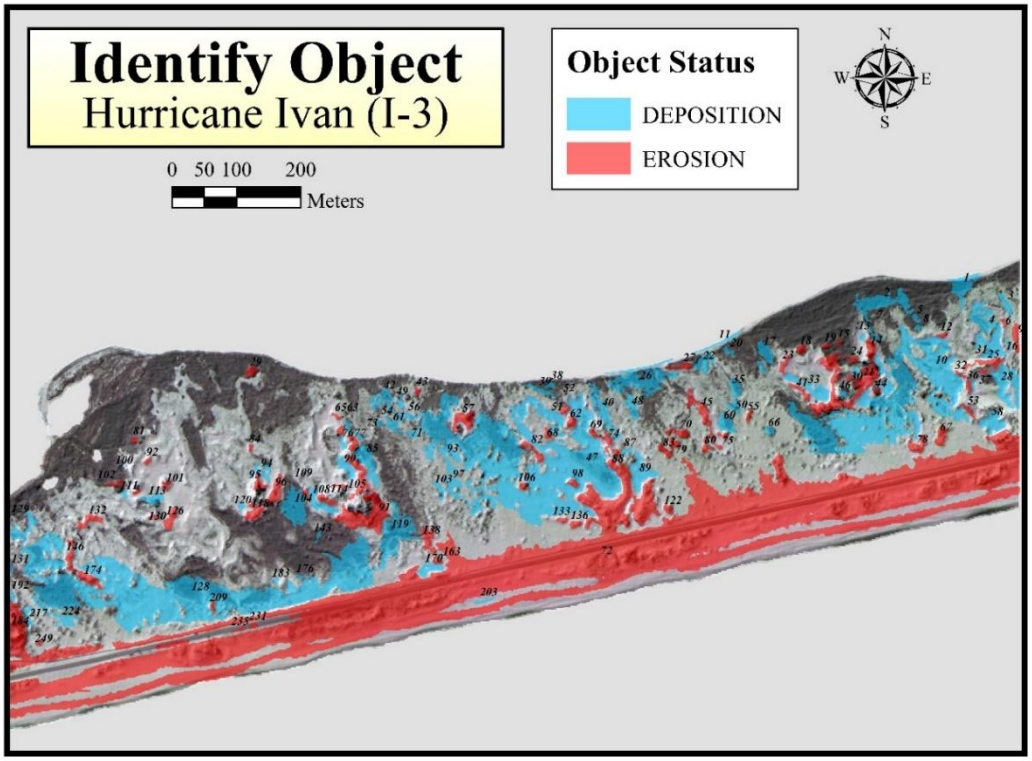

Figure 37 Spatial distribution of the identified objects post-Hurricane Ivan within (I-3). Background image acquired on March 1, 2004.

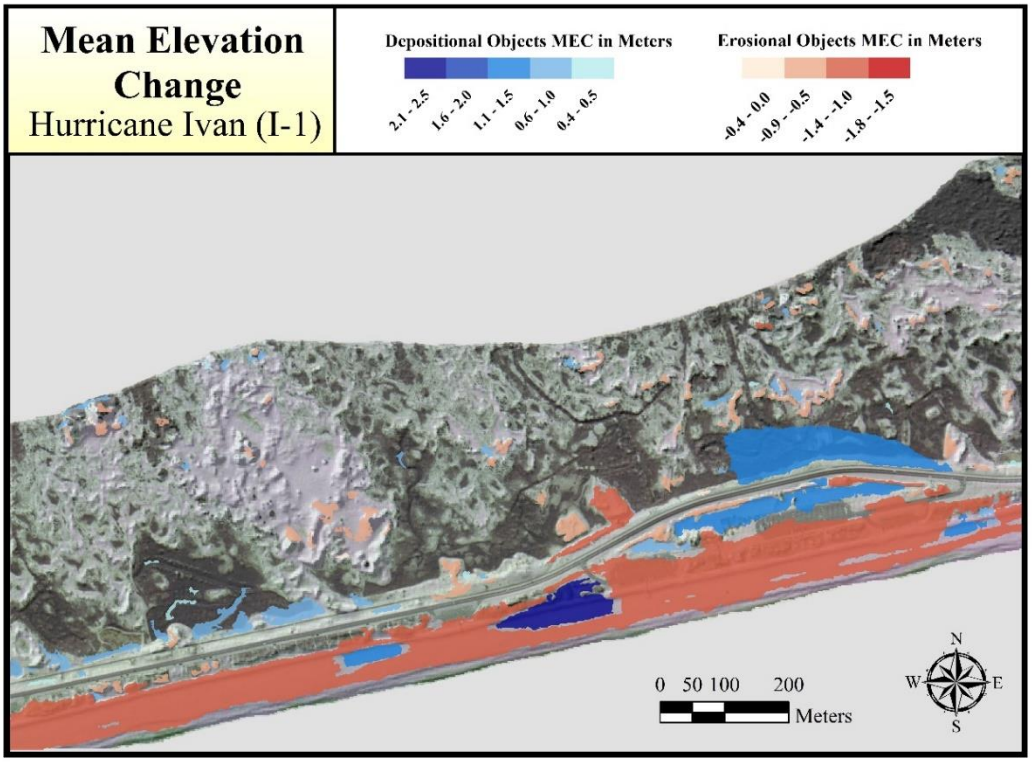

Figure 38 The mean elevation change distibution post-Hurricane Ivan within (I-1). Background image acquired on March 1, 2004.

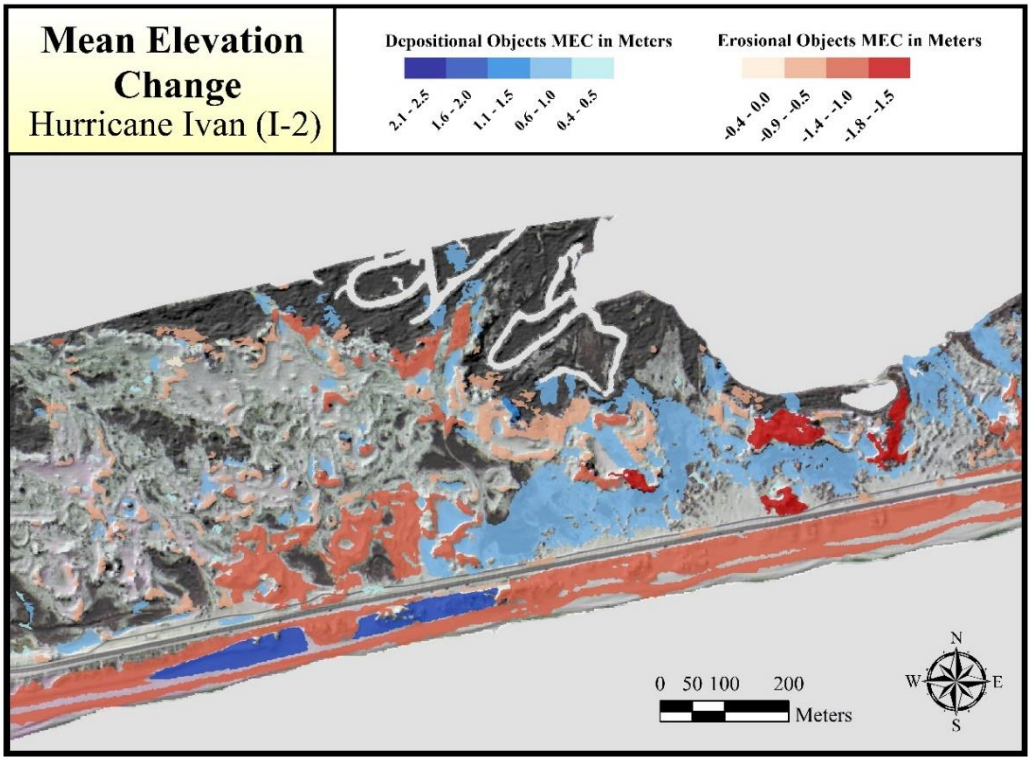

Figure 39 The mean elevation change distibution post-Hurricane Ivan within (I-2). Background image acquired on March 1, 2004.

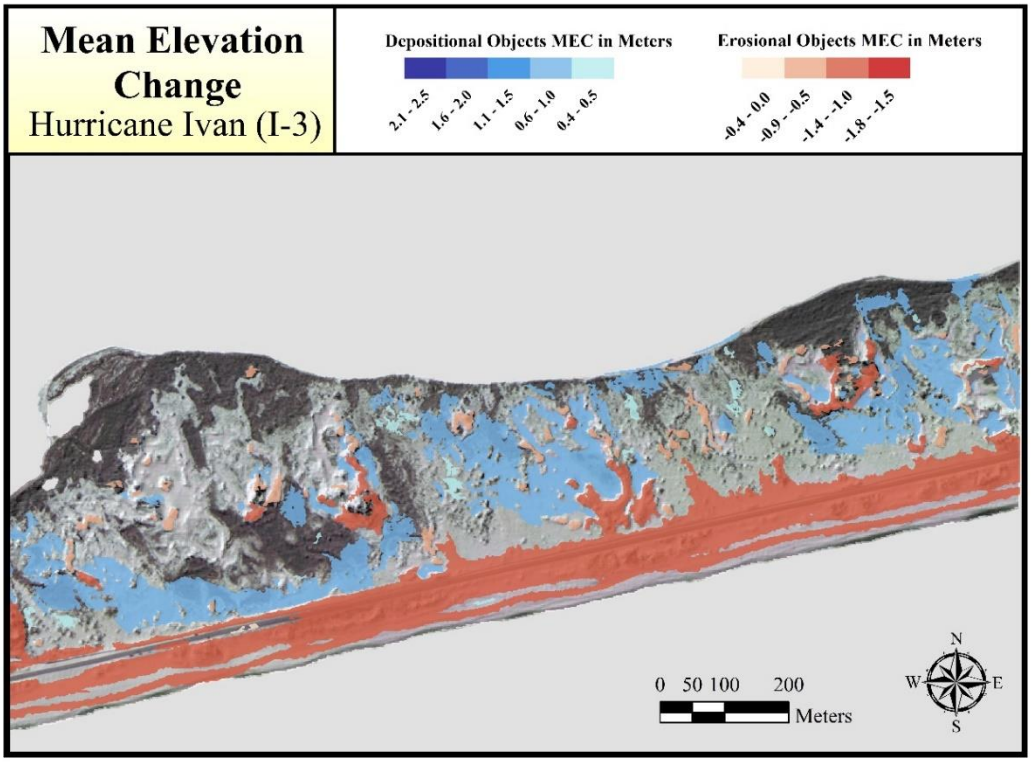

Figure 40 The mean elevation change distibution post-Hurricane Ivan within (I-3). Background image acquired on March 1, 2004.

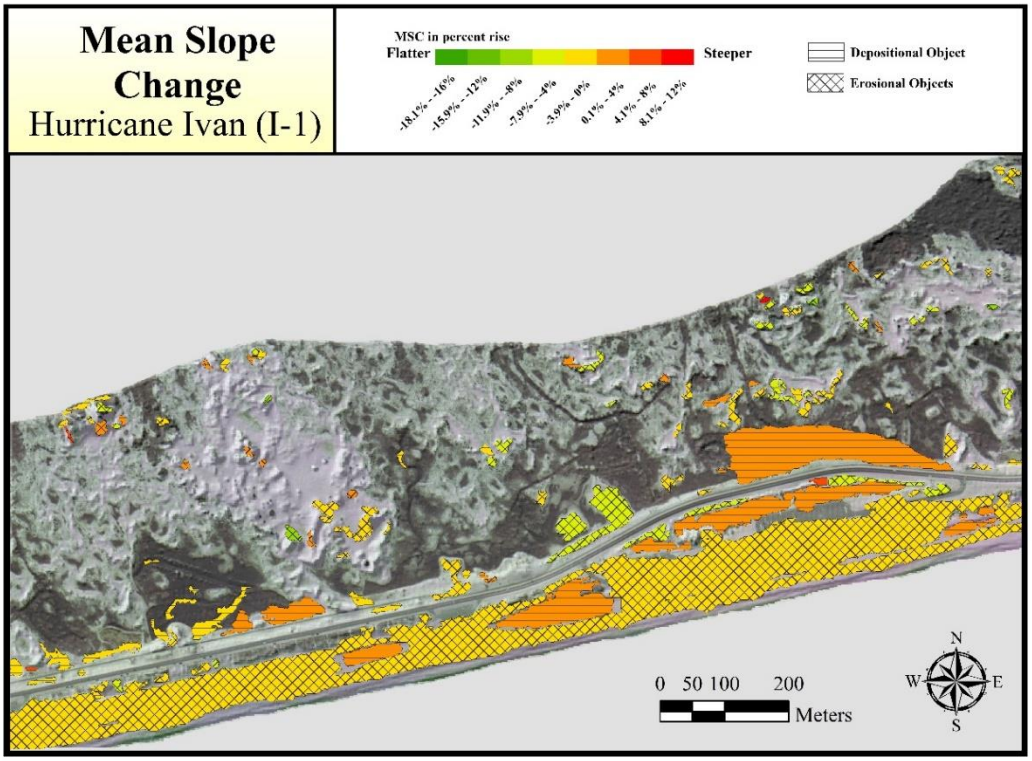

Figure 41 The mean slope change distibution post-Hurricane Ivan within (I-1). Background image acquired on March 1, 2004.

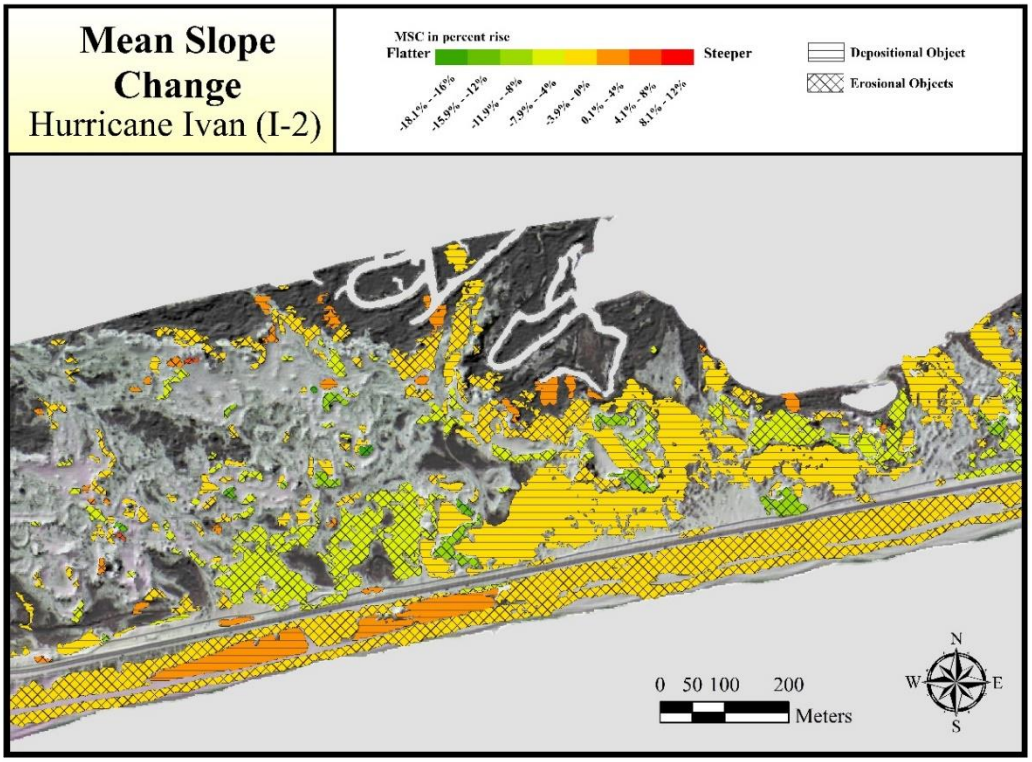

Figure 42 The mean slope change distibution post-Hurricane Ivan within (I-2). Background image acquired on March 1, 2004.

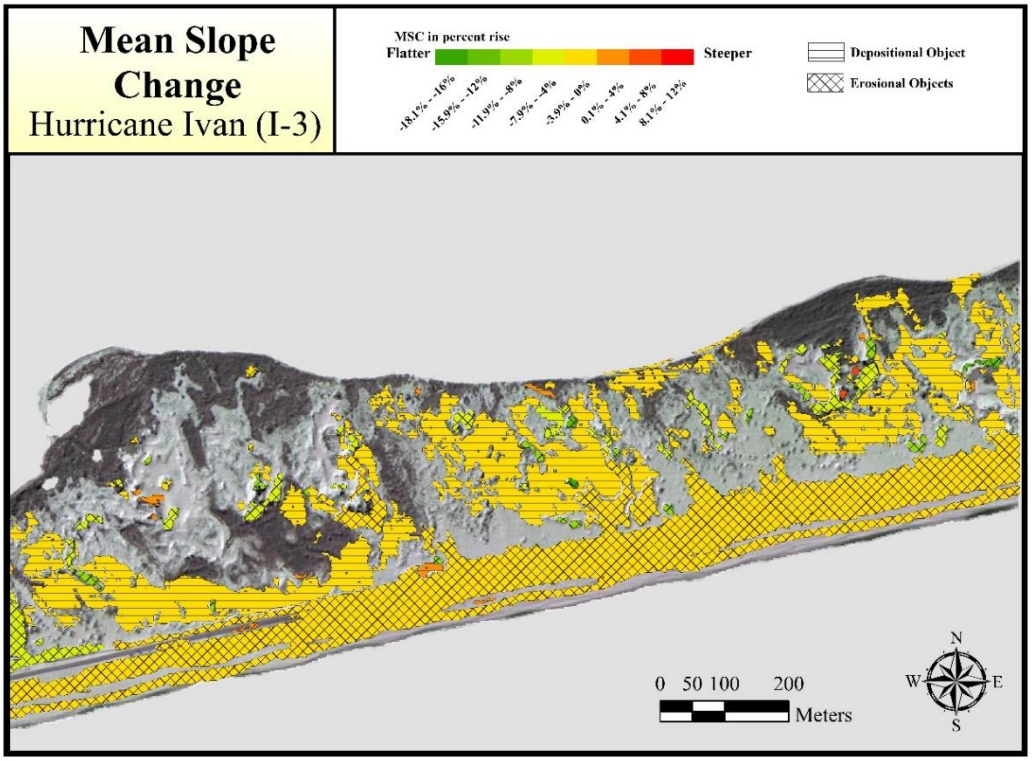

Figure 43 The mean slope change distibution post-Hurricane Ivan within (I-3). Background image acquired on March 1, 2004.

to 5.4 m prior to the hurricane. Some examples include OID 292 with its mean elevation of 2 m, OID 184 with its mean elevation of 3.1 m, and OID 91 with its mean elevation of 3.9 m.

The highest increase in mean elevation change of values > 1 m occurred in objects mostly situated along the coast within a 170 m extent inland—especially in section I-1 and the west of section I-2—with the maximum being in OID 459 at a mean vertical increase of 2 m. The other objects ranged from 2.0 m to 1.1 m, such as in the case of OID 415, 385, 471, 444, 431, and 432.

Several depositional patches occurred within the eroded elongated patch OID 72, such as OID 471, 459, 444, 442, 445, 415, 385, and 203. These depositional objects were redistributed as a result of swash and collision processes from the surrounding elevated surfaces elongating along the coast.

The area around OID 452, 432, and 431 in section I-1 mainly consisted of infrastructures, including one building and several parking lots and bridges, and as noticed, played a role in

disturbing and dissipating the energy of the dominating storm forces, hence depositing sediment around them with a volume increase recorded as 707 m^3, 8,541 m^3, and 254 m^3, respectively.

In the west side of section I-1 and the west side of section I-2, the adjacent roadbed played a role in dissipating the storm energy and depositing sediment behind the road, with elongated patches extending almost parallel to it—such as in the case of OID 478, 469, 465, 463, 414, 408, and 382—while others varied in orientation—such as in OID 470, 466, and 462. The road also aided in the erosional process where elongated erosional objects occurred almost parallel to the road, such as in the case of OID 439, 430, 378, 359, and 344. Observations after the storm indicate that once the overwashing waves had crossed the slightly elevated road they caused considerable linear scour along the landward edge of the road (Hesp, pers. Comm., 2012).

Moving inland, large depositional patches were redistributed into washover platforms, such as in the case of OID 186, 128, 47, and 10, and deposited into flatter surfaces with mean slope values of 3.1º, 3.2º, 3.0º, and 3.4º, respectively. Although those objects spread horizontally into large area sizes ranging between 18,504 m^2 and 47,472 m^2, the mean vertical increase in elevation was less than a meter, ranging between 0.71 m and 0.79 m. Those objects were a result of overwash processes completely eroding all foredunes along the coast in section I-3, as well as dunes in the east side of section I-2, and eventually penetrating landward. The curvature surface of all those objects changed to a more convex surface with mean curvature change values of 1.4, 1.5, 1.9, and 2.3, respectively. OID 10 and 186 washover was disturbed by large dunes as they moved inland, depositing sediment in the seaward edges of the foredunes, while OID 47 deposited in the lee side of the dunes, spreading landward.

Fifty-five depositional patches corresponded with vegetated patches comprising of a mean vegetation cover of >= 50% or more. For example, sediment accretion was found in OID 104, 125,

181, 196, and 398 with a mean vegetation cover of 100%, in OID 123 and 2 with 99% cover, in OID 199 with 92% cover, in OID 26 with 73% cover, and in OID 162 with 58% cover.

The majority of objects with smaller area sizes were dispersed in the back of the barrier island. Several depositional patches migrated landward, transgressing the barrier island toward the mainland, such as in the case of OID 154, 26, 11, and 1. Since the CMA tool only covers the change from two sequential pre-event survey and a post-event survey within the same extent and resolution, it was not possible to display the migration extent into the back of the barrier island as an object. Nevertheless, this inland migration can be displayed in the DTM, as shown in Figure 7, following Hurricane Ivan, especially in the east side of the study area that was comprised of a narrower width in the barrier island, and as a result, provided a shorter distance for the sediment to transport to the back.

It should be noted that OID 409 was not believed to be the result of natural processes, but rather, a product of human influence, such as debris accumulation from the storm which was distinguished from satellite images acquired on December 30, 2004, following Hurricane Ivan, as shown in Figure 44.

Figure 44 OID 409 distinguished-to-be human effect on the change using a Google Earth satellite image acquired on December 30, 2004 (Earth 2013).

4.7 Hurricane Dennis Spatial Distribution

Prior to Hurricane Dennis, the landform along the coast was mostly flat in section D-3, with a mostly complete destruction of foredunes, and also flat in the east side of section D-2 from the impact of Hurricane Ivan. Some foredunes in section D-1 and the west side of section D-2 survived the storm but still suffered from swash and collision processes. The crest elevation of the remaining foredunes and the depositional patches from the previous storm situated seaward from the road ranged between approximately 3 m and 7 m. The inland area was composed of several discrete high-elevated dunes that survived the previous storm, with crest elevations ranging from approximately 3 m to 9 m. The cross-shore width of the barrier island ranged from the minimum value of approximately 260 m to the maximum value of about 925 m. Roughly 16% of the study area was composed of vegetation cover, diminishing after Hurricane Ivan buried and destroyed a large amount of the cover. The survived vegetation was generally distributed in inland regions and along the bay in the back of the barrier island. In section D-3 a new road was reconstructed and situated more inland relative to the initial location of the road that was buried and breached during Hurricane Ivan.

Following Hurricane Dennis, the spatial variation in object distribution was noticeable. The identified object's status distribution maps are shown in shown Figure 45, Figure 46, and Figure 47; the mean elevation change maps are shown in Figure 48, Figure 49, and Figure 50; and the mean slope change maps are shown in Figure 51, Figure 52, and Figure 53.

The berm and foredunes along the coast suffered from erosional changes as a result of swash and collision processes represented in 13 discrete, elongated, non-vegetated, and mostly narrow erosional patches, within an extent of approximately 80 m inland, such as in the case of OID 72, 127, 153, 175, 222, 318, 383, 385, 414, 419, 426, 427, and 428. Those objects comprised

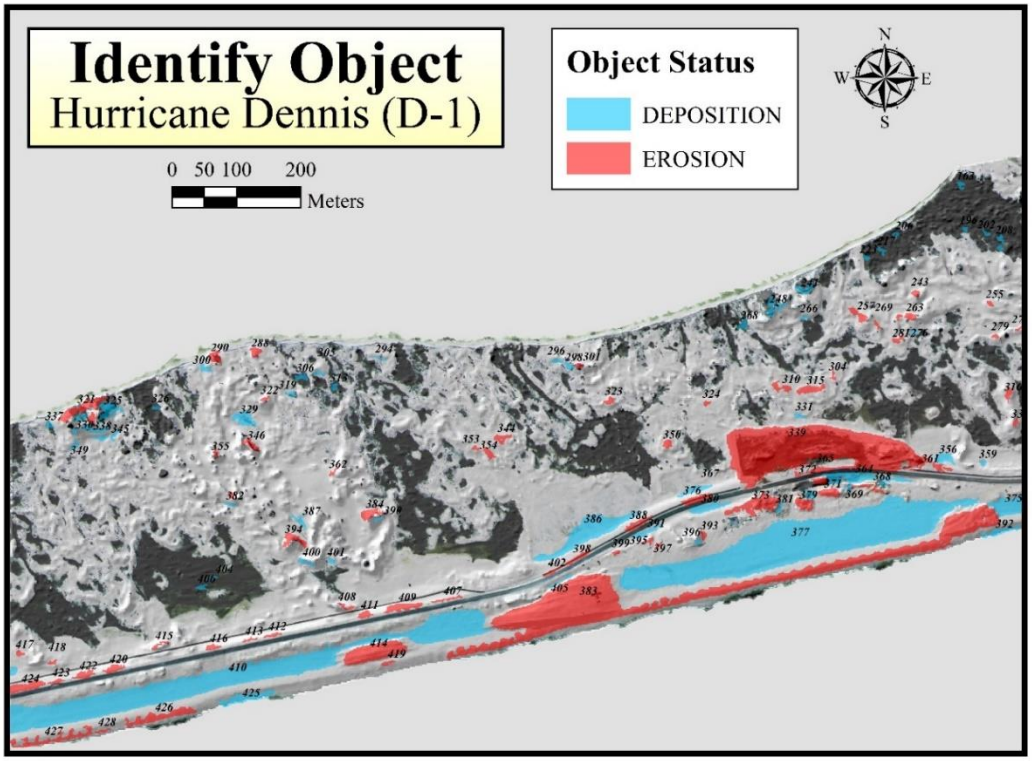

Figure 45 Spatial distribution of the identified objects post-Hurricane Dennis within (D-1). Background image acquired on February 27, 2005.

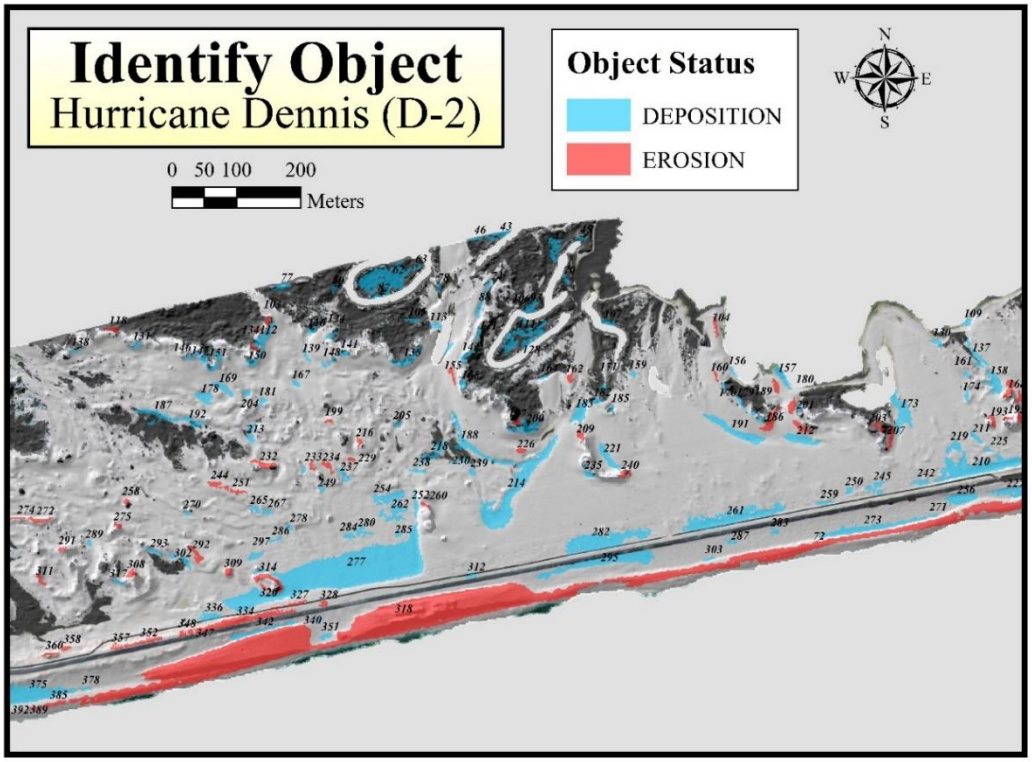

Figure 46 Spatial distribution of the identified objects post-Hurricane Dennis within (D-2). Background image acquired on February 27, 2005.

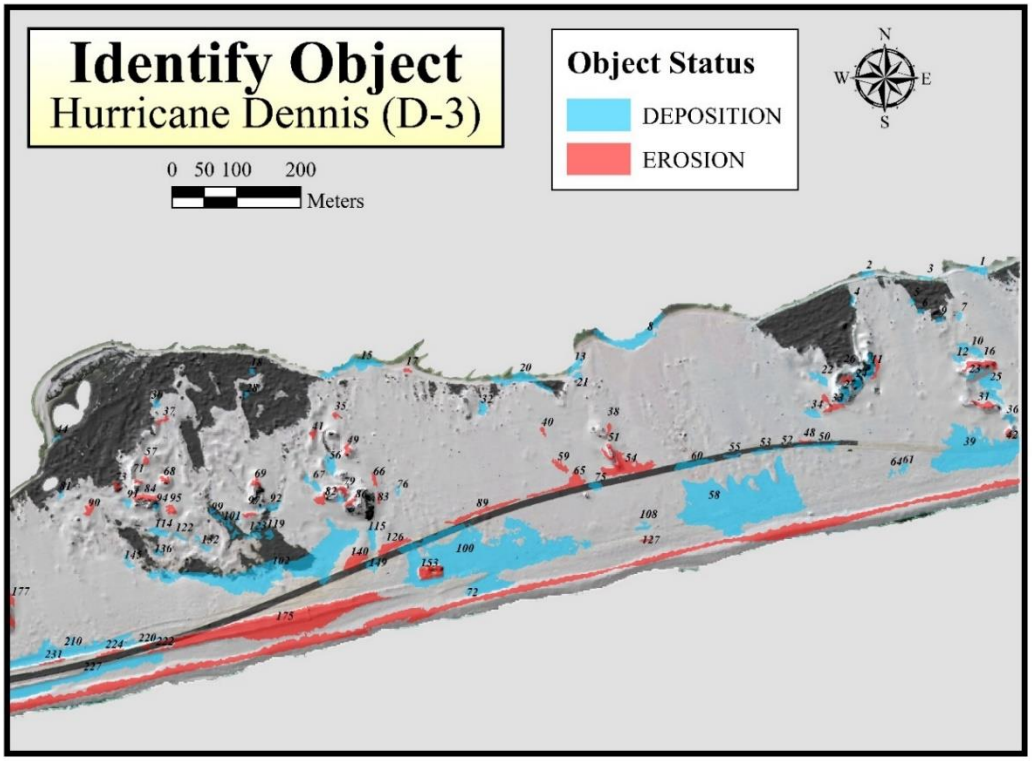

Figure 47 Spatial distribution of the identified objects post-Hurricane Dennis within (D-3). Background image acquired on February 27, 2005.

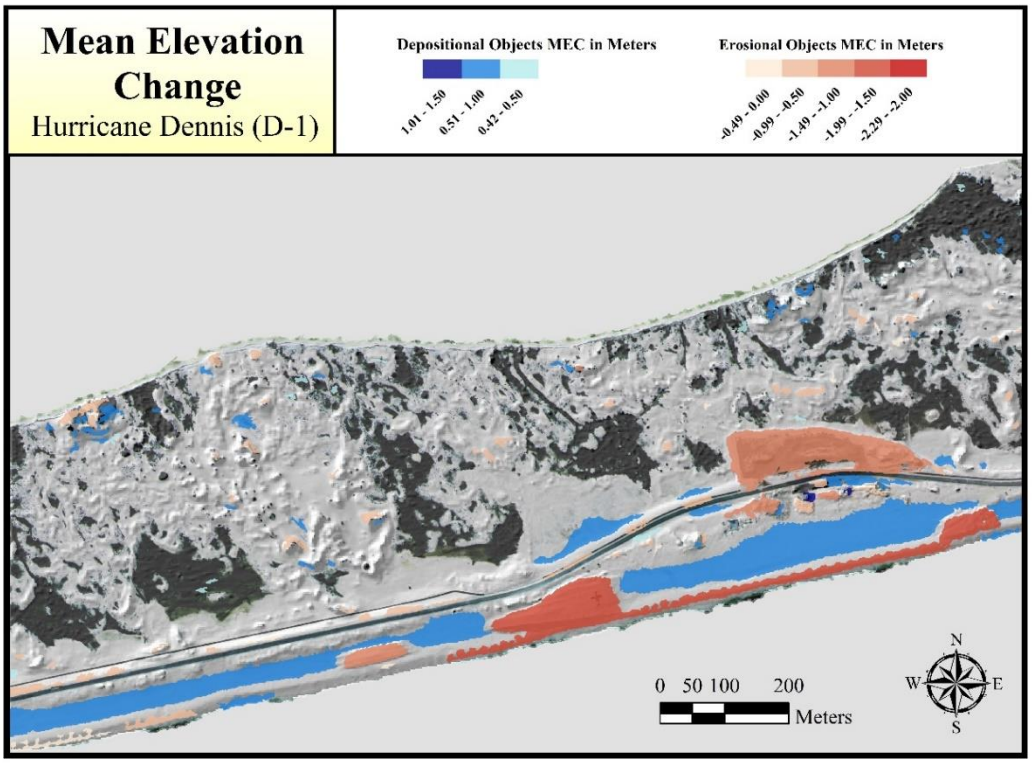

Figure 48 The mean elevation change distibution post-Hurricane Dennis within (D-1). Background image acquired on February 27, 2005.

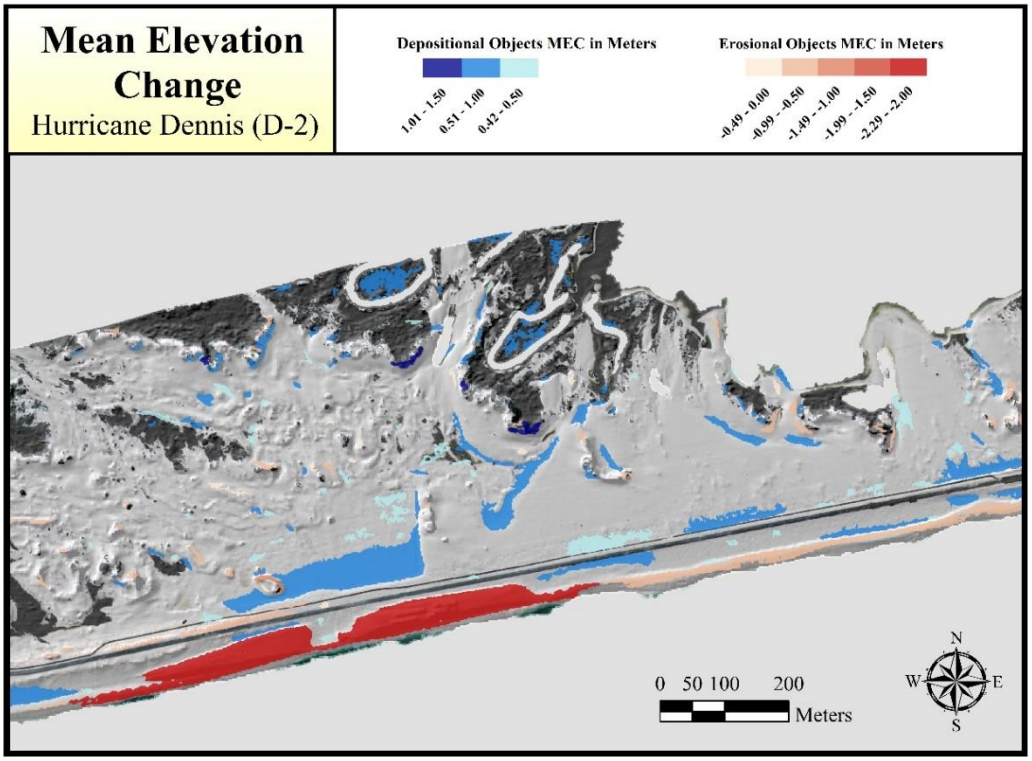

Figure 49 The mean elevation change distibution post-Hurricane Dennis within (D-2). Background image acquired on February 27, 2005.

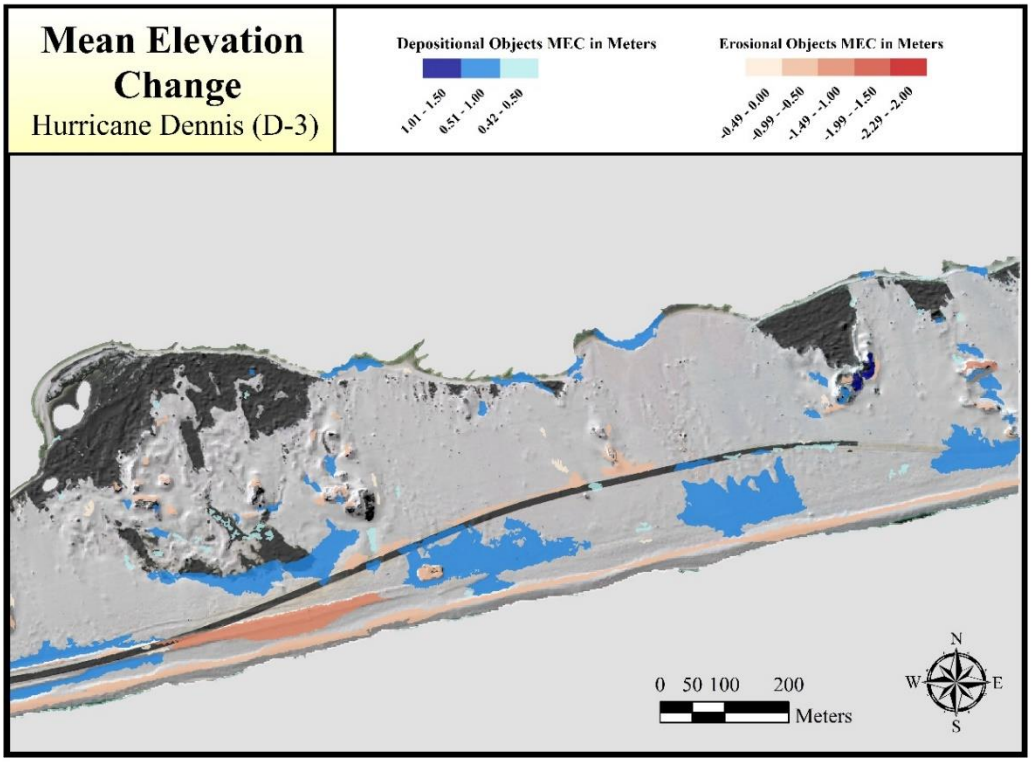

Figure 50 The mean elevation change distibution post-Hurricane Dennis within (D-3). Background image acquired on February 27, 2005.

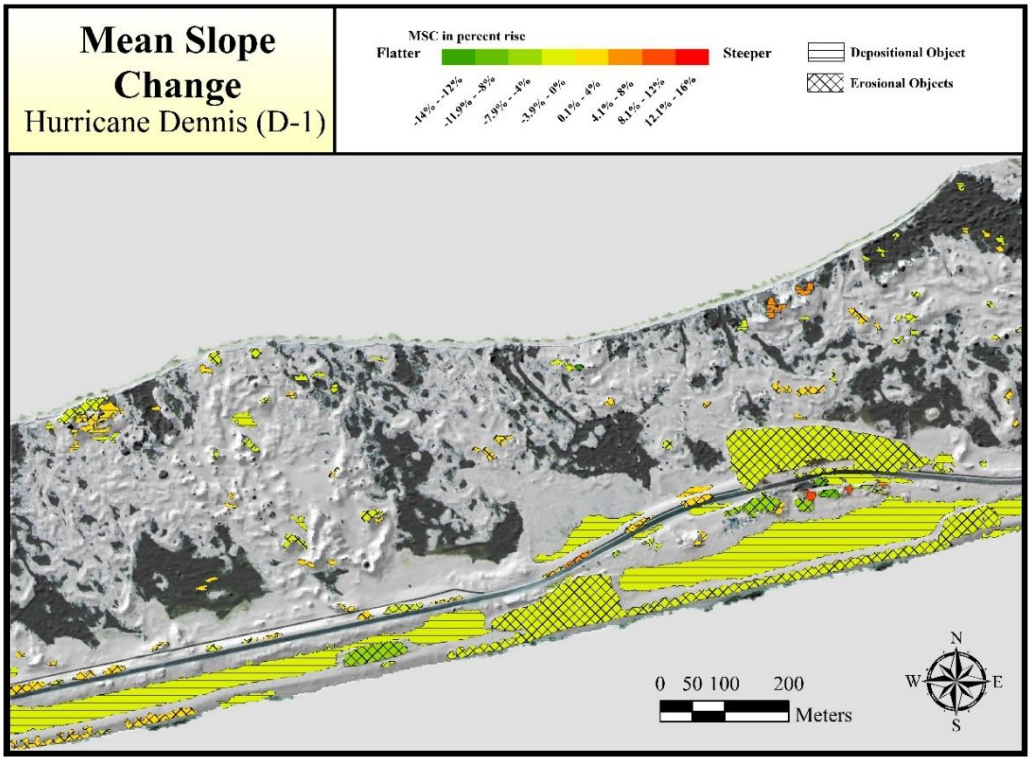

Figure 51 The mean slope change distibution post-Hurricane Dennis within (D-1). Background image acquired on February 27, 2005.

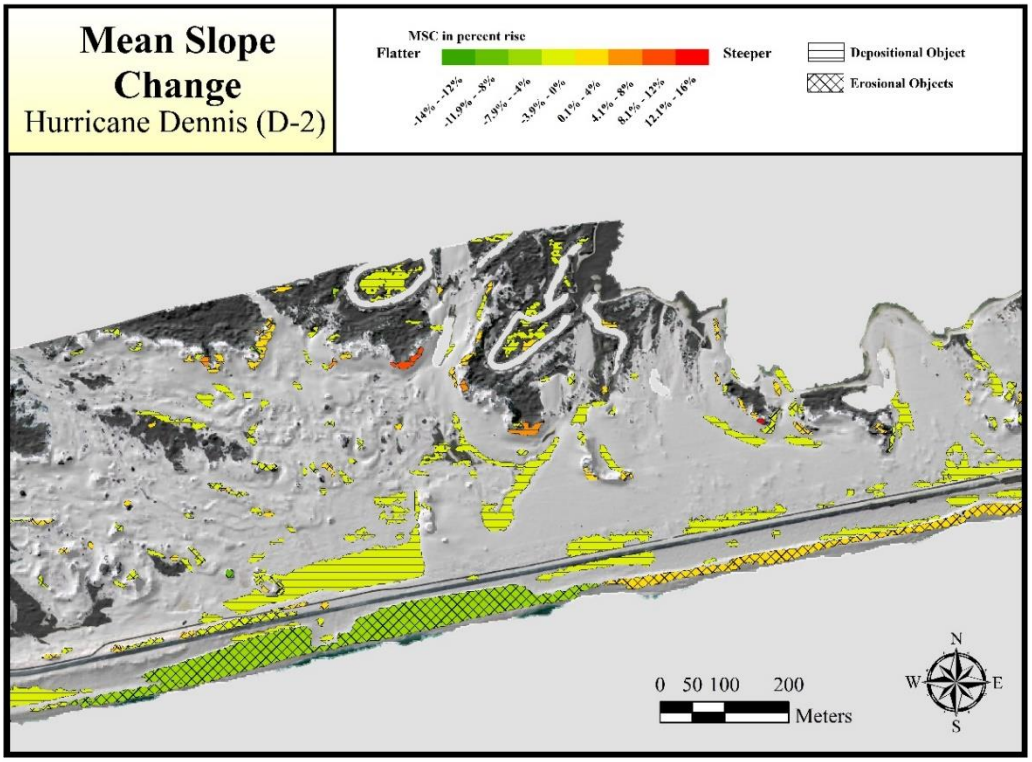

Figure 52 The mean slope change distibution post-Hurricane Dennis within (D-2). Background image acquired on February 27, 2005.

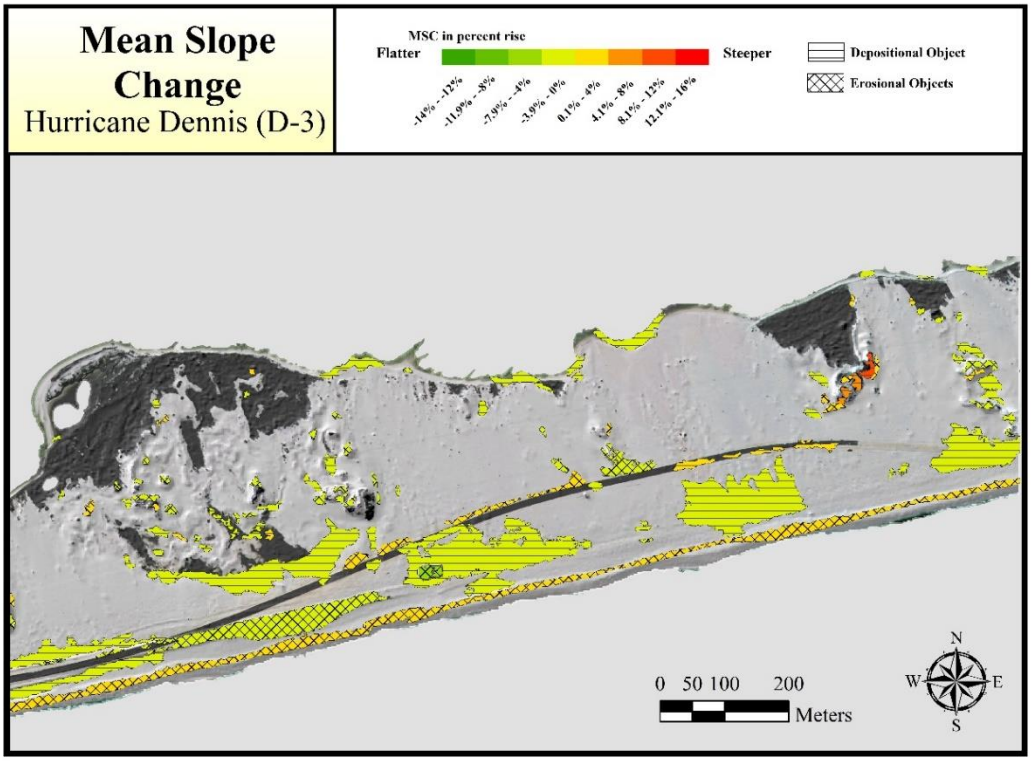

Figure 53 The mean slope change distibution post-Hurricane Dennis within (D-3). Background image acquired on February 27, 2005.

a total area size of 85,076 m^2, ranging from the minimum of 76 m^2 to the maximum of 26,204 m^2, and had a total volume change of -129,745 m^3. The mean elevation change values show a vertical elevation decline ranging from -2.2 m to -0.4 m. All the objects oriented with an azimuth angle ranging between 164.2º and 172.2º from true north (in other words, directed toward the E and ENE compass points). Around 76.9% of those objects became flatter in surface, ranging from -7.2º to -0.1º in mean slope change values. The two depositional patches accumulated from the previous hurricane within section I-1 comprising OID 471 and 459 were completely eroded in the second hurricane, as shown in D-1 in OID 414 and 383.

A total of 125 erosional objects, or in other words 74% of the erosional objects, had a mean elevation value ranging from >= 2 m up to 6.3 m prior to Hurricane Dennis, explaining that higher elevated surfaces were more vulnerable to erosional processes.

Some of the depositional objects with the highest volume increase and largest area sizes were distributed behind the elongated erosional patches and extended inland to about 200 m from the shoreline, such as in the case of OID 410, 377, 375, 277, 273, 227, 100, 58, and 39. All these objects were deposited within non-vegetated surfaces and had a mean elevation increase ranging between 0.5 m and 0.8 m.

The highest increase in mean elevation change values > 1 m occurred in smaller objects ranging in area size between 84 m^2 and 520 m^2 and were mostly distributed inland, such as in the case of OID 372, 369, 200, 165, 147, 135, 24, and 11.

Several erosional and depositional patches distributed along the adjacent road base and were almost parallel to the road with an elongated shape—for example, in the case of OID 424, 409, 398, 376, 352, 334, 126, and 89 as erosional patches and OID 386, 282, 295, 261, 210, 60, and 50 as depositional patches.

The inland accretion in section D-3 can be attributed to overwash processes because of the absence of foredunes previously destroyed by Hurricane Ivan along the coast, hence aiding in the penetration process of washover platforms into inland regions, such as in the case of OID 102, 100, 58, and 39. These objects were deposited into flatter surfaces with mean slope values of about 2º, 1.5º, 1.3º, and 1.3º, respectively. Despite the fact that those objects spread horizontally into large area sizes ranging between 6,096 m^2 and 15,396 m^2, the mean vertical increase in elevation after the hurricane was less than a meter, ranging between around 0.6 m and 0.7 m. The curvature surface of all the objects changed to a more convex surface, with mean curvature change values of about 1.0, 1.2, 0.5, and 0.5, respectively.

The majority of smaller area-sized objects were distributed inland and on the back of the barrier island. Numerous depositional objects migrated to the back of the barrier island,

transgressing the island toward the mainland, especially in the east side of section D-2 and in section D-3—for example, in the case of OID 157, 156, 130, 109, 44, 15, 20, 13, 8, 3, 2, and 1.

It should be noted that OID 339 was not believed to be the result of natural processes, but rather, a product of human influence, such as debris accumulation from the storm which was distinguished from satellite images acquired on December 30, 2004, following Hurricane Ivan, as shown in Figure 44.

4.8 Discussion and Conclusion

During Hurricane Ivan, which was characterized as a category 3 at landfall, 18.6% of the study area suffered from erosional processes, while 11.4% suffered from depositional processes. During Hurricane Dennis, also characterized as category 3 at landfall, 5.9% of the whole study area suffered from erosional processes while 8.2% suffered from depositional processes. In the quantitative volumetric assessment, both events experienced an overwhelming net volume loss of sediment. Hurricane Ivan produced a net sand loss of 283,167 m^3, and Hurricane Dennis produced a net sand loss of 52,450 m^3 in the study area which can be attributed to sediment lost offshore and/or transported toward the mainland to be deposited in the bay. During storms, waves and storm surges have the ability to transport the sediment to the back of barrier islands, which can contribute to losing sand into the lagoons (Beatley, Brower, and Schwab 2002). When comparing Hurricane Dennis to Hurricane Ivan, a decline in morphological changes is apparent after the second hurricane. This is consistent with the finding of Claudino-Sales, Wang, and Horwitz (2008), indicating that even though both hurricanes had very strong maximum sustained wind speed of approximately 200 km/hr during landfall, the impact of Hurricane Dennis was much less severe due to the fact that it had a smaller extent and size, and also because it was moving faster. It may also be that much of the damage was done by the first hurricane and so therefore less damage could

be wrought by the second. Giving the short time period between the two hurricanes from September 2004 to July 2005, whereas Hurricane Dennis occurred within less than a year from Hurricane Ivan, the study area was highly impacted from the first hurricane and did not have sufficient recovery time as the second hurricane took place.

The spatial analysis indicated that erosional and depositional objects varied spatially in sand relocation and distribution. Along the coast, erosional processes dominated the morphological change processes. During Hurricane Ivan a continuous wide patch of erosional processes along the coast occurred, while after Hurricane Dennis discrete patches were found with narrower width and smaller area sizes. The first hurricane completely destroyed most of the dunes along the coast in the east side of the study area, while in the west some dunes survived the hurricane. Several factors contributed to the erosional processes:

1. Storm Surge and Wave Height: Storm surge was measured from the Pensacola tide gauge to be a 2.06 m high surge above MLLW during Hurricane Ivan (Wang et al. 2006) and 1.5 m high above MLLW during Hurricane Dennis, and the wave height was recorded as 16 m during Hurricane Ivan and recorded as 10 m high during Hurricane Dennis (Claudino-Sales, Wang, and Horwitz 2008); hence, the reduction in storm severity provided a different response along the coast.
2. Dune Length and Continuity: The length and continuity of dunes played a role in the change. Prior to Hurricane Ivan the alongshore length of the dunes on the west side tended to be longer and more continuous in form, while in the east it tended to be shorter in length and discrete in form. This made the east side more vulnerable to overwash processes.
3. Dune Height: Prior to Hurricane Ivan, dune crests in the west side had a continuity within higher elevated values while dunes in the east had variation of vertical shifting between

higher and lower elevation values, and as a result this provided gaps for the wave run-up and high storm surge to penetrate inland and destroy dunes.

4. Location from Shoreline: Given that the backshore is the first line against most of the damaging high forces of the storm, such as strong waves, storm surge, and strong winds, it makes it the most vulnerable location for damage and erosional changes.
5. Vegetation Cover: In comparison to inland regions, the coast lacks vegetation cover and mostly consists of fine sand, therefore making it prone to erosional processes.

As a consequence of the vulnerability of the east side to the storm during both hurricanes, overwash deposits dominated the east side of the study area with massive deposits migrating landward. Sallenger (2000) indicated that overwash regime is one of the storm impacts that occur when R_{High} is higher than D_{High} and R_{Low} is lower than D_{High} and results in washover processes. Those washover platforms were distributed inland in flat surfaces with large areal dimensions, but it should be noted that the change was more of a horizontal spread and extent of sediment deposition rather than a vertical increase and accretion in elevation. As those objects migrated landward in its path, obstacles consisting of high elevated dune and/or vegetation cover dissipated the energy of the transportation.

After investigating different surface attributes, several consistent patterns are noticed. The mean elevation change attribute following Hurricane Ivan is perceived to be dominated by an incline in surface mean elevation, whereas following Hurricane Dennis the dominating change was an increase in the mean elevation change. Additionally, a consistent pattern of the object's mean curvature change in both hurricanes is also observed. The curvature mostly tends to transform to a concave surface in erosional objects, and mostly transforms to a convex surface in depositional

objects. Furthermore, the mean slope change showed a consistent pattern where the majority of landforms tended to flatten following a major storm.

Once several object shape attributes were examined, a consistent pattern is observed. Most objects tended to be irregular and asymmetrical, with smooth boundaries type of shapes. Most of the objects distributed along the coast tended to have an elongated type of a shape, and became even more elongated following Hurricane Dennis. This is attributed to the direct interaction of the waves along the shoreline, which aids in shaping elongated forms. Moving inland, shapes become more irregular depending on the obstacles they encounter.

After investigating the relationship between the morphological change orientations with the wind flow, wave run-ups were noticed to be more important to the model than wind as waves showed a great role in spreading objects and orienting them along the coast. The rest of objects were distributed all along the range of orientations. This can be attributed to the chaotic circumstances of wind flow during hurricanes. For example, during Hurricane Dennis the wind flow was blowing from two opposing prevailing directions, the north-northeast and the south-southwest. It can also be attributed to the orientation of obstacles in which dissipated the sediment around it, such as the roadbed, dunes, buildings, and vegetation cover. The only noted relationship was found during Hurricane Ivan within the depositional objects that followed and elongated toward the northwest direction point, which coincides within the range of the prevailing wind directions blowing from the south, southeast, and the south-southwest.

Chapter 5 Linear Regression Analysis

5.1 Introduction

In this chapter, OLS regression analysis was performed to find whether factors such as vegetation, slope, and elevation influenced the mean elevation change during a category 3 hurricane. First, OLS performed on Hurricane Ivan will be presented, and then OLS on Hurricane Dennis will be given. Finally, the discussion and conclusions are presented.

5.2 OLS Regression Analysis

The linear regression analysis was utilized to test for significant relationships of several factors on the morphological changes after two hurricanes. The dependent variable used here was the mean elevation change, which quantifies the vertical change in height measured in meters, and the explanatory variables used in the analysis included the mean vegetation, mean slope, and mean elevation. The analysis will be presented in different sections for each hurricane.

Since objects identified in this research varied in area size from very large sizes to very small sizes (for example, in the case of Post-Hurricane Ivan the range was between 295,708 m^2 and 72 m^2), those exceptionally high values skewed the distribution results during the linear regression analysis. In order to overcome outlying results, the segmented change map was used in this phase from Figure 16.

Two objects were omitted from the linear regression analysis—OID 409 from Figure 35 and OID 339 from Figure 45—because they were believed to be an unnatural change in the morphology and rather represented human interference with the surface after the hurricane occurred, such as debris accumulations.

The analysis was constructed in several stages for each hurricane separately: 1) an overall analysis on the region, including both depositional and erosional processes; 2) overall depositional

processes along the study area; 3) deposition processes along the coast within a strip of 200 meters from shoreline; 4) depositional processes inland behind the 200 meters strip extending to the back of the barrier island; 5) overall erosional processes along the study area; 6) Erosional processes along the coast within a strip of 200 meters from shoreline; and 7) erosional processes inland behind the 200 meters strip extending to the back of the barrier island.

5.2.1 OLS for Hurricane Ivan

The total observations reached 766l objects, consisting of 4811 erosional objects and 2850 depositional objects. The OLS regression analysis results are shown in Table 7 and Table 8. Numerous variables are statistically significant and suggest that the coefficient is important to the model.

In the overall analysis, the results reject the null hypothesis, as all variables in the model yielded significant statistical results with a confidence level of 0.00. The coefficients yield the expected signs in the tested variable. The vegetation coefficient value of 0.34 shows a positive association with mean elevation change, which is in accord with our expectations. This indicates that the more vegetation cover is found on the surface, the more increased elevation is expected to occur. The slope coefficient value of 0.02 shows that higher slope degrees yield more deposition of sediment. The elevation coefficient value of -0.66 indicates that with higher elevated morphology, more decline in vertical elevation height is expected. The adjusted r-square of 0.40 means that 40% of the total mean elevation change is explained by the selected variables in this study.

Depositional processes all along the study area provide more insight into the results. All variables continued to be statistically significant. In this case, a positive association, 0.05, is found between vegetation and mean elevation change, indicating that vegetation plays a role in capturing

Table 7 Hurricane Ivan Coefficient Report. * An asterisk next to a number indicates a statistically significant p-value ($p < 0.05$).

Variable	*Coef*	*StdError*	*t_Stat*	*Prob*	*Robust_SE*	*Robust_t*	*Robust_Pr*
Erosion & Deposition							
Intercept	0.80	0.02	34.18	0.00*	0.03	28.97	0.00*
Vegetation	0.34	0.03	10.19	0.00*	0.03	12.01	0.00*
Slope	0.02	0.00	7.97	0.00*	0.00	7.59	0.00*
Elevation	-0.66	0.01	-59.06	0.00*	0.01	-46.98	0.00*
Deposition							
Intercept	0.49	0.02	24.30	0.00*	0.03	18.22	0.00*
Vegetation	0.05	0.02	2.19	0.03*	0.02	2.63	0.01*
Slope	-0.02	0.00	-7.47	0.00*	0.00	-5.93	0.00*
Elevation	0.31	0.01	23.05	0.00*	0.03	12.77	0.00*
Deposition (Along the Coast <200 m extent)							
Intercept	0.45	0.04	11.99	0.00*	0.04	10.04	0.00*
Vegetation	0.15	0.04	3.68	0.00*	0.03	4.64	0.00*
Slope	-0.03	0.01	-5.20	0.00*	0.01	-4.40	0.00*
Elevation	0.37	0.02	16.98	0.00*	0.03	11.79	0.00*
Deposition (Inland >200 m extent)							
Intercept	0.67	0.01	52.30	0.00*	0.02	33.62	0.00*
Vegetation	-0.05	0.01	-3.86	0.00*	0.01	-3.69	0.00*
Slope	0.01	0.00	4.09	0.00*	0.00	3.67	0.00*
Elevation	-0.02	0.01	-1.37	0.17	0.02	-0.86	0.39
Erosion							
Intercept	-0.39	0.02	-16.19	0.00*	0.03	-11.65	0.00*
Vegetation	0.18	0.04	4.67	0.00*	0.04	4.86	0.00*
Slope	0.01	0.00	2.77	0.01*	0.00	2.50	0.01*
Elevation	-0.32	0.01	-30.89	0.00*	0.02	-20.54	0.00*
Erosion (Along the Coast <200 m extent)							
Intercept	-0.36	0.03	-11.87	0.00*	0.04	-8.67	0.00*
Vegetation	-0.01	0.08	-0.11	0.91	0.10	-0.09	0.93
Slope	-0.02	0.00	-6.15	0.00*	0.00	-5.38	0.00*
Elevation	-0.31	0.01	-23.80	0.00*	0.02	-16.85	0.00*
Erosion (Inland >200 m extent)							
Intercept	-0.48	0.03	-14.09	0.00*	0.04	-13.27	0.00*
Vegetation	0.05	0.04	1.35	0.18	0.03	1.64	0.10
Slope	-0.01	0.00	-2.67	0.01*	0.00	-2.20	0.03*
Elevation	-0.15	0.02	-9.80	0.00*	0.02	-6.58	0.00*

Table 8 Hurricane Ivan Diagnostic Report.

Diagnostic Name	***Diagnostic Values***						
	All	**Deposition**	**Deposition (<200 m)**	**Deposition (>200 m)**	**Erosion**	**Erosion (<200 m)**	**Erosion (>200 m)**
AIC	19,338.4	3,175.6	2,425.97	-780.22	7,878.15	6,196.12	1,110.16
AICc	19,338.5	3,175.6	2,426.01	-780.18	7,878.16	6,196.14	1,110.22
R2	0.40	0.17	0.17	0.03	0.20	0.25	0.18
AdjR2	0.40	0.17	0.17	0.02	0.20	0.25	0.18
F-Stat	1,719.90	196.59	102.36	11.73	403.14	406.33	78.12
F-Prob	0.00	0.00	0.00	0.00	0.00	0.00	0.00
Wald	5,045.26	180.67	141.02	38.79	521.74	496.17	148.67
Wald-Prob	0.00	0.00	0.00	0.00	0.00	0.00	0.00
K(BP)	295.52	332.75	168.03	24.78	860.48	549.32	147.91
K(BP)-Prob	0.00	0.00	0.00	0.00	0.00	0.00	0.00
JB	7,160.65	17,267.30	3,343.88	1,286.78	909.19	388.13	1,531.97
JB-Prob	0.00	0.00	0.00	0.00	0.00	0.00	0.00
Sigma2	0.73	0.18	0.28	0.03	0.30	0.31	0.16

the sediment and increasing the height in morphology. Slope, on the other hand, yielded a negative association with a coefficient of -0.02, indicating that higher gradient degree surfaces have less increase in mean elevation change. Areas with higher elevation prior to the hurricane show a positive relationship of 0.31, explaining that higher surfaces yield greater increase in elevation.

Since the processes may depend on spatial variation along the barrier island, results were conducted for coastal objects and for inland objects separately. In the case of vegetation, depositional processes showed different relationships closer to the coast and further from the coast. Along the 200 m strip from shoreline, the vegetation relationship showed a positive coefficient of 0.15, indicating that with higher vegetation cover, a greater increase in mean elevation change is found. On the contrary, moving inland, a negative relationship was found with a coefficient of -0.05, indicating that even with the existence of vegetation cover, it was less likely to deliver depositional processes. Slope also showed varying associations depending on distance from shoreline. Along the coast, a negative association of -0.03 was found, explaining that higher sloped

surfaces yielded less increase in mean elevation change. Within the inland regions, a contradicting positive association was found, 0.01, showing that higher slope gradient yielded greater increase in mean elevation change. Along the coast, elevation showed a positive relationship of 0.37, explaining that with higher elevation, an increase in mean elevation change was found. Moving inland, the p-value did not yield a statistically significant value.

Erosional processes suggested a different insight. For erosional processes all over the study area, all variables provided a statistically significant value with a confidence level of 0.00. Vegetation showed a positive association of 0.18 with mean elevation change, indicating that an increase in vegetation cover lessened the erosional processes, or in other words less elevation decline was found. Slope showed a positive association of 0.01, indicating that with an increase in slope degree, there was less decline in mean elevation change. Higher elevated areas showed a negative relationship of -0.32 explaining that higher surfaces were associated with more elevation loss.

Vegetation did not yield a statistically significant relationship when applying the regression on both coastal and inland objects. Slope showed a consistent negative association in both coastal and inland objects with coefficients of -0.02 and -0.01, respectively, indicating that higher surface gradients yielded more elevation loss. Elevation provided a consistent relationship on both coastal and inland objects with a negative relationship of -0.31 along the coast and with -0.15 in inland region.

5.2.2 OLS for Hurricane Dennis

The total observations reached 3572 objects, consisting of 1404 erosional objects and 2168 depositional objects. The OLS regression analysis results are shown in Table 9 and Table 10. Numerous variables are statistically significant in the model.

Table 9 Hurricane Dennis Coefficient Report. * An asterisk next to a number indicates a statistically significant p-value ($p < 0.05$).

Variable	*Coef*	*StdError*	*t_Stat*	*Prob*	*Robust_SE*	*Robust_t*	*Robust_Pr*
Erosion & Deposition							
Intercept	0.98	0.02	40.21	0.00*	0.03	28.93	0.00*
Vegetation	0.53	0.06	8.40	0.00*	0.09	5.94	0.00*
Slope	0.00	0.00	-0.90	0.37	0.01	-0.60	0.55
Elevation	-0.60	0.01	-46.01	0.00*	0.02	-26.15	0.000*
Deposition							
Intercept	0.57	0.01	77.76	0.00*	0.01	59.79	0.00*
Vegetation	0.04	0.02	2.75	0.01*	0.02	2.38	0.02*
Slope	0.00	0.00	2.30	0.02*	0.00	2.25	0.03*
Elevation	0.04	0.01	7.18	0.00*	0.01	5.37	0.00*
Deposition (Along the Coast <200 m extent)							
Intercept	0.65	0.01	54.80	0.00*	0.01	51.99	0.00*
Vegetation	0.06	0.04	1.51	0.13	0.05	1.28	0.20
Slope	0.00	0.00	1.89	0.06	0.00	2.06	0.04*
Elevation	-0.02	0.01	-2.04	0.04*	0.01	-1.96	0.05*
Deposition (Inland >200 m extent)							
Intercept	0.49	0.01	41.50	0.00*	0.01	43.81	0.00*
Vegetation	0.08	0.02	4.26	0.00*	0.02	4.53	0.00*
Slope	0.00	0.00	1.95	0.05	0.00	1.55	0.12
Elevation	0.06	0.01	7.03	0.00*	0.01	4.29	0.00*
Erosion							
Intercept	0.16	0.04	4.08	0.00*	0.05	3.33	0.00*
Vegetation	1.40	0.16	8.73	0.00*	0.21	6.58	0.00*
Slope	0.02	0.00	4.69	0.00*	0.00	3.85	0.00*
Elevation	-0.57	0.01	-41.30	0.00*	0.02	-27.54	0.00*
Erosion (Along the Coast <200 m extent)							
Intercept	0.27	0.04	6.48	0.00*	0.05	5.98	0.00*
Vegetation	3.07	0.42	7.31	0.00*	0.73	4.20	0.00*
Slope	0.00	0.00	-0.19	0.85	0.00	-0.16	0.87
Elevation	-0.60	0.01	-43.20	0.00*	0.02	-31.73	0.00*
Erosion (Inland >200 m extent)							
Intercept	-0.36	0.04	-10.22	0.00*	0.06	-6.65	0.00*
Vegetation	-0.13	0.06	-2.16	0.03*	0.08	-1.54	0.13
Slope	-0.01	0.00	-2.74	0.01*	0.00	-1.83	0.07
Elevation	-0.07	0.02	-4.00	0.00*	0.04	-2.13	0.04*

Table 10 Hurricane Dennis Diagnostic Report.

Diagnostic Name	***Diagnostic Values***						
	All	**Deposition**	**Deposition (<200 m)**	**Deposition (>200 m)**	**Erosion**	**Erosion (<200 m)**	**Erosion (> 200 m)**
AIC	8,495.33	-1,426.74	-1,158.30	-352.81	2,743.26	2,307.50	-72.97
AICc	8,495.34	-1,426.71	-1,158.27	-352.70	2,743.30	2,307.55	-72.63
R2	0.47	0.05	0.01	0.29	0.56	0.62	0.43
AdjR2	0.47	0.05	0.00	0.28	0.56	0.62	0.42
F-Stat	1,057.26	40.82	2.93	68.31	594.06	658.97	45.03
F-Prob	0.00	0.00	0.03	0.00	0.00	0.00	0.00
Wald	1,288.65	53.13	8.78	89.52	772.35	1,036.61	69.50
Wald-Prob	0.00	0.00	0.03	0.00	0.00	0.00	0.00
K(BP)	1,186.50	88.38	4.41	48.19	494.98	328.12	33.20
K(BP)-Prob	0.00	0.00	0.22	0.00	0.00	0.00	0.00
JB	311.23	1,553.10	544.25	1,879.04	6.45	1.47	1,395.71
JB-Prob	0.00	0.00	0.00	0.00	0.04	0.48	0.00
Sigma2	0.63	0.03	0.03	0.03	0.41	0.39	0.04

In the overall analysis, the vegetation and elevation results reject the null hypothesis, as the model yielded significant statistical results with a confidence level of 0.00, while slope did not show significance. Vegetation yielded the expected sign with a positive association of 0.53 with the mean elevation change. This indicates that the more vegetation cover is found on the surface, the greater the increase is expected to occur in the surface elevation. Elevation also showed a negative association similar to our expectations with a coefficient of -0.60, indicating that with higher elevated morphology prior to a hurricane, more loss in surface elevation is expected after a hurricane hits. The adjusted R-square of 0.47 means that 47% of the total mean elevation change is explained by the selected variables in this study.

Depositional processes all along the study area provide more insight into the results. All variables tended to be statistically significant. In this case, vegetation showed a positive association of 0.04, indicating that with the increase in vegetation cover, an increase in mean elevation change was found within the depositional processes. Slope yielded a positive association

with a coefficient of 0.00, indicating that higher gradient degree surfaces are associated with greater elevation increase. Higher elevated areas showed a positive relationship of 0.04, explaining that higher surfaces showed greater vertical rise in surface elevation.

Results over spatial variation were calculated for coastal objects and inland objects separately. In the case of depositional objects along the coast, vegetation and slope did not yield statistically significant results with probability values of 0.13 and 0.06, respectively. Elevation showed a negative association in objects along the coast with a coefficient value of -0.02, explaining that higher elevated surfaces yielded less vertical increase in surface. In inland regions, vegetation showed a positive relationship with a coefficient of 0.08 to explain that with higher vegetation cover, more increase in mean elevation change was found. Elevation showed a positive relationship in inland objects with a coefficient value of 0.06, explaining that with higher elevation in surface prior to a hurricane, greater increase was found in mean elevation change.

Erosional processes suggest a different insight. In the case of R^2 values, erosional processes in general suggest a high value of 0.56, meaning that 55.9% of the total change in mean elevation change is explained by the three factors.

For erosional processes all over the study area, all variables provided a statistically significant value with a confidence level of 0.00. Vegetation showed a positive association of 1.40 with mean elevation change, indicating that the increase in vegetation cover is associated with less decline in mean elevation change value. Slope showed a positive association of 0.02 indicating that with the increase of slope degree, there was less decline in mean elevation change. Higher elevated areas showed a negative relationship of -0.57, explaining that higher surfaces are associated with more decline in mean elevation change.

Along the coast, the same results were shown in erosional processes for both vegetation and elevation variables as they showed statistically significant results with coefficients of 3.07 and -0.60, respectively, while slope on the other hand did not yield a statistically significant result. For inland objects, vegetation showed a negative association of -0.13, indicating that with higher vegetation cover, more decline in elevation is expected. Slope showed a negative relationship of -0.01, demonstrating that an increase in slope degree was associated with greater decrease in surface elevation. Elevation showed a negative association of -0.07, indicating that higher elevation surfaces prior to a hurricane are expected to lose more vertical elevation.

5.3 Discussion and Conclusion

In the OLS regression analysis, the results varied spatially, and the significance of certain variables changed with spatial variation across the study area. The observations indicated that a simple relationship between morphological processes and the selected variables cannot be explained only within a universal level along the barrier island; instead, distance from the shoreline has to be put into account. Several factors were examined in controlling the morphological change of erosional and depositional processes, and the following are some of the consistent findings:

- The mean elevation values of the erosional processes were noticed to be consistent in having a negative association with the mean elevation change values, whether during Hurricane Ivan or Hurricane Dennis, and also whether located in coastal or inland regions. This consistency means that higher elevated surfaces coincided with more erosional processes and vertical loss in surface.
- The mean elevation values of the depositional processes did not seem to establish a consistent relationship with mean elevation change when looking at coastal or inland region. However, the overall depositional processes did show a consistency of a positive

association with the mean elevation change values during the first and second hurricane, meaning that with higher surface elevation prior to a hurricane, more increase in surface elevation is expected after a hurricane hits.

- The mean vegetation values for erosional processes along the study area were consistent in presenting positive association with the mean elevation change values in both hurricanes. This means that it is common that if the vegetation cover increases, the loss of sediment is less expected.
- The mean vegetation values for depositional processes along the study area were consistent in showing a positive relationship with the mean elevation change in both hurricanes. This means that the more vegetation cover that was present, the more deposition and vertical accretion is found. Consistent with (Hesp 2002), wind velocity changes as it reaches the plant by decelerating quickly, which explains the sediment deposition in vegetated areas.
- The mean slope values for erosional processes showed contradicting results. In the overall study area, a positive association with mean elevation change is found to be consistent in both hurricanes; however in inland regions, a negative association with the mean elevation change is found to be consistent in both hurricanes.

The analysis provides important predictions for coastal management decision-making. First, the best conditions to lessen erosional processes during hurricanes of a category 3 are found within environment conditions of a steep, and is highly vegetated surfaces. In addition, the best conditions for sediment entrapment are found within environment condition of higher elevation surfaces, and with highly vegetated cover.

Chapter 6 Non-linear Regression Analysis

6.1 Introduction

In this chapter, CART analysis was performed to find whether factors such as vegetation, slope, and elevation influenced the mean elevation change during a category 3 hurricane. This analysis was performed in two stages: First the Classification Tree, followed by the Regression Tree, using the segmented change map shapefile. Finally, the discussion and conclusions are presented.

6.2 Classification Tree

The classification tree model classified cases into group values of the categorical dependent variable based on the values of independent variables. In this case, the object's status of erosional and depositional processes is the dependent or target variable, and the mean vegetation, the mean slope, and the mean elevation are the independent variables. This tree is used to identify which class the target or dependent variable will fall under, erosion or deposition, within every hurricane. Two tree-based classification models were generated for all objects during Hurricane Ivan as shown in Figure 54, and Hurricane Dennis as shown in Figure 55. Each node showed several pieces of information such as: the node number, a frequency table with percentages and count *n* of cases, a chart, and each predicted category containing the highest count or percentage is highlighted in grey.

In the case of Hurricane Ivan (Figure 54), a total of 17 nodes were generated, from which 9 are terminal nodes. From the first node of the tree, Node 0, it can be indicated that erosional processes dominated the tree model by 62.8%, while the remaining 37.2% were depositional processes. In addition, within this node, it is noticed that the split was based on the mean elevation independent variable, indicating that it represents the most important predictor to the model. The

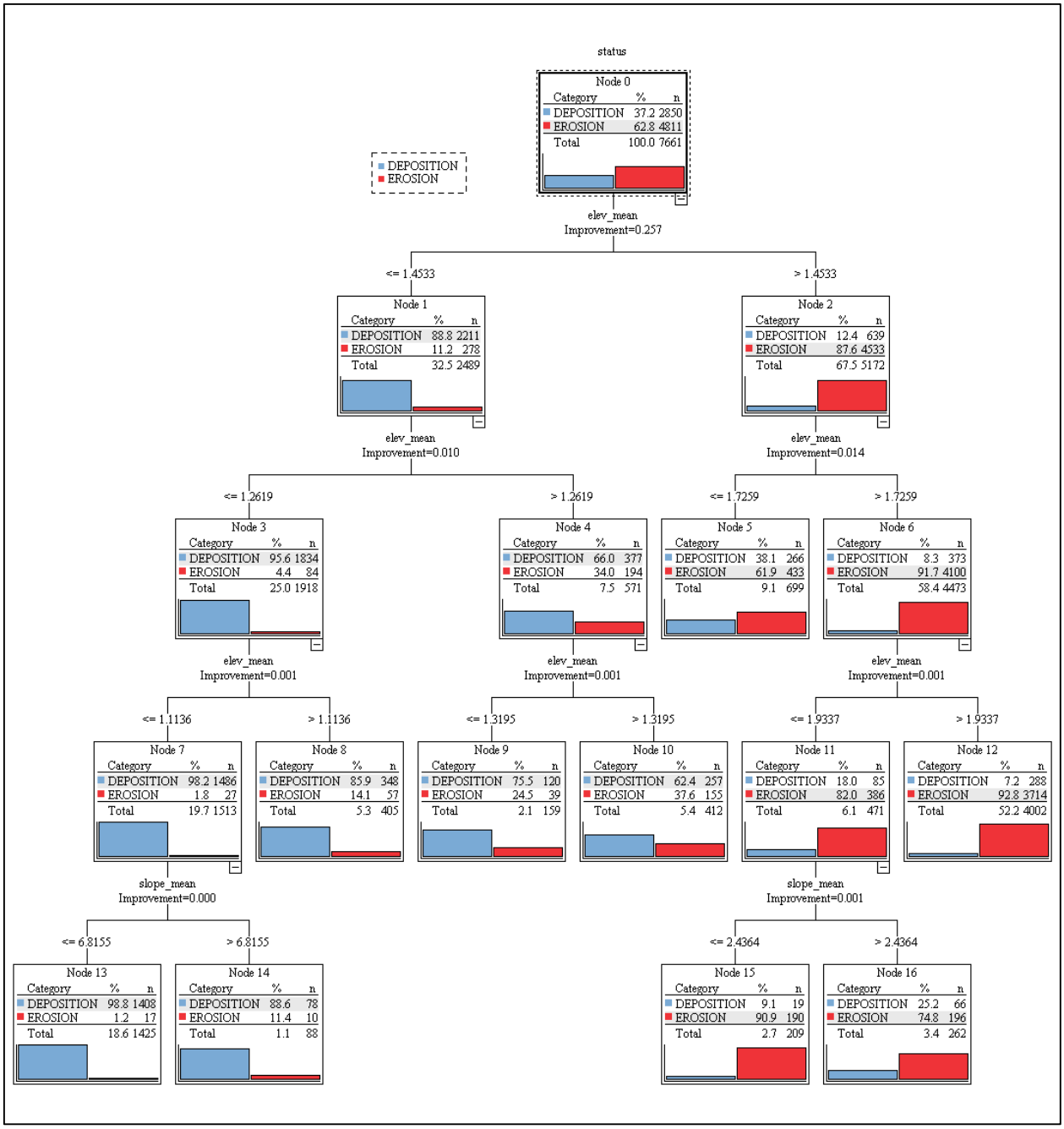

Figure 54 Classification tree during Hurricane Ivan.

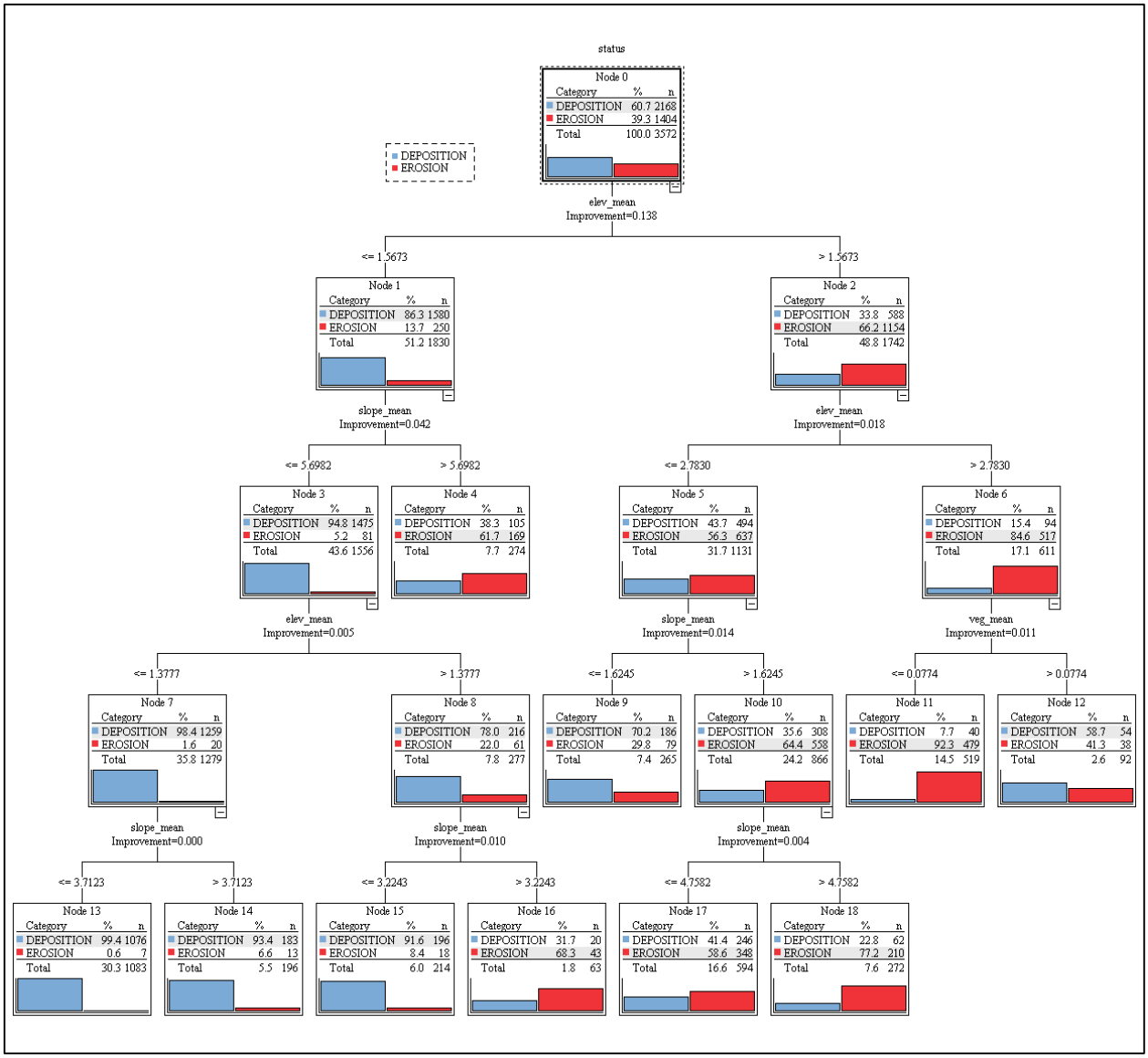

Figure 55 Classification tree during Hurricane Dennis.

first split was based on the posed question, "Is the mean elevation value greater than 1.5 m?" For the cases with an answer of "No" indicating that it is less or equal to 1.5 m, the classes fall on the left side of the tree in Node 1. For answers with "Yes", the classes fall on the right side of the tree in Node 2. For the cases under Node 2, it can be determined that within surfaces with mean elevation of height > 1.5 m, the erosional processes dominated these cases, while depositional processes in Node 1 dominated lower height surfaces with mean elevation <= 1.5 m. The same consistent pattern continues from Node 3 to 12 where all of those nodes were split by the variable,

the mean elevation, but with different splitting values. For mean elevation values <= 1.1 m from Node 7, which represent the lowest case of elevation height in the study area, a split is generated by the mean slope variable, and in terminal Node 13 the depositional processes dominated surfaces with gradient values <= 6.8º with a total count of 1408 cases. It can be concluded that depositional processes usually occur in the lowermost elevation surfaces, but with slope gradients of around or less than 6º, for example at the toe of a dune. The split from Node 11 is also by the mean slope variable, and terminal Node 15 and terminal Node 16 are both dominated by erosional processes, whether in cases with slope gradient <= 2.4º or in > 2.4º. Terminal Node 12 showed that most erosional cases occurred in mean elevation surfaces >1.9 m.

For Hurricane Dennis (Figure 55), a total of 19 nodes were partitioned, and 10 of them were terminal nodes. In Node 0, it was indicated that depositional processes dominated this hurricane by 60.7%, while the remaining 39.3% were for erosional processes. The split of this node was by the mean elevation variable, indicating that it represents the most important predictor to the model. The split from this node was based on the posed question, "Is the mean elevation value greater than 1.6 m?" Answers with "No" fell on the left side of the tree in Node 1, and answers with "Yes" fell on the right side in Node 2. It was noticed from Node 1 that 86.3% of the depositional processes were dominating lower elevation surfaces of <= 1.6 m. Node 2, on the other hand, with higher elevated surfaces > 1.6 m, was dominated by erosional processes by 66.2%. This finding is similar to the case of Hurricane Ivan but with slightly different splitting values. Following the sequence of node split from Node 1, Node 3, Node 7, and until terminal Node 13, it was indicated that depositional processes were dominating areas with the lowest elevated surfaces of <= 1.4 m and with flatter terrain of <= 3.7º with a total of 1076 cases recorded. Terminal Node 11 showed that 479 erosional cases were recorded with elevation higher than 2.8 m and with

vegetation <= 0.08 (around 8% cover). Node10 and its split through terminal Node 17 and terminal Node 18 displayed that 558 erosional cases were recorded with mean elevation between values > 1.6 m and <= 2.8 m and with mean slope gradient > 1.6º. This indicates that erosional processes are found more in higher elevated and steeper surfaces.

6.3 Regression Tree

The regression tree uses a numerical continuous dependent or target variable. In this case, mean elevation change is the dependent variable, and the mean vegetation, the mean slope, and the mean elevation are the independent variables. The analysis was conducted in two separate processes within each hurricane: first for erosional processes and second for depositional processes. Tree models were generated for Hurricane Ivan erosional and depositional processes as shown in Figure 56 and Figure 57, respectively, and for Hurricane Dennis erosional and depositional processes as shown in Figure 58 and Figure 59, respectively. Within each node, several pieces of information is presented, such as: the node number, the mean value and standard deviation value of the dependent variable, count *n* of cases, frequency percentage, and the predicted value.

In the case of erosional processes during Hurricane Ivan (Figure 56), a total of 29 nodes were generated, from which 15 were terminal nodes. Node 0 showed that the overall mean elevation loss was 1.2 m occurring in 4811 cases. The first split was by the mean elevation variable based on the following question, "Is the mean elevation value greater than 3.2 m?" Answers with "No" fell on the left side of the tree in Node 1 with a total of 3687 cases (76.6%), and answers with "Yes" fell on the right side in Node 2 with a total of 1124 cases (23.4%). Node 1 showed that the mean elevation change reached a mean value of -1.0 m, and Node 2 with -1.6 m. This indicated that erosional processes were frequently occurring in areas <= 3.2 m, but the higher vertical loss

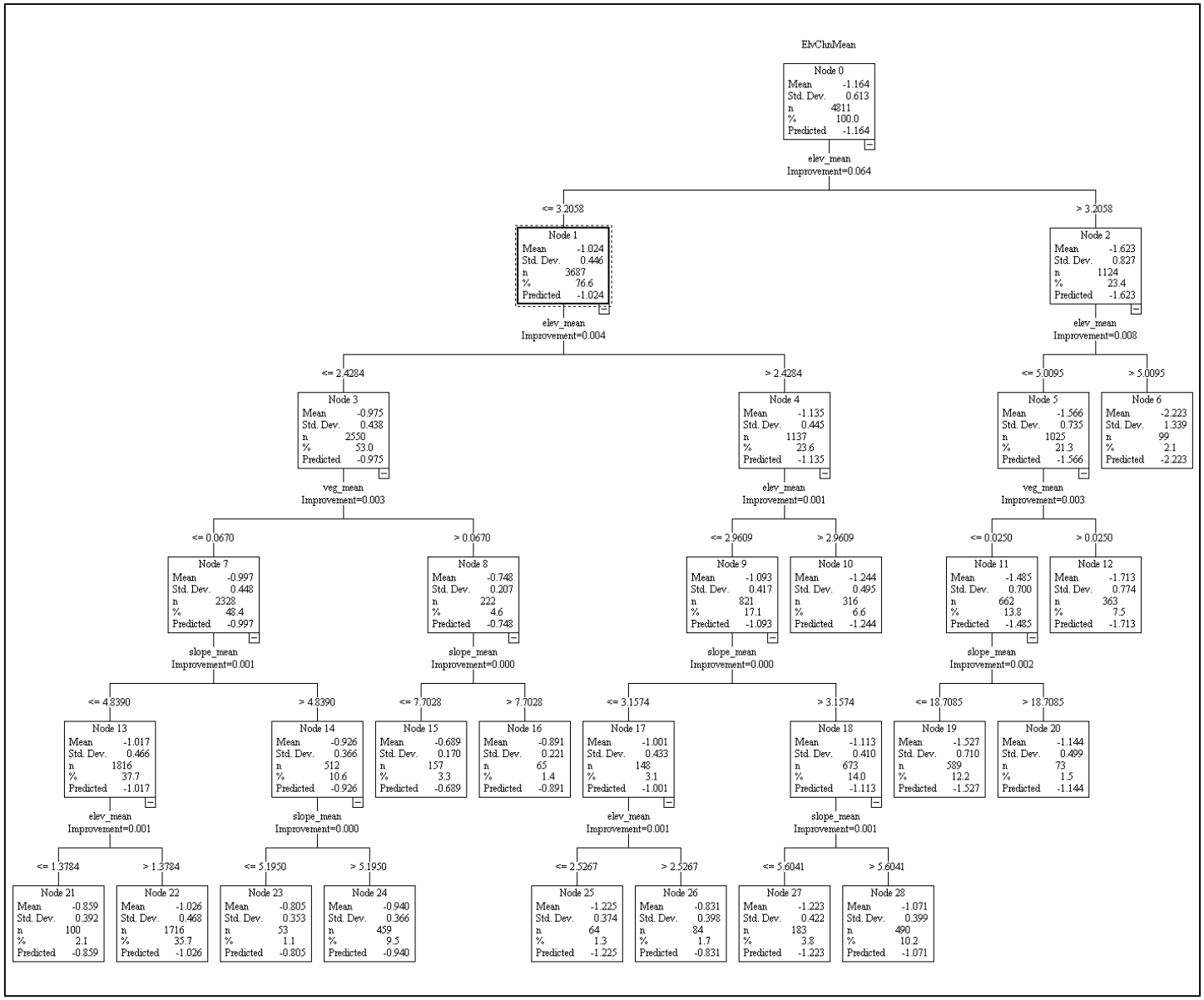

Figure 56 Regression tree for erosional processes during Hurricane Ivan.

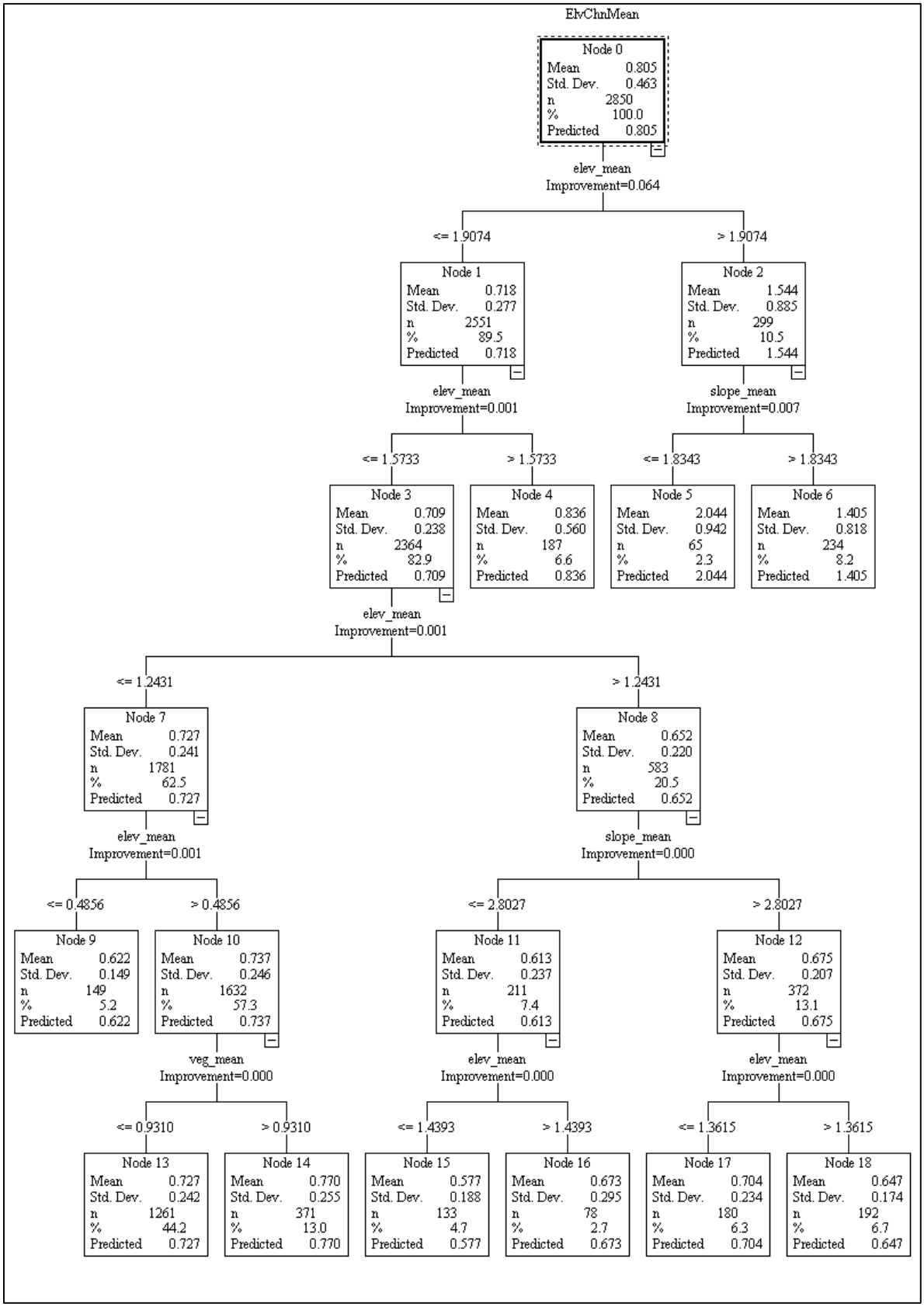

Figure 57 Regression tree for depositional processes during Hurricane Ivan.

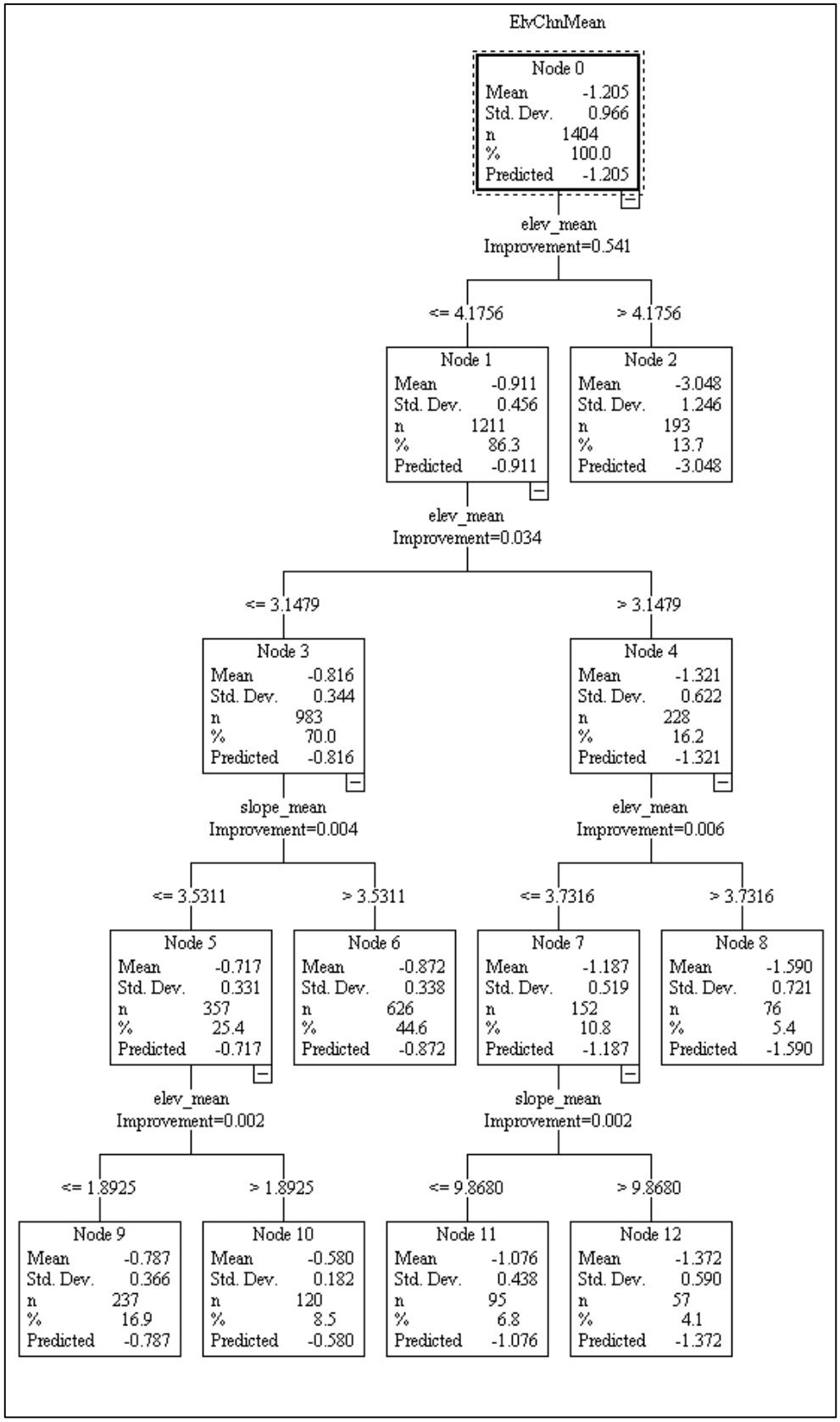

Figure 58 Regression tree for erosional processes during Hurricane Dennis.

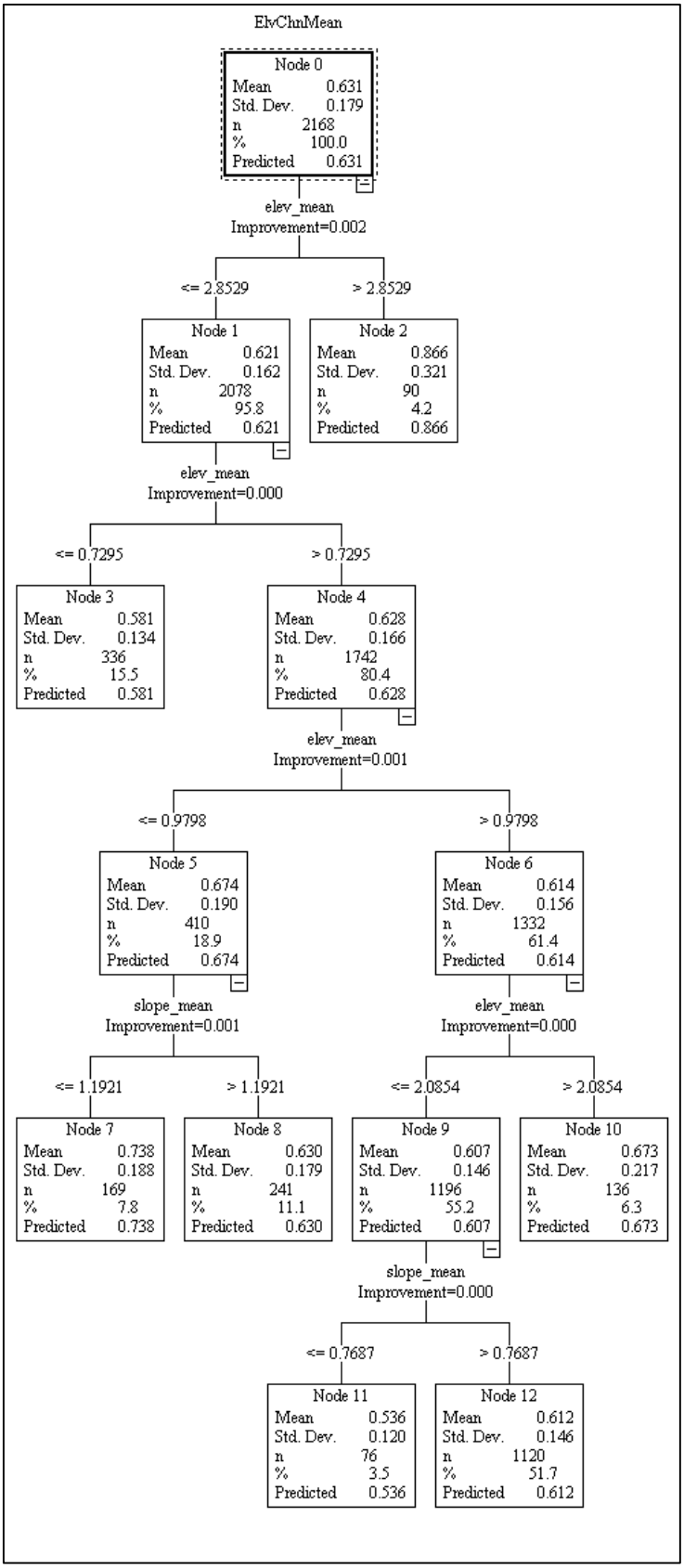

Figure 59 Regression tree for depositional processes during Hurricane Dennis.

was within surfaces > 3.2 m. Terminal Node 22 had the most frequent cases and conveyed an important prediction that 1716 cases (35.7%) with elevation between > 1.4 m and <= 2.4 m, with vegetation cover less than 7%, and with flatter surface of less than 4.8º encountered erosional loss of 1.0 m after Hurricane Ivan. Another important prediction was observed from terminal Node 19 that areas with elevation > 3.2 m and <= 5.0 m, with vegetation cover less than 2%, and with slope <= 18.7º encountered 1.5 m loss in vertical change. The maximum mean elevation change loss of 2.2 m was noticed in terminal Node 6 in the highest elevated surfaces of greater than 5.0 m.

For depositional processes during Hurricane Ivan (Figure 57), a total of 19 nodes were created, from which 10 were terminal nodes. Node 0 presented that the overall mean elevation increase was 0.8 m and occurred in 2850 cases. The first split was by the mean elevation variable based on the following question: "Is the mean elevation value greater than 1.9 m?" Answers with "No" fell on the left side of the tree in Node 1 with a total of 2551 cases (89.5%), and answers with "Yes" fell on the right side in Node 2 with a total of 299 cases (10.5%). Node 1 displayed that the mean elevation change reached a mean value of 0.7 m and Node 2 with 1.5 m. From this, it was indicated that depositional processes mostly occur in lower elevated surfaces of <= 1.9 m but that is not necessarily an indication of higher vertical accretion in elevation, which occurred in surfaces > 1.9 m. Terminal Node 13 had the most frequently occurring cases, and conveyed an important prediction in that 1261 cases (44.2%) with elevation between > 0.5 m and <= 1.2 m, and with vegetation cover less than 93% encountered depositional accumulation of 0.7 m after Hurricane Ivan. A similar prediction to terminal Node 13 is found in terminal Node 14 where 371 cases had mean elevation change of 0.8 m between surfaces > 0.5 m and <= 1.2 m, but this time it occurred within vegetation cover > 93%. The maximum mean elevation increase was predicted to be 2.0 m as noticed in terminal Node 5 within surfaces of > 1.9 m and flatter surfaces of <= 1.8º.

For erosional processes during Hurricane Dennis (Figure 58), a total of 13 nodes were generated, from which 7 were terminal nodes. Node 0 displays that the overall mean elevation loss was 1.2 m, occurring in 1404 cases. The first split was by the most important predictor to the model, the mean elevation variable, based on the following question: "Is the mean elevation value greater than 4.2 m?" Answers with "No" fell on the left side of the tree in Node 1 with a total of 1211 cases (86.3%), and answers with "Yes" fell on the right side in terminal Node 2 with a total of 193 cases (13.7%). Node 1 shows that the mean elevation change reached a mean value of -0.9 m, and terminal Node 2 with -3.0 m in which the maximum mean elevation loss was during Hurricane Dennis. This showed that most erosional cases occurred in surfaces <= 4.2 m, but the higher vertical loss is within surfaces > 4.2 m. The most frequently occurring cases were found in terminal Node 6 where 626 cases (44.6%) had a mean elevation loss of 0.9 m in surfaces <= 3.1 m and with slope > 3.5º.

In the case of depositional processes during Hurricane Dennis (Figure 59), a total of 13 nodes were generated, from which 7 were terminal nodes. Node 0 demonstrated that the overall mean elevation change was 0.6 m and occurred in 2168 cases. The first split was by the most important variable to the model, the mean elevation, and was based on the following question: "Is the mean elevation value greater than 2.9 m?" Answers with "No" fell on the left side of the tree in Node 1 with a total of 2078 cases (95.8%), and answers with "Yes" fell on the right side in terminal Node 2 with a total of 90 cases (4.2%). Node 1 displayed that the mean elevation change reached a mean value of 0.6 m, and terminal Node 2 with 0.9 m in which the maximum mean elevation accretion was during Hurricane Dennis. From this, it was indicated that depositional processes mostly occurred in lower elevated surfaces of <= 2.9 m, but that is not necessarily an indication of higher vertical accretion in elevation, which occurred in surfaces > 2.9 m. For

partitions on the left side within the split of <= 2.9 m, it was noticed that terminal Node 7 had the highest predicted sediment accretion of 0.7 m with 169 cases recorded, and this prediction was found in environmental conditions with elevation <= 1.0 m and with slope <= 1.2º. However, the most frequently occurring cases were found in terminal Node 12 where 1120 cases (51.7%) predicted an accretion of 0.6 m within environmental conditions consisting of mean elevation between > 1.0 m and <= 2.1 m and slope > 0.8º.

In addition to the tree model, the independent variable normalized importance to model bar chart is generated as shown in Figure 60 and Figure 61 for erosional and depositional processes, respectively, during Hurricane Ivan, and Figure 62 and Figure 63 for erosional and depositional processes, respectively, during Hurricane Dennis. Each independent variable, in this case the mean elevation, the mean slope, and the mean vegetation, is ranked in relation to its importance to the model for the dependent variable, in this case the mean elevation change. The predictor importance represented variables that are most important in the partitioning process of the tree where higher percentages are the most important and lower percentages are least important. Based on all the bar chart of all conditions, the mean elevation change was explained in order of importance by the 1) mean elevation, 2) mean slope, and 3) mean vegetation.

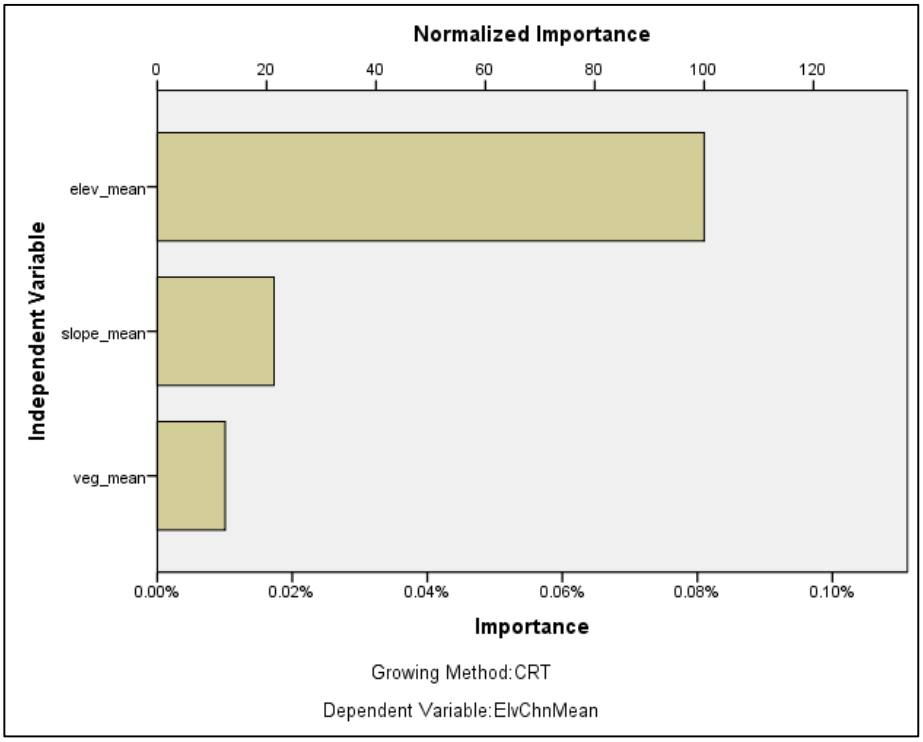

Figure 60 Normalized importance of the independent variables to the mean elevation change for erosional processes during Hurricane Ivan. The mean elevation change was explained in order of importance by the 1) mean elevation, 2) mean slope, and 3) mean vegetation.

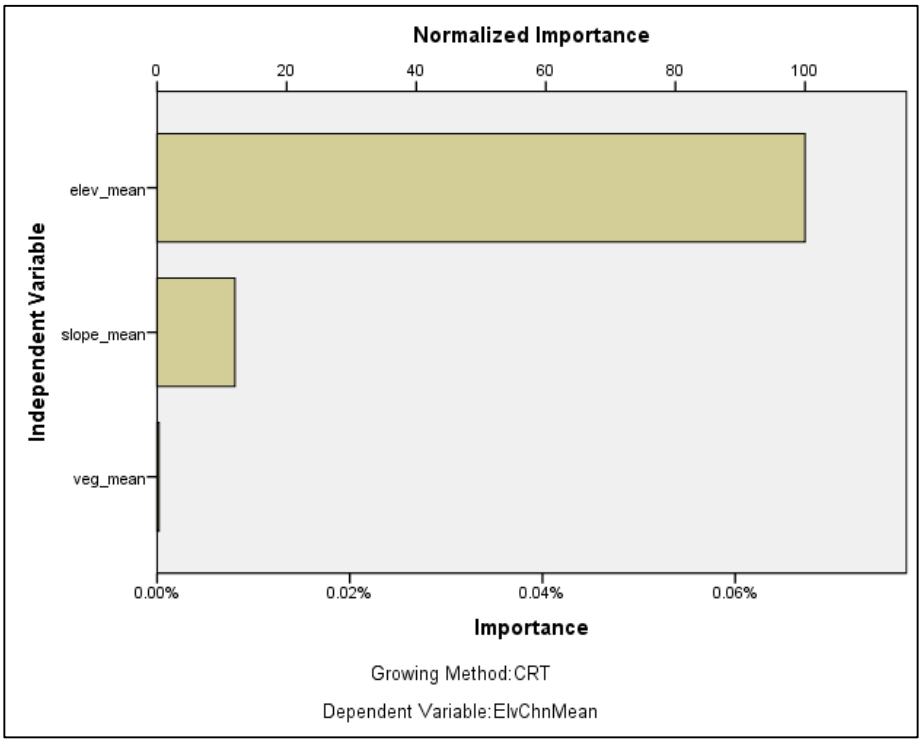

Figure 61 Normalized importance of the independent variables to the mean elevation change for depositional processes during Hurricane Ivan. The mean elevation change was explained in order of importance by the 1) mean elevation, 2) mean slope, and 3) mean vegetation.

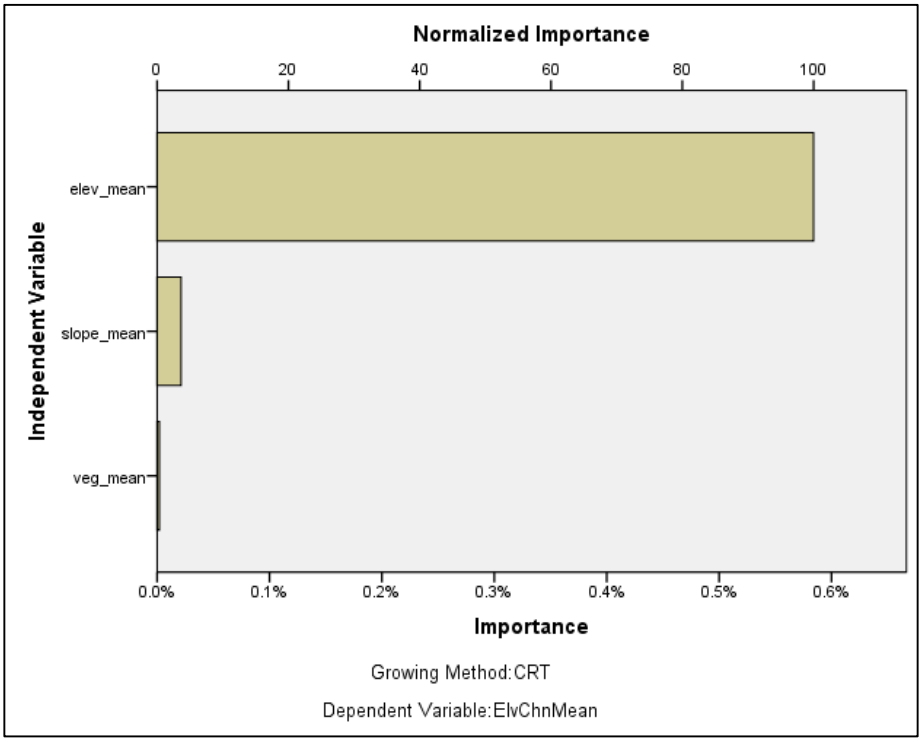

Figure 62 Normalized importance of the independent variables to the mean elevation change for erosional processes during Hurricane Dennis. The mean elevation change was explained in order of importance by the 1) mean elevation, 2) mean slope, and 3) mean vegetation.

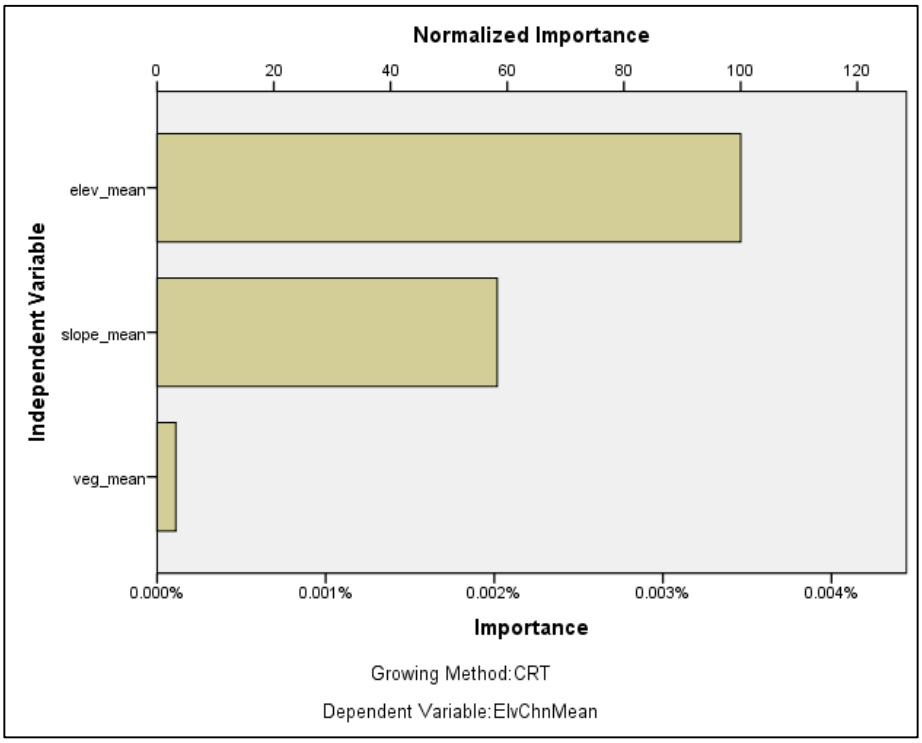

Figure 63 Normalized importance of the independent variables to the mean elevation change for depositional processes during Hurricane Dennis. The mean elevation change was explained in order of importance by the 1) mean elevation, 2) mean slope, and 3) mean vegetation.

6.4 Discussion and Conclusion

In the case of CART analysis, the test performed better in giving management prediction and decisions rather than just proving or disapproving a relationship significance in the traditional linear regression using OLS. In addition, assembling a global model using OLS in the case of our research produced complicated, difficult results, while CART was easy in terms of interpretation.

Based on the analysis in both hurricanes, the mean elevation each time ranked in first place as the most important factor in predicting the mean elevation change, followed by the mean slope variable ranked in second place, and finally the mean vegetation variable ranked in third place. It should be put in consideration that the barrier island in general lacked vegetation cover, especially following Hurricane Ivan that destroyed and buried a great amount of it, hence explains the low ranking in comparison with the other factors. Several consistent finding and predictions are found as followed:

- For erosional processes in both hurricanes, a consistent response is noticed. The most frequently occurring cases leading to a mean elevation loss of around 1 meter were found in surfaces around 1 m and 3 m, with slope gradient around 3º and 5º, and with vegetation cover less than 7%. This may be represented in flatter surfaces found on the crest of smaller foredunes, or low-hummocky dunes. This provides be a vital prediction for coastal managers to focus on stabilizing the first line of defense in foredunes along the coast by establishing greater than 7% cover of vegetation.
- Another prediction for erosional processes was found in cases that suffered the maximum mean elevation change of 2 m and 3 m during both hurricanes. These cases were found mostly in conditions with very high elevation of 4 m and 5 m, which can be explained as the top of the high elevated foredunes. This bring the attention for coastal managers to focus on these areas

that seems to suffer the most vertical loss of sediment during hurricanes, and apply stabilization techniques within it.

- For depositional processes during both hurricanes, the most frequently occurring cases that led to a vertical accretion of about 0.6 m and 0.7 m were found in surfaces with mean elevation around 0.4 m and 2 m, flat surfaces with slope less than 1º, and with vegetation cover less than 93%. This may be represented by the large amount of washover platforms that spread in a great size horizontally, but did not count for a vertical rise in elevation. These cases emphasize the role of vegetation in capturing and depositing the sediment where these objects encountered great amount of vegetation cover that aided in dissipating the energy of sediment.
- Finally, depositional objects in both hurricanes encountering the maximum mean elevation rise of 0.8 m and 2 m where found in surfaces with mean elevation of around 1 m and 2 m, and with slope around 2º. These cases may be found around the toe of dunes or within the depositional lobe in the back of the dune in which has lowest surface and almost flat gradient, and may perform as an obstacle in dissipating the energy of sediment transportation. The distribution of wind speed tends to change in elevated areas in contrast to flat surfaces, in which can be explained by the increase in pressure as airflow reaches the dune, decreasing wind speed, and hence results in deposition processes around the dune toe (Hesp et al. 2005). A protection mechanism for coastal management is to build continuous foredune in the back of the barrier island in order to avoid loss of sediment by the overwash processes in which can be susceptible to be lost in the bay area.

Chapter 7 Conclusion

In GIS, there are two models representing spatial information: 1) Field-based; and 2) Object-based (Shekhar and Chawla 2003). This research has utilized the object-based approach to study the coastal morphological changes that occurred after two major hurricanes, Hurricane Ivan in 2004 and Hurricane Dennis in 2005, using LiDAR data.

In contrary to previous research, this study was the first to examine and apply an object-based representation with a purpose of understanding the morphological changes occurring after a hurricane. The analysis was indicative of the efficiency of the object-based approach as it provided an abundant set of detailed information, geometric properties, and a spatial pattern analysis that could not be extracted using only the field-based approach. This research quantitatively linked the change to the contributing factors rather than just providing a qualitative assessment. The focus of this study was on the physical processes of the change by classifying and applying only the bare earth or ground data, and excluding vegetation, building, and noise points within the area. Therefore it provided new insight into the academic literature. Coastal management and planning becomes a challenge when dealing with the impacts of strong storms, and hence short-term quantification and evolution of the coastal landscapes and landscape change is needed to understand beach and barrier responses. This study provided several predictions and recommendations that can be further used by coastal managers for restoration projects.

7.1 Limitations and Future Suggestions

Although the CMA tool was efficient in the analysis of erosional and depositional objects, the performance of the tool covered the change within two sequential datasets, a pre-event survey and a post-event survey, whilst having the same spatial extent and resolution. Hence bringing its limitation in presenting the migration extent of the sediment into the back of the barrier island.

Given that the data in this research was relatively old, the downloaded datasets were unclassified to several class codes. This became one of the major limitations during the pre-processing stage as it was time-consuming to manually classify the LiDAR cloud points and extract bare-earth points. Accordingly, it would be more appropriate to find datasets previously classified. It is recommended that researchers use data with higher point cloud density to provide higher accuracy in the analysis and avoid confliction of the data error with the morphology change. In addition, color-infrared aerial photographs would have had higher accuracy in the estimation of vegetation cover, which was not found in the case of this research. For future research, a recommendation is to add more variables in the linear regression analysis, such as surface orientation, wave height, distance from the shoreline, and/or precipitation.

References

Beatley, T., D. J. Brower, and A. K. Schwab. 2002. *An introduction to coastal zone management*. 2nd ed. ed. Washington, D.C.: Island ; London : Kogan Page.

Beraldin, J.-A., F. Blais, and U. Lohr. 2010. Laser scanning technology. In *Airborne and terrestrial laser scanning*, eds. G. Vosselman and H.-G. Maas. Dunbeath, UK: Whittles.

Berk, R. A. 2008. *Statistical learning from a regression perspective*: Springer.

Beven, J. 2005. Tropical Cyclone Report. Hurricane Dennis. 4 – 13 July 2005: National Hurricane Center.

Bird, E. C. F. 2008. *Coastal geomorphology : an introduction*. 2nd ed. ed. Chichester: John Wiley.

Brock, J. C., C. W. Wright, A. H. Sallenger, W. B. Krabill, and R. N. Swift. 2002. Basis and Methods of NASA Airborne Topographic Mapper Lidar Surveys for Coastal Studies. *Journal of Coastal Research* 18 (1):1-13.

Carson, R. 1955. *The edge of the sea*. Boston,: Houghton Mifflin.

Carter, R. W. G. 1989. *Coastal Environments: An Introduction to the Physical, Ecological and Cultural Systems of Coastlines*: Academic Press.

Chang, K.-T. 2013. *Introduction to Geographic Information Systems*: McGraw-Hill Education.

Channel, T. W. *Hurricanes and Tropical Storms: Saffir-Simpson Hurricane Scale*. The Weather Channel 2012 [cited 12 September 2013. Available from **http://www.weather.com/encyclopedia/charts/tropical/saffirscale.html**.

CHL. *CEM Appendix A - Glossary of Coastal Terminology*. U.S. Army Corps of Engineers, Coastal and Hydraulics Laboratory, Engineer Research and Development Center 2003 [cited 2 July 2014. Available from **http://chl.erdc.usace.army.mil/cemglossary**.

Claudino-Sales, V., P. Wang, and M. H. Horwitz. 2008. Factors controlling the survival of coastal dunes during multiple hurricane impacts in 2004 and 2005: Santa Rosa barrier island, Florida. *Geomorphology* 95:295–315.

———. 2010. Effect of Hurricane Ivan on Coastal Dunes of Santa Rosa Barrier Island, Florida: Characterized on the Basis of Pre- and Poststorm LIDAR Surveys. *Journal of Coastal Research* 26 (3):470–484.

Cowell, P. J., and B. G. Thom. 1997. Morphodynamics of coastal evolution. In *Coastal evolution, Late Quaternary shoreline morphodynamics*, eds. R. W. G. Carter and C. D. Woodroffe. United Kingdom: Cambrige University Press.

Dolan, R., and P. Godfrey. 1973. Effects of Hurricane Ginger on the barrier islands of North Carolina. *Geological Society of America Bulletin* 84 (4):1329-1334.

Dolan, R., B. Hayden, and J. Heywood. 1978. A new photogrammetric method for determining shoreline erosion. *Coastal Engineering* 2:21–39.

Earth, G. *Google Earth*. Google Earth 2013 [cited 12 September 2013. Available from **http://www.google.com/earth/index.html**.

ESRI. *ArcGIS Help 10.1: Ordinary Least Squares (OLS) (Spatial Statistics)*. ESRI 2013a [cited 03 November 2013. Available from **http://resources.arcgis.com/en/help/main/10.1/index.html#//005p00000022000000**.

———. 2013b. ESRI Basemap.

Everitt, B. S. 2002. The Cambridge dictionary of statistics. *Cambridge: Cambridge*.

FDEP. 2004. Hurricane Ivan: Beach and Dune Erosion and Structural Damage Assessment and Post-storm Recovery Plan for the Panhandle Coast of Florida: Bureau of Beaches and Coastal Systems, Division of Water Resource Management, Department of Environmental Protection State of Florida.

———. 2005. Hurricane Dennis: Beach and Dune Erosion and Structural Damage Assessment and Post-storm Recovery Recommendations for the Panhandle Coast of Florida: Florida Department of Environmental Protection, Division of Water Resource Management, Bureau of Beaches and Coastal Systems.

Gares, P. A., Y. Wang, and S. A. White. 2006. Using LIDAR to Monitor a Beach Nourishment Project at Wrightsville Beach, North Carolina, USA. *Journal of Coastal Research* 22 (5):1206-1219.

Goudie, A. 2004. *Encyclopedia of geomorphology*. London ; New York: Routledge : International Association of Geomorphologists.

Gutierrez, R., James C. Gibeaut, R. C. Smyth, T. L. Hepner, and J. R. Andrews. 2001. Precise airborne lidar surveying for coastal research and geo-hazards applications. *International Archives of Photogrammetry and Remote Sensing* XXXIV-3/W4:185–192.

Hapke, C. J., D. Reid, B. M. Richmond, P. Ruggiero, and J. List. 2006. National assessment of shoreline change part 3: Historical shoreline change and associated coastal land loss along sandy shorelines of the California coast. *Open-File Report 2006-1219*:79.

Hayes, M. O. 1967. Hurricanes as geological agents: case studies of Hurricanes Carla, 1961, and Cindy, 1963.54 p.

Hesp, P. 2002. Foredunes and blowouts: initiation, geomorphology and dynamics. *Geomorphology* 48 (1):245-268.

Hesp, P. A., R. Davidson-Arnott, I. J. Walker, and J. Ollerhead. 2005. Flow dynamics over a foredune at Prince Edward Island, Canada. *Geomorphology* 65:71–84.

Hesp, P. A., and A. D. Short. 1999. Barrier Morphodynamics. In *Handbook of beach and shoreface morphodynamics*, ed. A. D. Short. Chichester: John Wiley.

Hinrichsen, D. 1999. Trends and Future Challenges for U.S. National Ocean and Coastal Policy.

———. *Ocean planet in decline*. People & the Planet 2010 [cited 22 July 2013. Available from **http://www.peopleandplanet.net/?lid=26188&section=35&topic=44**.

Houser, C., C. Hapke, and S. Hamilton. 2008. Controls on coastal dune morphology, shoreline erosion and barrier island response to extreme storms. *Geomorphology* 100:223–240.

Jensen, J. R. 2009. *Remote sensing of the environment: an earth resource perspective*. 2 ed. Upper Saddle River, NJ: Pearson Education.

Keen, T. R., and G. W. Stone. 2000. Anomalous response of beaches to hurricane waves in a low-energy environment, northeast Gulf of Mexico, USA. *Journal of Coastal Research* 16 (4):1100-1110.

Kish, S. A., and J. F. Donoghue. 2013. Coastal Response to Storms and Sea-Level Rise: Santa Rosa Island, Northwest Florida, U.S.A. *Journal of Coastal Research* SI (63):131–140.

Liu, H., L. Wang, D. Sherman, Y. Gao, and Q. Wu. 2010. An object-based conceptual framework and computational method for representing and analyzing coastal morphological changes. *International Journal of Geographical Information Science*:1–27.

Lutgens, F. K., and E. J. Tarbuck. 2007. *The Atmosphere: An Introduction to Meteorology*. 10th ed. Upper Saddle River, New Jersey: Pearson Prentice Hall.

Moore, L. J. 2000. Shoreline Mapping Techniques. *Journal of Coastal Research* 16 (1):111-124.

Morton, R. A. 2002. Factors controlling storm impacts on coastal barriers and beaches: a preliminary basis for near real-time forecasting. *Journal of Coastal Research*:486-501.

Morton, R. A., and T. L. Miller. 2005. National assessment of shoreline change: Part 2, Historical shoreline changes and associated coastal land loss along the U.S. southeast Atlantic coast. *Open-File Report 2005-1401*:40.

Morton, R. A., T. L. Miller, and L. J. Moore. 2004. National assessment of shoreline change: Part 1, Historical shoreline changes and associated coastal land loss along the U.S. Gulf of Mexico. *U.S. Geological Survey Open-File Report 2004-1043*:44.

NOAA. 2013. *Frequently Askes Questions: Subject: A2) What is a "Cape Verde" hurricane?* Hurricane Research Division, Atlantic Oceanographic & Meteorological Laboratory,

National Oceanic & Atmospheric Administration 2006 [cited 15 September 2013 2013]. Available from **http://www.aoml.noaa.gov/hrd/tcfaq/A2.html**.

———. 2013. *NOAA National Weather Service to Use New Hurricane Wind Scale: Storm Surge and Flooding Prediction Dropped in New Scale*. National Oceanic and Atmospheric Administration 2010 [cited 13 September 2013 2013]. Available from **http://www.noaanews.noaa.gov/stories2010/20100217_hurricane.html**.

———. 2012. *Lidar 101: An Introduction to Lidar Technology, Data, and Applications*. Charleston, SC: National Oceanic and Atmospheric Administration (NOAA) Coastal Services Center.

———. 2013. *Digital Coast: NOAA Coastal Services Center*. United States Department of Commerce, National Oceanic and Atmospheric Administration, July 2013 2013a [cited 1 July 2013 2013]. Available from **http://www.csc.noaa.gov/dataviewer/#app=f8ce&6ba3-selectedIndex=0**.

———. 2013b. National Coastal Population Report: Population Trends from 1970 to 2020.

———. 2013. *Ocean Facts: Storm surge is the rise in seawater level caused solely by a storm; storm tide is the observed seawater level during a storm.* National Ocean Service (NOS), National Oceanic and Atmospheric Administration (NOAA), Department of Commerce 2013c [cited 25 September 2013 2013]. Available from **http://oceanservice.noaa.gov/facts/stormsurge-stormtide.html**.

———. 2013. *Saffir-Simpson Hurricane Wind Scale*. National Weather Service, National Centers for Environmental Prediction, National Hurricane Center 2013d [cited 3 September 2013]. Available from **http://www.nhc.noaa.gov/aboutsshws.php**.

———. 2014. *National Climatic Data Center (NCDC)*. National Oceanic and Atmospheric Administration, September 2014 2014a [cited 7 September 2014 2014]. Available from **http://www.ncdc.noaa.gov/data-access/quick-links#loc-clim**.

———. 2014. *National Climatic Data Center (NCDC)*. National Oceanic and Atmospheric Administration, September 2014 2014b [cited 13 September 2014 2014]. Available from **http://www.ncdc.noaa.gov/ibtracs/index.php?name=ibtracs-data**.

NWS, I. S. T. *National Weather Service Glossary*. US Dept of Commerce, National Oceanic and Atmospheric Administration, National Weather Service 2009 [cited 14 September 2013. Available from **http://w1.weather.gov/glossary/**.

Price, M. 2013. *Mastering ArcGIS with Video Clips DVD-ROM*: McGraw-Hill Education.

Robertson, W., V, D. Whitman, K. Zhang, and S. P. Leatherman. 2004. Mapping shoreline position using airborne laser altimetry. *Journal of Coastal Research* 20 (3):884-892.

Robertson, W., V, K. Zhang, and D. Whitman. 2007. Hurricane-induced beach change derived from airborne laser measurements near Panama City, Florida. *Marine Geology* 237 (3–4):191–205.

Sallenger, A. H., Jr. 2000. Storm Impact Scale for Barrier Islands. *Journal of Coastal Research* 16 (3):890-895.

Sallenger, A. H., Jr., W. B. Krabill, R. N. Swift, J. Brock, J. List, M. Hansen, R. A. Holman, S. Manizade, J. Sontag, A. Meredith, K. Morgan, J. K. Yunkel, E. B. Frederick, and H. Stockdon. 2003. Evaluation of airborne topographic lidar for quantifying beach changes. *Journal of Coastal Research* 19 (1):125-133.

Sallenger, A. H., H. F. Stockdon, L. Fauver, M. Hansen, D. Thompson, C. W. Wright, and J. Lillycrop. 2006. Hurricanes 2004: An Overview of Their Characteristics and Coastal Change. *Estuaries and Coasts* 29 (6A):880-888.

Schwartz, M. L. 2005. *Encyclopedia of coastal science*. Dordrecht ; [London]: Springer.

Shekhar, S., and S. Chawla. 2003. *Spatial databases : a tour*. Upper Saddle River, N.J.: Prentice Hall.

Shepard, F. P. 1950. Beach Cycles in Southern California. *CORPS OF ENGINEERS WASHINGTON DC BEACH EROSION BOARD* (TM-20).

Shepard, F. P., and E. C. LaFond. 1940. Sand movements along the Scripps Institution Pier. *American Journal of Science* 238 (4):272-285.

Short, A. D. 1999. Beaches. In *Handbook of beach and shoreface morphodynamics*, ed. A. D. Short. Chichester: John Wiley.

Shrestha, R. L., W. E. Carter, M. Sartori, B. J. Luzum, and K. C. Slatton. 2005. Airborne Laser Swath Mapping: Quantifying changes in sandy beaches over time scales of weeks to years. *ISPRS Journal of Photogrammetry & Remote Sensing* 59 (4):222– 232.

Stewart, R. 2013. *Oceanography in the 21st Century - An Online Textbook*. Department of Oceanography, Texas A&M University 2009 [cited 22 July 2013]. Available from **http://oceanworld.tamu.edu/resources/oceanography-book/coastalzone.htm**.

Stewart, S. R. *Tropical Cyclone Report. Hurricane Ivan. 2 - 24 September 2004*. NOAA/ National Weather Service, National Centers for Environmental Prediction, National Hurricane Center 2006 [cited 14 September 2013. Available from **http://www.nhc.noaa.gov/2004ivan.shtml**.

Stockdon, H. F., K. S. Doran, and A. H. Sallenger, Jr. 2009. Extraction of lidar-based dune-crest elevations for use in examining the vulnerability of beaches to inundation during hurricanes. *Journal of Coastal Research* SI (53):59–65.

Stockdon, H. F., A. H. Sallenger, Jr., J. H. List, and R. A. Holman. 2002. Estimation of shoreline position and change from airborne scanning lidar. *Journal of Coastal Research* 18 (3):502-513.

Stone, G. W., B. Liu, D. A. Pepper, and P. Wang. 2004. The importance of extratropical and tropical cyclones on the short-term evolution of barrier islands along the northern Gulf of Mexico, USA. *Marine Geology* 210:63–78.

Stone, G. W., and F. W. Stapor, Jr. 1996. A Nearshore Sediment Transport Model for the Northeast Gulf of Mexico Coast, U.S.A. *Journal of Coastal Research* 12 (3):786-793.

Thomas, D. S. G., A. Goudie, and D. Dunkerley. 2000. *The dictionary of physical geography*. 3rd ed. ed. Oxford: Blackwell Publishers.

USGS. 2014. *EarthExplorer*. U.S. Department of the Interior, U.S. Geological Survey, January 2014 2014 [cited 1 January 2014 2014]. Available from **http://earthexplorer.usgs.gov/**.

Wang, P., J. H. Kirby, J. D. Haber, M. H. Horwitz, P. O. Knorr, and J. R. Krock. 2006. Morphological and Sedimentological Impacts of Hurricane Ivan and Immediate PoststormBeach Recovery along the Northwestern Florida Barrier-Island Coasts. *Journal of Coastal Research* 22 (6):1382-1402.

Weisstein, E. W. *Least Squares Fitting*. MathWorld--A Wolfram Web Resource 2013 [cited 3 November 2013. Available from **http://mathworld.wolfram.com/LeastSquaresFitting.html**.

Wentz, E. A. 2000. A shape definition for geographic applications based on edge, elongation, and perforation. *Geographical Analysis* 32 (2):95-112.

White, S. A., and Y. Wang. 2003. Utilizing DEMs derived from LIDAR data to analyze morphologic change in the North Carolina coastline. *Remote Sensing of Environment* 85 (2):39–47.

Woodroffe, C. D. 2002. *Coasts : form, process, and evolution*. Cambridge: Cambridge University Press.

Yan, X., and X. G. Su. 2009. *Linear regression analysis: theory and computing*. New Jersey: World Scientific.

Zhang, K., D. Whitman, S. Leatherman, and W. Robertson. 2005. Quantification of beach changes caused by Hurricane Floyd along Florida's Atlantic coast using airborne laser surveys. *Journal of Coastal Research* 21 (1):123-134.

Zhou, G., and M. Xie. 2009. Coastal 3-D Morphological Change Analysis Using LiDAR Series Data: A Case Study of Assateague Island. *Journal of Coastal Research* 25 (2):435–447.

Appendix A: Permission Letter to Redraw Figure

Gmail

Bedoor Mohammad <bedoor11@gmail.com>

RE: [EXTERNAL] Fwd: Permission to Redraw a Figure
1 message

Morang, Andrew ERDC-RDE-CHL-MS <Andrew.Morang@erdc.dren.mil> Mon, Jul 7, 2014 at 8:55 AM
To: Bedoor Mohammad <bedoor11@gmail.com>

Dear Sir,
You may use this illustration freely because it is from an official U.S. Government publication and therefore does not have copyright. But we certainly do appreciate your noting the source. As I recall, this figure originally was drawn in Autocad. I can send the original if you want to use Autocad to modify it. Some other engineering packages may also open Autocad files.

All the best,

Andrew Morang, Ph.D.
Coastal and Hydraulics Laboratory, HN-CE
Engineer Research and Development Center
3909 Halls Ferry Road
Vicksburg, Mississippi 39180 USA
.....
Tel: 601 634 2064
Facsimile: 601 634 3080

(P.S., I, too was a Tiger years ago, Ph.D. in geology)

-----Original Message-----
From: Bedoor Mohammad [mailto:bedoor11@gmail.com]
Sent: Friday, July 04, 2014 21:31
To: andrew.morang@erdc.usace.army.mil
Subject: [EXTERNAL] Fwd: Permission to Redraw a Figure

Hello,

I am a graduate student in Louisiana State University working on my dissertation. I am interested in redrawing one illustration found in your website and to include the redrawn copy in my dissertation. The original illustration I would like to redraw is found in this link below:

http://chl.erdc.usace.army.mil/cemglossary

titled "Definition of terms and features describing the coastal zone."

I also attached a file of the illustration I mentioned.

I will cite your original source of the illustrations in my dissertation.

Please let me know at your earliest convenience if I have your permission to redraw the illustration. Thank you for your time and consideration.

Sincerely,

Bedoor Mohammad, M.A.

PhD Candidate
Department of Geography and Anthropology Louisiana State University
Email: bmoham1@lsu.edu
bedoor11@gmail.com

Appendix B: Shape Attributes Definitions.

Attributes	Definitions
Compactness index *(CI)*	$CI = \frac{4\pi A}{P^2}$
Elongatedness *(ELG)*	$ELG = \frac{l}{w}$ l and w are the length and width of the minimum bounding rectangle.
Asymmetry *(ASM)*	$ASM = 1 - \frac{b}{a}$ $\quad \mu_{pq} = \sum_{i-1}^{n}(x_i - \bar{x})^p\,(y_i - \bar{y})^q$ $a = \sqrt{\frac{2(\mu_{20} + \mu_{02} + \sqrt{(\mu_{20} - \mu_{02})^2 + 4\mu_{11}^2})}{\mu_{00}}}$ $b = \sqrt{\frac{2(\mu_{20} + \mu_{02} - \sqrt{(\mu_{20} - \mu_{02})^2 + 4\mu_{11}^2})}{\mu_{00}}}$ a and b are the semi-major and semi-minor of the best-fit ellipse, μ_{pq} are the central moments
Orientation *(∅)*	$\emptyset = \frac{1}{2}\tan^{-1}\left(\frac{2\mu_{11}}{\mu_{20} - \mu_{02}}\right)$ μ_{pq} are the central moments, ∅ is defined as an angle in degree between the x-axis and the major axis of the best-fit ellipse measured counterclockwise [0, 180º].
Fractal dimension (*D*)	$N(r) = cr^{1-D}$ r is the width of box, $N(r)$ is the counts of the boxes contain the object.
Ellipticity (*ELP*)	$ELP = \begin{cases} 16\pi^2 I_1 & if\ I_1 \leq 1/16\pi^2 \\ \frac{1}{16\pi^2 I_1} & otherwise \end{cases}$ $I_1 = \frac{\mu_{20}\mu_{02} - \mu_{11}^2}{\mu_{00}^4}$ μ_{pq} are the central moments, and I_1 is the affine moment invariant.

Source (Liu et al. 2010)

Vita

Bedoor Adel Mohammad was born and raised in Kuwait. She received her bachelor's degree from the Department of Geography at Kuwait University in 2005, and she earned her Masters of Art degree from the Department of Geography at California State University, Northridge in 2009. She entered graduate school in 2010 to pursue a Doctor of Philosophy degree in the Department of Geography and Anthropology at Louisiana State University, and she expects to complete her Ph.D. in May 2015.